

**SYNTHESIS AND CHARACTERIZATION OF POLYIMIDE  
COBALT FERRITE NANOCOMPOSITES FOR POTENTIAL  
APPLICATIONS IN MEMS**

By

Jesús David Mazuera Robledo

A thesis submitted in partial fulfillment of the requirements for the degree of

MASTER OF SCIENCE

in

MECHANICAL ENGINEERING

UNIVERSITY OF PUERTO RICO

MAYAGÜEZ CAMPUS

2009

Approved by:

\_\_\_\_\_  
Oscar Juan Perales Pérez, Ph.D.  
President, Graduate Comité

\_\_\_\_\_  
Date

\_\_\_\_\_  
Ricky Valentín, Ph.D.  
Member, Graduate Committee

\_\_\_\_\_  
Date

\_\_\_\_\_  
Gustavo Gutiérrez, Ph.D.  
Member, Graduate Committee

\_\_\_\_\_  
Date

\_\_\_\_\_  
Mercedes Ferrer, ME.  
Representative of Graduate Studies

\_\_\_\_\_  
Date

\_\_\_\_\_  
Ramón E. Vásquez, Ph.D.  
Dean of Engineering  
ME Director Representative

\_\_\_\_\_  
Date

## **ABSTRACT**

In the present work, cobalt ferrite nanocrystals were synthesized under size-controlled conditions in aqueous phase and incorporated into a polyimide matrix at various volumetric loads. Synthesized 20nm-cobalt ferrite single crystals, which exhibited a coercivity of 2.9kOe at room-temperature, were dispersed in polyimide precursor using two dispersion techniques: (homogenizer and ball mill) and cured to develop the polyimide matrix in the resulting nanocomposites. Produced films were characterized by Fourier transform infrared spectroscopy, X-ray diffraction and vibrating sample magnetometry, which confirmed the formation of the nanocomposite. As expected, the saturation magnetization in the nanocomposites varied according to the Polyimide/Ferrite weight ratio, while coercivity remained at the value corresponding to pure cobalt ferrite nanocrystals. In addition, thermal degradation, thermal stability and dynamic mechanical analyses tests were conducted to assess the viability of the two selected nanocomposites fabrication processes and thus to establish the temperature range in which produced composites can be used.

## RESUMEN

En el presente trabajo, nanocristales de ferrita de cobalto fueron sintetizados en fase acuosa en condiciones de control de tamaño de cristal y fueron incorporadas en una matriz de poliimida a diferentes fracciones volumétricas. Los monocristales sintetizados de 20nm que exhiben una coercitividad de 2.9kOe a temperatura ambiente fueron dispersados en un precursor de poliimida usando dos técnicas de dispersión: homogenizador y molino de bolas, y curados para obtener la matriz de poliimida en los compuestos resultantes. Las películas producidas fueron caracterizadas usando espectroscopía infrarroja con transformada de Fourier, difracción de rayos X y magnetometría de muestra vibrante. Como se esperaba, la magnetización de saturación en los nanocompuestos varió de acuerdo con la razón en peso de poliimida a ferrita mientras que la coercitividad se mantuvo en el mismo valor obtenido para los nanocristales de ferrita de cobalto puros. Además, pruebas de degradación térmica, estabilidad térmica y análisis dinámico mecánico fueron llevados a cabo para evaluar la viabilidad de los dos procesos de fabricación seleccionados y de esta manera establecer los rangos de temperatura en los que los nanocompuestos producidos pueden ser usados.

Copyright © by  
Jesús David Mazuera Robledo  
2009

*To SRT...*

*To my Family...*

*To the memory of Cecilia Franco...*

## ACKNOWLEDGEMENTS

There are a lot people that have contributed to the achievement of this goal and to make of me the person and professional that I actually am. In first place I would like to acknowledge the University of Puerto Rico Mayaguez Campus for giving me the opportunity of conduct my graduate studies in this academia. In particular I would like to acknowledge the Engineering Science and Materials Department for the support given to me during the last two years.

I'm grateful with Dr. Oscar Perales, my advisor for giving me the opportunity to work with him and join his research group at the Nanomaterials processing lab. I'm also grateful with Dr. Marcelo Suarez and the PREM program for supporting me and my research project.

To my beloved girlfriend, Sandra, for being my force, support and inspiration during every single day of this adventure, and most important, for her pattiencie. I would like to thank to my parents and aunts Cecilia, Olga and Betty for their support and love.

I'm grateful with Jorge Giraldo, M.Sc., Eng. Cesar Chaves, Eng. Jorge Ivan Alvarez and Dr. Alejandro Toro at Universidad Nacional de Colombia Sede Medellin for inspiring me and thought me that engineering is a lifestyle and that to train an engineer is more than repeat information from a book. To my colleagues and friends in Medellin: Eng. John

Suarez and Monica Builes who highly contributed to sculpt my professional profile.

I also have to thank to my friends and coworkers at the nanomaterials processing lab: Boris Renteria, M.Sc., Andres Velasco, M.Sc., Lic. Yarilyn Cedeño, Cristina Rodriguez, Celia Osorio, M.Sc., Eric Calderon, M.Sc., Liliana Rizo, M.Sc. and Sandra Pedraza, M.Sc; for their support and kindly comments and cooperation in my research.

Finally I thank to HD Microsystems, Kenrich Petrochemicals and Mettler Toledo for the support given to my research project.

## TABLE OF CONTENTS

<b>SYNTHESIS AND CHARACTERIZATION OF POLYIMIDE COBALT FERRITE NANOCOMPOSITES FOR POTENTIAL APPLICATIONS IN MEMS</b>	<b>I</b>
<b>ABSTRACT</b>	<b>II</b>
<b>RESUMEN</b>	<b>III</b>
<b>ACKNOWLEDGEMENTS</b>	<b>VI</b>
<b>TABLE OF CONTENTS</b>	<b>VIII</b>
<b>LIST OF TABLES</b>	<b>XII</b>
<b>LIST OF FIGURES</b>	<b>XIII</b>
<b><u>1. INTRODUCTION</u></b>	<b>1</b>
1.1 JUSTIFICATION OF THIS RESEARCH	2
1.2 OBJECTIVES	3
1.2.1 Main Objective.....	3
1.2.2 Specific Objectives.....	4
1.3 MAGNETIC COMPOSITES AND MAGNETIC MATERIALS FOR MEMS: LITERATURE REVIEW	4
1.3.1 Magnetic Composites .....	4
1.3.1.1 Polymer Matrices	5
1.3.1.2 Magnetic Phases	6
1.3.1.3 Fabrication and Processing	7
1.3.1.4 Characterization of Magnetic Composites	8
1.3.2 Magnetic Materials for MEMS .....	10

1.3.2.1	Candidate Materials	10
1.3.2.2	Materials Selection	11
<b>2.</b>	<b>THEORETICAL BACKGROUND</b>	<b>13</b>
<hr/>		
2.1	POLYIMIDES	13
2.1.1	Synthesis and Processing of Polyimides .....	14
2.1.2	Structural Features of Polyimides .....	17
2.1.3	Thermomechanical Properties of Polyimides .....	19
2.2	THE MAGNETIC DISPERSE PHASE: COBALT FERRITE	20
2.2.1	Introduction to Magnetism.....	20
2.2.1.1	Diamagnetism	20
2.2.1.2	Paramagnetism	21
2.2.1.3	Ferromagnetism	21
2.2.1.4	Antiferromagnetism	21
2.2.1.5	Ferrimagnetism	22
2.2.1.6	Superparamagnetism	22
2.2.2	Magnetic Hysteresis.....	23
2.2.2.1	Magnetic parameters	25
2.2.3	Permanent Magnets.....	26
2.2.4	Ferrites: Structural and Functional properties .....	26
2.2.5	The Cobalt Ferrite Dispersoids .....	27
2.3	POLYMER BASED NANOCOMPOSITES	28
2.4	INTRODUCTION TO THERMAL ANALYSIS	30
2.4.1	Thermogravimetry (TG).....	31
2.4.2	Dynamic Mechanical Analysis.....	34
2.4.2.1	Principles of the Technique	34
2.4.2.2	Application of DMA to polymers characterization	39
<b>3.</b>	<b>METHODOLOGY</b>	<b>42</b>
<hr/>		

<b>3.1</b>	<b>MATERIAL SELECTION</b>	<b>42</b>
<b>3.1.1</b>	<b>Polymer Matrix: Polyimide (PI).....</b>	<b>42</b>
<b>3.1.2</b>	<b>The Magnetic Disperse Phase: Cobalt Ferrite Nanoparticles .....</b>	<b>42</b>
<b>3.2</b>	<b>MATERIALS SYNTHESSES AND PROCESSING</b>	<b>43</b>
<b>3.2.1</b>	<b>Synthesis of Cobalt Ferrite Nanocrystals .....</b>	<b>43</b>
<b>3.2.2</b>	<b>Synthesis of Polyimide.....</b>	<b>46</b>
<b>3.2.3</b>	<b>Preparation of Polyimide-CoFe<sub>2</sub>O<sub>4</sub> Nanocomposites .....</b>	<b>47</b>
<b>3.2.3.1</b>	Composite Preparation by High Energy Dispersion	49
<b>3.2.3.2</b>	Composite preparation by Low Energy Dispersion	53
<b>3.2.4</b>	<b>Pure Polyimide and Composite Films Processing .....</b>	<b>53</b>
<b>3.3</b>	<b>MATERIALS CHARACTERIZATION</b>	<b>55</b>
<b>3.3.1</b>	<b>X-Ray Diffraction (XRD).....</b>	<b>55</b>
<b>3.3.2</b>	<b>Fourier Transform Infrared Spectroscopy (FT-IR).....</b>	<b>58</b>
<b>3.3.3</b>	<b>The Vibrating Sample Magnetometer (VSM).....</b>	<b>59</b>
<b>3.4</b>	<b>THERMAL ANALYSIS</b>	<b>61</b>
<b>3.4.1</b>	<b>Thermogravimety (TG).....</b>	<b>61</b>
<b>3.4.2</b>	<b>Dynamic Mechanical Analysis (DMA) .....</b>	<b>63</b>
<b>4.</b>	<b>RESULTS AND DISCUSSION</b>	<b>64</b>
<hr/>		
<b>4.1</b>	<b>STRUCTURAL ANALYSIS</b>	<b>64</b>
<b>4.1.1</b>	<b>FTIR Analyses .....</b>	<b>64</b>
<b>4.1.2</b>	<b>XRD Analyses .....</b>	<b>66</b>
<b>4.2</b>	<b>DISPERSION ASSESSMENT</b>	<b>69</b>
<b>4.3</b>	<b>MAGNETIC CHARACTERIZATION</b>	<b>70</b>
<b>4.4</b>	<b>THERMAL ANALYSES</b>	<b>78</b>
<b>4.4.1</b>	<b>Thermal Degradation Tests .....</b>	<b>79</b>
<b>4.4.2</b>	<b>Thermal Stability .....</b>	<b>84</b>
<b>4.4.3</b>	<b>Dynamical Mechanical Analysis.....</b>	<b>88</b>
<b>5.</b>	<b>CONCLUDING REMARKS</b>	<b>96</b>
<hr/>		



## LIST OF TABLES

Table 1.	Materials for permanent magnet films [5].....	11
Table 2.	Typical magnetic properties of rare earth alloys and ceramic ferrites [7] .....	11
Table 3.	FTIR absorption bands for imides and related compounds [21] .....	17
Table 4.	Typical values for selected properties of polyimides .....	19
Table 5.	Common thermal analysis techniques [24] .....	31
Table 6.	Specification for PI2555 (as supplied by DuPont Company).....	47
Table 7.	Typical properties of KR-TTS (supplied by Kenrich Petrochemicals) .....	50
Table 8.	Theoretical and experimental values of saturation magnetization for films produced at different volume fractions. Low-energy ball mill was used as a dispersing tool. ....	77
Table 9.	Theoretical and experimental values of saturation magnetization for films produced at different volume fractions. High-energy homogenizer was used as a dispersing tool. ....	77
Table 10.	Summary of Thermal Degradation Results .....	82
Table 11.	Weight loss rates for composite films produced at different volume fractions .....	87
Table 12.	Glass transition temperature determined from $M^2$ -T plots for composite films produced at different ferrite volume fractions .....	91
Table 13.	Glass transition temperature determined from $\text{Tan}\delta$ -T plots for composite films produced at different ferrite volume fractions .....	93

## LIST OF FIGURES

Figure 1.	Imide group .....	13
Figure 2.	Typical aromatic polyimide repeat group.....	14
Figure 3.	Classical polyimide two steps synthesis.....	16
Figure 4.	Typical polyimide FTIR spectra [21] .....	18
Figure 5.	WAXD transmission (T) and reflection (R) for a PMDA/ODA polyimide [21] .....	18
Figure 6.	Schematic of magnetic behavior in materials.....	24
Figure 7.	Typical hysteresis loop for ferro- ferri-magnetic materials [25] .....	25
Figure 8.	The spinel structure [26].....	27
Figure 9.	Variation of surface area per unit volume vs. particle size for various volumetric loads of homogeneously distributed dispersoids within a polymeric matrix[22].....	29
Figure 10.	Schematic view of a thermobalance.....	32
Figure 11.	Typical TG curves .....	33
Figure 12.	Variation of stress-strain curves with temperature [24] .....	35
Figure 13.	Schematic view of a DMA unit [32] .....	36
Figure 14.	Response of materials for oscillatory loading [32].....	37
Figure 15.	Typical output profiles from a DMA-temperature scan [32] .....	39
Figure 16.	Crankshaft model of a polymer molecule [32] .....	40
Figure 17.	Idealized DMA curve for a thermoplastic polymer [32] .....	40
Figure 18.	Actual DMA curve showing structural transitions in polymers [32] .....	41
Figure 19.	Chemical reactions involved with the formation of cobalt ferrite.....	43
Figure 20.	Experimental setup used to synthesize cobalt ferrite.....	44
Figure 21.	HRTEM micrograph of cobalt ferrite nanocrystals used in this thesis.....	44
Figure 22.	Experimental procedure for cobalt ferrite synthesis.....	45
Figure 23.	PI2555 polyimide repeat unit .....	47

Figure 24. IKA T-8 basic homogenizer (right) and the corresponding dispersing accessory (left). .....	48
Figure 25. Cole Parmer labmill 8000 one-tier mill.....	49
Figure 26. Chemical structure of KR-TTS .....	50
Figure 27. Burundum grinding media used in the present research.....	51
Figure 28. Experimental procedure for nanocomposite film synthesis and processing .....	52
Figure 29. Stereo images of produced films and scheme of the used molds.....	54
Figure 30. Details of the curing cycle used to produce pure PI and PI-based nanocomposite films.....	55
Figure 31. Siemens D500 XRD – Engineering Science and Materials Department at UPRM.....	57
Figure 32. Basic features of the Siemens D500 powder diffractometer .....	57
Figure 33. Schematic of the diffraction phenomenon.....	58
Figure 34. Scimitar FTS 2000 Digilab Spectrometer – Physics Department UPRM.....	59
Figure 35. Lake Shore 7400 Series VSM – Engineering Science and Materials Department UPRM.....	60
Figure 36. Schematic of a Vibrating Sample Magnetometer [26] .....	61
Figure 37. Mettler Toledo Thermogravimetric Analyzer – Engineering Science and Materials Department UPRM.....	62
Figure 38. Mettler Toledo Dynamic Mechanical Analyzer – Engineering Science and Materials Department UPRM.....	63
Figure 39. FTIR Spectra for the polyamic precursor .....	65
Figure 40. FTIR Spectra of bare polyimide and different volume fraction composite films produced after curing the dispersion treated by the IKA T-8 high-energy homogenizer .....	65
Figure 41. FTIR Spectra of bare polyimide and different volume fraction composite films produced after curing the dispersion treated by the Labmill 8000 ball mill.....	66

Figure 42. XRD patterns for cobalt ferrite powder, bare polyimide and different volume fraction composite films produced after dispersing the ferrite nanoparticles in PI precursor using the IKA T-8 homogenizer.....	68
Figure 43. XRD for cobalt ferrite powders, bare polyimide and different volume fraction composite films produced after dispersing the ferrite nanoparticles in PI precursor using the Labmill 8000 ball mill.....	68
Figure 44. 100X Stereographs of composites produced after curing the ferrite-precursor solution using the IKA T-18 high energy homogenizer.....	69
Figure 45. 100X Stereographs Stereographs of composites produced after curing the ferrite-precursor solution using the Labmill 800 ball mill.....	70
Figure 46. Room temperature M-H loops for cobalt ferrite powders and composite films produced at different volume fractions. High-energy homogenizer was used as a dispersing tool. The external field was applied along the parallel direction.....	71
Figure 47. Room temperature M-H loops for cobalt ferrite powders and composite films produced at different volume fractions. High-energy homogenizer was used as a dispersing tool. The external field was applied along the transverse direction.....	72
Figure 48. Room temperature M-H loop for composite film containing 0.1% v/v cobalt ferrite. High-energy homogenizer was used as a dispersing tool. The external field was applied along the parallel direction.....	72
Figure 49. Room temperature M-H loop for composite film containing 0.1% v/v cobalt ferrite. High-energy homogenizer was used as a dispersing tool. The external field was applied along the transverse direction.....	73
Figure 50. Room temperature M-H loops for cobalt ferrite powders and	

	composite films produced at different volume fractions. Low-energy ball mill was used as a dispersing tool. The external field was applied along the parallel direction .....	74
Figure 51.	Room temperature M-H loops for cobalt ferrite powders and composite films produced at different volume fractions. Low-energy ball mill was used as a dispersing tool. The external field was applied along the transverse direction .....	75
Figure 52.	Room temperature M-H loop for composite film containing 0.1% v/v cobalt ferrite. Low-energy ball mill was used as a dispersing tool. The external field was applied along the parallel direction.....	75
Figure 53.	Room temperature M-H loop for composite film containing 0.1% v/v cobalt ferrite. Low-energy ball mill was used as a dispersing tool. The external field was applied along the transverse direction .....	76
Figure 54.	Theoretical and experimental values of saturation magnetization for films produced at different volume fractions. Low-energy ball mill was used as a dispersing tool.. The dotted lines are presented as eye guides only.....	77
Figure 55.	Theoretical and experimental values of saturation magnetization for films produced at different volume fractions. High-energy homogenizer was used as a dispersing tool. The dotted lines are presented as eye guides only. ....	78
Figure 56.	Thermal degradation curve for bare PI produced without using the high-energy homogenizer.....	80
Figure 57.	Thermal degradation curve for PI synthesized after using high-energy IKA T-18 homogenizer.....	80
Figure 58.	Thermal degradation curves for composites containing 0.1% and 1% ferrite volume fractions .....	81
Figure 59.	Thermal degradation curves for composites containing 10% and 20% ferrite volume fractions.....	83
Figure 60.	Schematic interpretation of the ferrite particles-polymeric matrix	

interaction.....	84
Figure 61. Thermal stability curve for bare PI.....	86
Figure 62. Thermal stability curve for bare PI pre-treated with the high-energy IKA T-8 homogenizer.....	86
Figure 63. Thermal stability curves for composites containing 0.1% and 1% ferrite volume fractions .....	87
Figure 64. Thermal stability curves for composites containing 10% and 20% ferrite volume fractions .....	88
Figure 65. Storage Modulus ( $M'$ ) against Temperature for bare PI and different volume fraction films previously dispersed by using the high-energy IKA T-8 homogenizer .....	91
Figure 66. Variation of $\tan \delta$ with temperature for bare PI and different volume fraction films previously dispersed by using the high-energy IKA T-8 homogenizer.....	92
Figure 67. Storage Modulus ( $M'$ ) against Temperature for bare PI and different volume fraction films previously dispersed by using ball milling.....	92
Figure 68. Variation of $\tan \delta$ with temperature for bare PI and different volume fraction films previously dispersed by using ball milling .....	93
Figure 69. Inflated composite film. 20% ferrite volume fraction film produced using the Labmill 800 ball mill. DMA tested from room temperature to 400°C.....	94
Figure 70. Fibrous-like microstructure of inflated film. 20% ferrite volume fraction film produced using the Labmill 800 ball mill. DMA tested from room temperature to 400°C.....	95

## 1. INTRODUCTION

Since 1959 human being began to think about the potential of fabricating very small machines; it wasn't until the 70's when such devices became designed and only during the 90's that were commercialized as the so-called Micro Electromechanic systems (MEMS) in the USA, microsystem technology (MST) in Europe and micromachines in Japan [1]. Those devices combine mechanical and electrical components in a single package to create small scale sensors, actuators, power generators, pumps, chemical reactors and biomedical devices [2]. Micro actuators, micro motors and micro pumps usually are driven by electrostatic or electromagnetic forces which are scale depending and therefore become a constraint within the design and materials selection processes [1-3]. These devices have feature lengths ranging between 1mm and  $1\mu\text{m}$  [1, 2, 4].

Regarding to actual or potential materials for MEMS devices driven by electromagnetic forces, a variety of composite magnetic materials had been suggested as suitable candidates. A particular type of composite is the one consisting of polymeric matrices hosting ceramic ferrimagnetic particles, ferrite, as dispersed phase [6-8]. Although suggested systems recommend the use of a high-coercivity magnetic phase to be dispersed in a flexible and mechanically resistant matrix, the technical literature disregard the use of such ceramic ferrites (e. g. cobalt ferrite,  $\text{CoFe}_2\text{O}_4$ ) because of the limited availability of extremely fine (nanosize) crystals with high enough magnetic properties (coercivity and magnetization of saturation). Ferrite particles that have been evaluated for such a purpose were micrometric in size. The magnetic properties of those ferrites became very poor at smaller size [6, 7, 9]. A ferrite material which combines the availability of nanosize

crystals, i.e. far below 100nm, and outstanding coercivity at room-temperature conditions will become the optimum magnetic material to manufacture the magnetic nanocomposite for MEMS applications. This problem has been solved by Y. Cedeño *et al* [9] who have developed a novel method to produce 20nm cobalt ferrite nanocrystals with room temperature coercivity above 5 kOe.

## 1.1 JUSTIFICATION OF THIS RESEARCH

The combination of magnetic properties and size control at the nanoscale, enables cobalt ferrite to be considered as component (dispersoids) for polymer-based magnetic nanocomposite with potential application in the fabrication of MEMS requiring permanent magnets (e. g. microactuators).

Polyimide-based composites have been considered promising materials mainly because of the low price of polymer precursor (polyamic acid), its wide use (and therefore, current availability) in microelectronics processing, as well as the simplicity of polyimide processing and curing [7, 10-12]. In addition, as discussed more detailed in further sections, among reviewed works regarding magnetic composites and nanocomposites there was not found a systematic study in which structural, functional and thermomechanical properties of produced materials were evaluated neither for the selected system (polyimide and cobalt ferrite) nor for other polymer/magnetic phase combinations. Some works only centered the attention on functional and structural analyses, some others based the discussion on the processing/fabrication techniques and few of them make discussion about the thermal and/or mechanical behavior of materials they were dealing with. The present work intends to get a wider view in which functional, structural and thermomechanical properties of

produced nanocomposites will be evaluated not only for different ferrite volume fractions but for two dispersion (or fabrication) techniques to assess its influence on the composite properties. This type of approach is essential to determine the applicability ranges of produced materials towards an adequate performance.

Based on above criteria, the present research addresses the fabrication of polyimide-cobalt ferrite nanocomposites for potential application in MEMS. High-coercivity cobalt ferrite nanocrystals will be synthesized and dispersed in polyamide precursor under suitable mixing conditions (homogenizing or ball milling). The ferrite-polymer precursor mixture will be deposited on a substrate and cured to develop the polyimide structure. Produced films will be characterized on a structural (using X-ray diffraction and Fourier transform infrared spectroscopy) and functional (magnetization and coercivity measured in a vibrating sample magnetometer) basis.

Thermogravimetric analysis (TGA) will be used to conduct measurements of degradation temperature and thermal stability. Dynamical mechanical analysis (DMA) measurements of  $\tan \delta$  and storage modulus ( $E'$ ) as a function of temperature will be used to determine the viscoelastic behavior. TGA and DMA tests will be used to assess the viability of nanocomposites fabrication process.

## **1.2 OBJECTIVES**

### **1.2.1 Main Objective**

The main goal of the present research is to prepare and characterize a magnetic nanocomposite consisting of polyimide as matrix and cobalt ferrite powders as disperse phase for potential application in MEMS.

### 1.2.2 Specific Objectives

To achieve the main objective it was necessary to prepare composites with different amounts (loading) of magnetic powder in order to determine the following: (i) The most suitable conditions to achieve a homogeneous dispersion of cobalt ferrite nanoparticles in the polymeric matrix; (ii) the relationship between magnetic response (magnetization, coercivity) and ferrite/polymer volumetric or weight ratio; (iii) the effect of ferrite loading on the viscoelastic properties of the resulting composite. All those measurements must be conducted for a range of temperature and characteristic lengths corresponding with the same parameters of the intended application.

Magnetic characterization and thermal analysis of the magnetic nanocomposite are fundamental to assess the applicability of such a composite for MEMS fabrication.

## 1.3 MAGNETIC COMPOSITES AND MAGNETIC MATERIALS FOR MEMS: LITERATURE REVIEW

### 1.3.1 Magnetic Composites

Among the recently developed materials there is one type commonly called *magnetic polymers*, which consist of polymeric matrices hosting dispersed magnetic particles. This kind of polymers has been widely studied; Yañez-Flores and coworkers [13] prepared and characterized a PVC-Magnetite composite in an attempt to probe a new method which increases magnetite dispersion. Also using a PVC matrix Slama and coworkers [14] prepared a composite with Lithium ferrite for application in electromagnetic shielding in the X-Band frequency range. Polyimide- $\gamma\text{Fe}_2\text{O}_3$  composites for possible application in high

density storage media where prepared by Lim and coworkers [10] and Zhan and coworkers [12] using different preparation techniques. Other application of magnetic polymers is in devices known as *piezomagnetic sensors*. In this regard Sasso and coworkers [15, 16] prepared composites for the latter application using polymer bonded cobalt ferrite particles. The following sections summarize commonly used polymeric matrices and magnetic dispersed materials, characterization techniques used for magnetic composites, and finally some approaches for its processing and fabrication.

#### **1.3.1.1** *Polymer Matrices*

Polymer matrices for these magnetic composites may be very varied depending basically on the requirements of each application. In the case of MEMS, SU-8 epoxy resin [17] and polyimide [7] have been reported as suitable candidates for MEMS since they are compatible with MEMS fabrication techniques such as LIGA (Lithography + galvanofarming). However processing methods for those polymers are quite different and therefore depending on the characteristic length selected for a particular application they could require prolonged time and additional processing steps (which will be discussed later) to complete the fabrication of a device.

For application oriented toward magneto optical devices poly methylmethacrylate (PMMA) or poly carbonate (PC) are the common choices due to their transparency; however, other trademarked polymers (i. e. CYTOP) are used for specialized applications such as optical communications [18].

When a polymer bonded magnet is the objective epoxy resins, phenolic resins, poly vinyl alcohol (PVA) and natural rubber have been used and reported [6, 15, 16, 19]. Finally, it must be pointed out that polymer matrices mentioned for the former two applications can

also be used in the case of the latter application. However some of those polymers, as can be seen in further sections, require particular processing conditions that become a drawback that turns into an additional and useless spent of money.

### **1.3.1.2**     *Magnetic Phases*

Magnetic dispersoids to be used in the fabrication of magnetic polymers are materials exhibiting ferromagnetic or ferrimagnetic behavior. Materials meeting the latter criteria can be divided in two groups according to their magnetic properties: magnetically hard and magnetic soft materials [8].

Magnetically hard materials could be rare earth alloys (samarium-cobalt, neodymium-iron-boron) or ceramic ferrites (barium ferrite, strontium ferrite, cobalt ferrite) which could be good candidates for applications such as MEMS and data storage; however, as mentioned before, possible difficulties with the former due to lack of availability in fine particle size and trend to oxidation and corrosion (especially in fine-powder form) must be taken into account and therefore, although ceramic ferrites may exhibit comparatively lower values for certain magnetic properties, they are recently being preferred since they overcome the drawbacks related to rare earth alloys and have a lower price [5, 7].

Magnetically soft materials include iron, nickel and some ceramic ferrites (nikel ferrite, manganese zinc ferrite, etc) and are typically thought as candidates for applications such as magneto optic devices and electromagnetic shielding [10, 13, 14, 18].

In addition the development of nanotechnology has allowed the possibility of tuning magnetic properties of a material and thus the same material could exhibit magnetically soft, magnetically hard and even super paramagnetic behavior when particle size is controlled thus materials as cobalt ferrite could become a versatile option for magnetic

dispersoids since it can be used in polymer magnet for very different applications which include even sensing [4-6, 12].

### **1.3.1.3**     *Fabrication and Processing*

Aside of materials selection the main concern in producing magnetic polymers is to achieve a good dispersion of the magnetic phase in the polymer matrix, especially when magnetically hard powders are used as dispersoids since grains are essentially little magnets stick to each other forming an aggregated.

To avoid agglomeration of magnetic particles one attempt is in situ formation of the magnetic phase as presented by Garcia-Cerda and coworkers [6] to produce cobalt-ferrite PVA nanocomposite in which cobalt ferrite were synthesized in an aqueous solution of PVA. The results presented in such study didn't report the particle size of ferrite however it could be estimated using the results of magnetic measurements which showed a sample exhibiting super paramagnetic behavior and another one responding as a combination of ferrimagnetic and super paramagnetic phases. The latter approach didn't show evidence such a TEM micrograph that allow the assessment of particle dispersion inside the matrix and also didn't say anything about the volume fraction achieved. Therefore the latter work is a start point for other works tending to combine this technique with other processes reported to produce cobalt ferrite in aqueous media obtaining controlled crystal sizes [9]. The drawback of this technique clearly arises when a polymer matrix insoluble in aqueous media is desired to be used with a magnetic phase that is chemically synthesized from aqueous solutions.

To overcome the latter problem is necessary to obtain the particles separately and then try to disperse them into the matrix. In this regard Lagorce and coworkers [7] used isopropyl

trisostearyl titanate (KR-TTS), a commercial additive used to disperse inorganic material in polymeric matrices such as pigments in paints, to treat polyimide which was further mixed with strontium ferrite micron sized particles inside a ball milling. However the roll of that dispersing aid was not discussed in their work neither the dispersion is confirmed by photomicrographs and taking into account the high volume fractions (55%, 65%, 80%) used in that work dispersion definitely must be assessed.

Another attempt is to functionalize the particles with a chemical agent, generally a polymer, which attaches to its surface and thus putting a physical obstacle between the particles that avoid the aggregation [12, 13]. This techniques allows to obtain a better matrix-dispersoid interaction when the reagent selected to functionalize the particles has functional groups that are also present in the molecular structure of the polymer matrix as presented by Zhan and coworkers [12] who try to disperse  $\gamma\text{-Fe}_2\text{O}_3$  nanoparticles in a polyimide matrix obtaining a result that could be satisfactory depending on the application since TEM micrographs showed nanoparticles forming clouds that are uniformly dispersed and within the nanoparticles are physically separated.

Finally, Kim and coworkers [12] as well as Lim and coworkers [10] presented another technique to disperse magnetic phases in polymeric matrices. In their method a thin layer of polymer is deposited onto a substrate, then magnetic material is sputtered over the film and finally another polymer film is deposited onto the magnetic layer, repeating this sequence until the desired thickness is achieved. Based on the TEM this method gives the better dispersion results among the reviewed works; however the use of sputtering constraints the magnetic phases that can be used in the composites as well as the particles size and shape.

#### **1.3.1.4**     *Characterization of Magnetic Composites*

The characterization stage in most of the reviewed papers is focused on the functional property of the composite which is for this case related with magnetic behavior. In this regard vibrating sample magnetometer (VSM) [6, 13, 20] and SQUID magnetometer [10, 11, 19] were used to pick the magnetic response up. Mossbauer spectroscopy was also used in other works [14]. It would be also recommended to conduct magnetic measurements of the bare magnetic phase to be compared with those conducted for the composite to verify that magnetic behavior remain unchanged specially for those polymer matrices requiring curing inside an oven. However this kind of analysis was rarely carried out in the reviewed papers.

With regard to the crystalline structure (for magnetic phase) and molecular structure (for polymer matrices) X-ray diffraction (XRD) and Fourier transform infrared spectroscopy (FTIR) respectively are the techniques to be used. However, paper by Lagorce and coworkers [7] didn't present such spectra and thus is not possible to determine if polyimide structure is effectively formed in the composite neither is possible to verify that crystalline structure didn't undergo changes after curing process.

As mentioned before, most papers focused on magnetic properties but little attention is paid to mechanical behavior and how is affected by the particle content. This kind of analysis was conducted in the work by Zhan and coworkers [12] and by Lagorce and coworkers [7]. The better choice to evaluate mechanical behavior is using dynamical mechanical analysis (DMA) as presented in the work by Makled and coworkers [19]. With this analysis is possible to know changes in the molecular structure of the polymer matrices as well as defects that can arise in the composite fabrication. Information obtained by DMA could also be complemented using thermo gravimetric analysis (TGA) for degradation temperature as presented by Sindhu and coworkers [20].

### 1.3.2 Magnetic Materials for MEMS

When dealing with magnetic materials for MEMS two main factors have to be considered. One of them deals with the development of criteria for materials selection and, after identifying suitable candidates, to optimize their syntheses conditions. In the following section the state of the art for both factors is summarized.

#### 1.3.2.1 Candidate Materials

Chin *et al.* [5] made a review of promising permanent magnets (PM) as possible candidates for applications in MEMS reported in available literature. They are summarized in *Table 1* with some relevant properties.

In table 1, the expression ‘Hi-T anneal’ involves the need of high annealing temperature (>450°C) or when the material is deposited at a substrate temperature higher than 450°C.

Magnetic polymers for MEMS have been studied by various groups [6-7]. According to Lagorce and Allen [7], the dispersed phase could be rare-earth alloys (samarium-cobalt, neodymium-iron-boron) or ceramic ferrites (barium ferrite, strontium ferrite) remarking possible difficulties with the former due to lack of availability in fine particle size and trend to oxidation and corrosion (especially in fine-powder form). Therefore, although ceramic ferrites may exhibit comparatively lower of magnetic properties, they could be preferred since they overcome the drawbacks related to rare earth alloys and have a lower price. Typical magnetic properties of both types of ferrites are listed in *Table 2*.

MATERIAL	Br[kG]	Hc[kOe]	CORROSION RESISTANCE	HI-T ANNEAL REQUIRED
----------	--------	---------	-------------------------	-------------------------

SmCo <sub>5</sub>	8	23	POOR	NO
Sm <sub>2</sub> (Co,Fe,Zr) <sub>17</sub>	9-11	7	POOR	YES
Nd <sub>2</sub> Fe <sub>14</sub> B	7-12	8-15	POOR	YES
Nd(Fe,Ti) <sub>12</sub> N <sub>8</sub>	12-15	8.7	FAIR	YES
PtCo/Ag	---	1-17	EXCELLENT	YES
Pt/Fe	10	10	GOOD	YES
CoNiMnP	2-3	0.8-1.3	GOOD	NO
CoCrTaX	7-9	2-4	GOOD	NO
FeCrCo	8-12	0.7	EXCELLENT	YES
MnAl	4-5	3	GOOD	NO
RESIN + RPM	8-10	8.5	FAIR	NO
RESIN + FERRITE	3	4	EXCELLENT	NO
Ba/Sr-Ferrite	2-3	3-4	EXCELLENT	YES
$\gamma$ -Fe <sub>2</sub> O <sub>3</sub>	3	2-4	EXCELLENT	NO

**Table 1. Materials for permanent magnet films [5]**

MATERIAL CLASS	RARE EARTH ALLOYS	CERAMIC FERRITES
RESIDUAL INDUCTION	~9kG	~3.6kG
INTRINSIC COERCIVITY	~15kOe	>4kOe
MAX ENERGY PRODUCT	~19MOe	~3MOe

**Table 2. Typical magnetic properties of rare earth alloys and ceramic ferrites [7]**

### 1.3.2.2 Materials Selection

Some criteria and recommendations for MEMS-materials selection have been elaborated by various authors [1-3, 5], each of them focusing on different issues that might be taken into account regardless of the intended application. According to Spearing [2], special attention must be paid to the characteristic length of the application because material's properties are scale dependent but do not vary in the same way and thus a material that has certain desired behavior at some scale could rapidly lose that properties because of the scale effect. For the particular case of transducers that intend to convert an electrical input into a mechanical

output it is possible to use electrostatic or electromagnetic principles to operate the device; however, the force generated using the electrostatic principle varies with the square of the characteristic length while in the case of electromagnetic forces they vary with the fourth power of characteristic length. The latter principles could be useful to solve tribological issues commonly encountered in MEMS [1].

## 2. THEORETICAL BACKGROUND

### 2.1 POLYIMIDES

Imides is the name given to any organic substance in which a nitrogen atom is single bonded with two carbonyl groups (figure 1), therefore any polymer consisting of such molecules as repeating unit would be called polyimide. However the name polyimide often is associated with a particular polyimide class: aromatic polyimides (figure 2) which have been classified as “high performance polymers” due to their exceptional thermo-oxidative stability [21]. In addition, the morphology of long linear ordered chains conducts to aromatic polyimides to be insoluble/intractable [21] and to show high glass transition temperatures ( $T_g$ ) which makes that fully cured polyimides cannot be processed without thermal degradation; thus polyimide are commonly treated as thermosetting polymers.

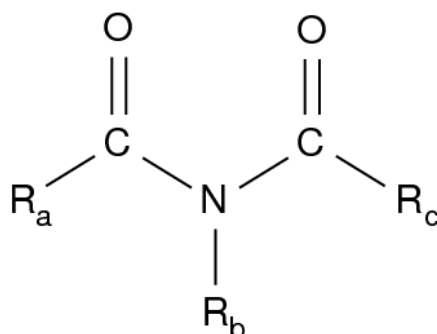


Figure 1. Imide group

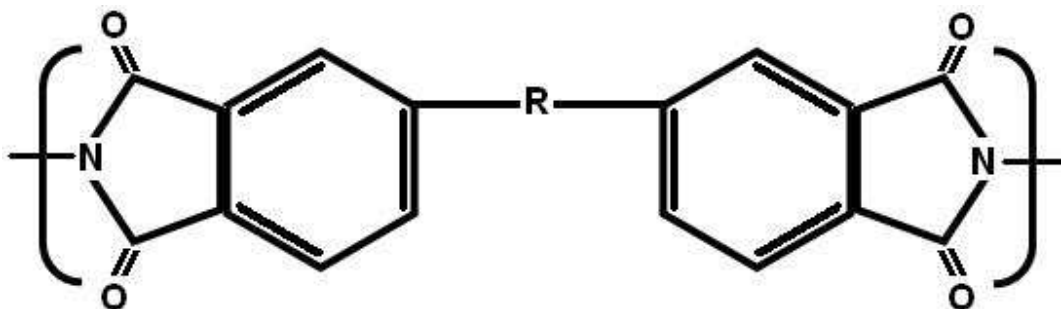


Figure 2. Typical aromatic polyimide repeat group

Another features of aromatic polyimides include low dielectric constant, high glass transition temperature, selective permeability to gases, film toughness under rigorous conditions of air aging, and retention of high mechanical strength over a wide temperature range [21]; which led to its wide current use in microelectronics industry (dielectric in electronic packaging, birefringent compensator for LCD displays), aerospace (engine components, electrical insulations, bearings) and the increased interest in expanding its application fields (e. g. in polymer matrix nanocomposites) [21, 22].

### 2.1.1 Synthesis and Processing of Polyimides

Classical aromatic polyimide synthesis is a two step reaction developed by DuPont in the 50's decade. This method allows to obtain polyimide through soluble intermediates referred to as poly(amic acid)s which can be further processed into desirable shape to finally obtain polyimide structure. The first step in the reaction to prepare a solution of an aromatic diamine with a solvent such as N-methyl-pyrrolidone (NMP) or dimethylacetamide (DMAC) which is further put in contact with a dianhydride, this reaction is known as polycondensation and produces poly(amic acid) [21, 22]. As mentioned before, the poly(amic acid) solution could be processed into desired shape The second step in the

polyimide synthesis is referred to as cyclodehydration (imidization) of polyamic acid and could be achieved by both thermal or chemical ways, from which the former is the typical used in microelectronics [21]. As an example figure 3 shows a schematically view of the two steps reaction to produce polyimide using 4,4'-diaminodiphenylether and pyrometllic dianhydride dissolved in DMAC.

As mentioned above thermal imidization (also commonly referred to as curing) is the method used in microelectronics as well as in research dealing with polyimide based composites. This process is carried out in two steps: soft-bake and hard-bake; the former has as objective to remove solvent and begin the imidization process while the second attempts to achieve almost complete solvent removal and imidization. Time and temperature for soft bake are selected depending on the thickness of intended shape. Hard-bake parameters depend on the desired microstructure and thickness. Most research work used a hard bake temperature of 300°C [7, 10, 11, 21, 22] while in industrial environments this parameter ranged from 350 to 400°C [21]. It must be taken into account that at 300°C imidization is achieved but if a cross-linked polyimide is desired a minimum temperature of 350°C has to be selected. It is also important to point out that temperature must be gradually increased to hard bake set point in order to reduce defects and allow enough time for solvent removal. It has been reported that full solvent removal is almost unreachable [21].

Other synthesis routes to produce polyimide in one step have been reported [21, 23] but so far have not reached the popularity of classical to step method because some of that works are in a preliminary research stage.

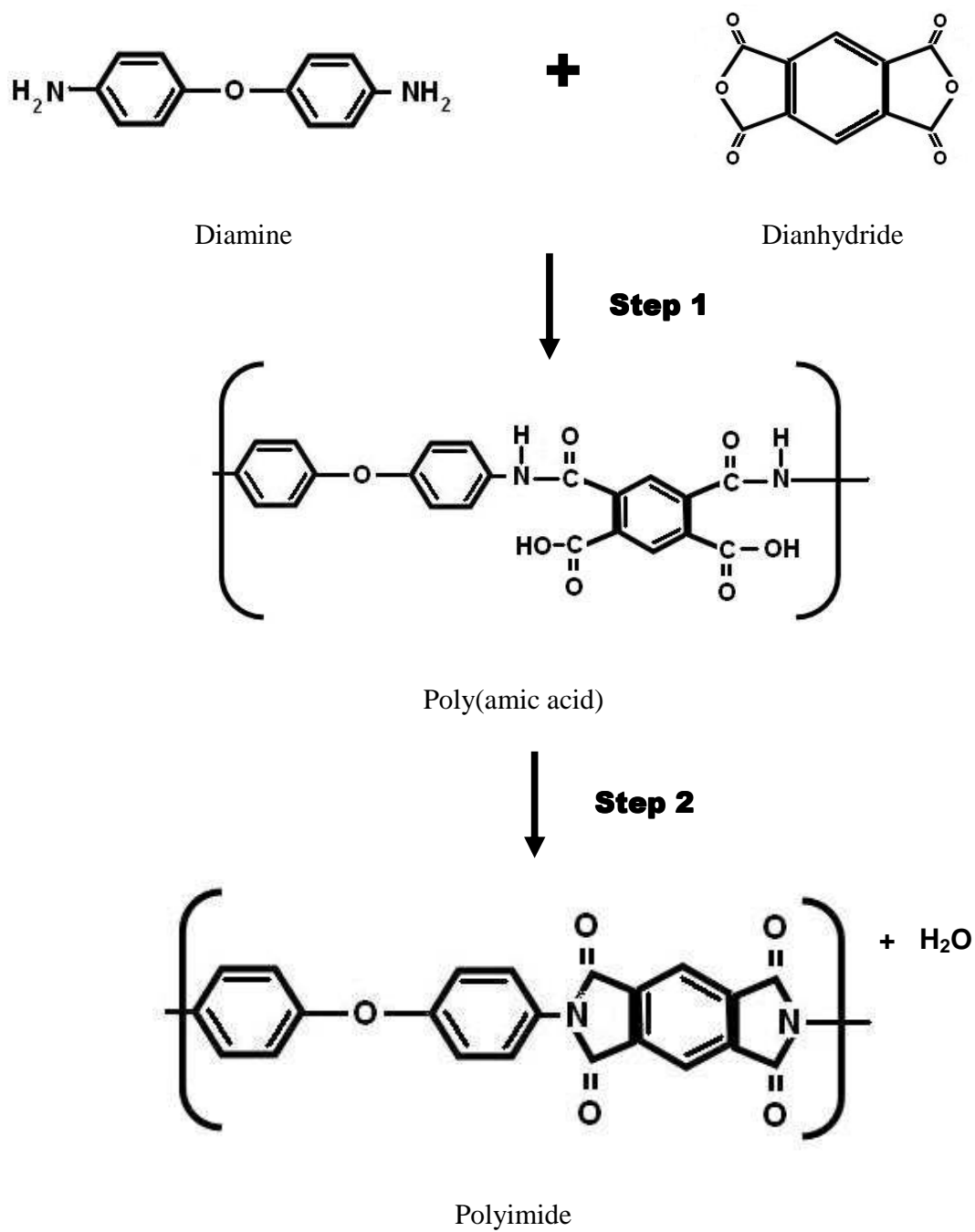


Figure 3. Classical polyimide two steps synthesis

### 2.1.2 Structural Features of Polyimides

Aromatic polyimides consist of heterocyclic imide and aryl groups, which are linked sequentially by simple atoms or groups [21] as can be seen in the typical repeat unit depicted in figure 2. The most used technique to determine the presence of functional groups in both polyimide and poly(amic acid) is Fourier transform infrared spectroscopy (FTIR). Table 3 shows various absorption bands corresponding to functional groups present in polyimides and poly(amic acid)s and a typical polyimide FTIR spectra is depicted on figure 4.

	Absorption band (cm <sup>-1</sup> )	Intensity	Origin
Aromatic Imides	1780	s	C=O Asymmetrical stretch
	1720	vs	C=O Symmetrical stretch
	1380	s	C-N Stretch
	725		C=O Bending
Amic acids	2900-3200	m	COOH and NH <sub>2</sub>
	1710	s	C=O (COOH)
	1660	s	C=O (COOH)
	Amide I		
	1550	m	C-NH
	Amide II		
Anhydres	1820	m	C=O
	1780	s	C=O
	720	s	C=O
Amines	~3200		NH <sub>2</sub> symmetrical structure
	Two bands	w	NH <sub>2</sub> asymmetrical structure

**Table 3. FTIR absorption bands for imides and related compounds [21]**

Wide angle x-ray diffraction (WAXD) has been also used to determine the morphology of polyimide film. It was found that certain polyimides exhibit a short range crystalline structure evidenced by a broad peak in WAXD transmission pattern. This broad peak is centered near  $2\theta$  value of  $18^\circ$ . As an example, figure 5 shows a WAXD pattern corresponding to a polyimide produced from 4,4'-oxydianiline (ODA) and pyromellitic dianhydride [21].

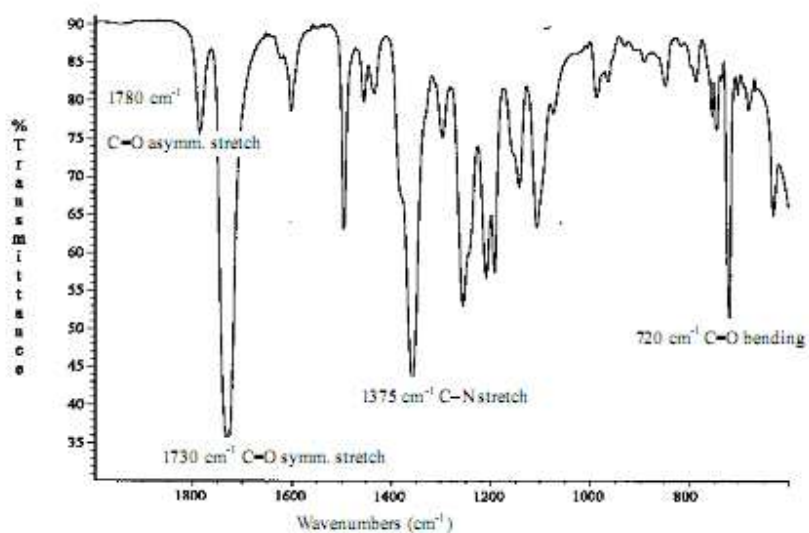


Figure 4. Typical polyimide FTIR spectra [21]

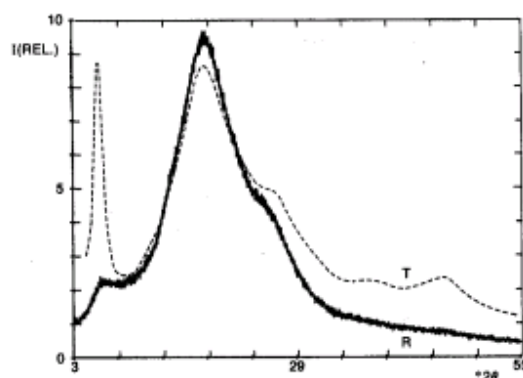


Figure 5. WAXD transmission (T) and reflection (R) for a PMDA/ODA polyimide [21]

### 2.1.3 Thermomechanical Properties of Polyimides

Thermomechanical properties of polyimides are often determined using different thermal analysis techniques such as: thermogravimetric analysis (TGA), dynamical mechanical analysis (DMA), thermomechanical analysis (TMA), thermodilatometry (TD) and differential scanning calorimetry (DSC) [24]; some of these techniques are going to be briefly addressed in a later section. Other conventional techniques are also used to determine properties such as modulus of elasticity.

The more common reported properties for polyimides include glass transition temperature ( $T_g$ ), degradation temperature, coefficient of thermal expansion (CTE or  $\alpha$ ), elastic modulus (E) and tensile strength (UTS). Other properties such as  $\beta$  and  $\gamma$  relaxation temperatures ( $T_\beta$  and  $T_\gamma$  respectively) are less common presented [21]. Typical values for some of these properties as well as the techniques used to determine them are summarized in table 4.

Property	Value	Techniques
Elastic modulus, GPa	3	TMA, DMA, tensile test
Tensile strength, GPa	01-0.2	Tensile test
Degradation temperature	>450°C	TGA
Glass transition temperature	400 °C	TMA, DMA, DSC
Coefficient of thermal expansion, ppm/ °C	20-70	TMA, TD

**Table 4.** Typical values for selected properties of polyimides

## 2.2 THE MAGNETIC DISPERSE PHASE: COBALT FERRITE

### 2.2.1 Introduction to Magnetism

All materials known so far in nature can interact with magnetic fields and exhibit a magnetic response as product of that interaction; therefore materials can be classified according with their magnetic behavior. A very simplified way to explain this interaction relays on classical physical principle: Ampere's law, which states that every electric current produces a magnetic field. With this in mind and taking into account that an electric current is a movement of charge carriers, is easy to visualize that an electron moving in an orbital has a magnetic field (and moment) associated with that movement; moreover, an additional magnetic moment associated with electron spin. This way it could be state that depending on the electronic distribution atoms could have net magnetic moments due to unpaired electron magnetic fields. The way these magnetic moments interact with an external magnetic field determines the magnetic response of a material. The following sections address each type of magnetic behavior of materials. It must be emphasized that a fully comprehension of magnetic behavior of materials involves elements and concepts of quantum mechanics which are out of the scope of this work, the model exposed above is a strong simplification for introduction purpose. Figure 6 shows a schematic representation of each type of magnetic response of a material for an applied field and in the absence of it.

#### 2.2.1.1 *Diamagnetism*

Diamagnetic materials have no unpaired electrons and thus have no net magnetic moments. However when an external magnetic field is applied magnetic dipoles are induced, this dipoles has associated magnetic moments that oppose to the direction of the external

applied field. Materials such as copper, silver, silicon, gold and alumina are diamagnetic at room temperature [8].

#### **2.2.1.2**    *Paramagnetism*

Atoms possessing unpaired electrons exhibit a net magnetic moment associated with electron spin. However, those moments are randomly oriented in such a way that bulk material does not show any magnetic response in absence of an external magnetic field. When a magnetic field is applied dipoles align in the field direction but since those moments do not interact, a very large magnetic field is needed to align all of them. In addition this effect remains only while the field is applied; once the field is removed the dipoles return to their random distribution.

#### **2.2.1.3**    *Ferromagnetism*

Ferromagnetic behavior is attributed to unfilled 3d energy levels of some atoms [8, 25] which cause permanent net magnetic moments that easily line up with an imposed magnetic field due to mutual reinforcement or exchange interaction. This behavior is only observed when materials are arranged in a lattice. Classical theory for this behavior was presented in 1907 by Weiss who explained the phenomena based on the presence of a molecular field inside the ferromagnetic material. However, as mentioned before a more accurate explanation relies on quantum mechanics theories. It is also important to point out that in ferromagnetic materials large magnetization is achieved for small field [8].

#### **2.2.1.4**    *Antiferromagnetism*

This behavior was discovered as a result of Heusler observations in certain ternary

intermetallic compounds containing elements such as manganese which were capable of deriving a magnetic moment from its unfilled 3d level that were expected to behave in a ferromagnetic way but instead no external magnetic response was observed. This dilemma was solved by Néel in 1932 by the introduction of the ferromagnetic state in which magnetic moments produced in neighboring atoms are aligned antiparallel to one another in the presence of an external magnetic field and thus no magnetization in the material as a whole is produced even when the strength of individual moments are very high [8,21]. Néel theory was further confirmed by neutron diffraction technique.

#### **2.2.1.5** *Ferrimagnetism*

Ceramic ionic materials are composed by two or more ions and thus two or more types of magnetic moments corresponding to each kind of atom (ion); when an external magnetic field is applied the moments corresponding to one kind of ion may align in the field direction while the moments of the other kind of ion are aligned in the opposite direction. Since the strength of moment belonging to each ion are different the material as a whole exhibits a net magnetization that as in the case of ferromagnetic materials remains even in when the external field is removed. Ceramic materials exhibiting this type of magnetic behavior are commonly referred to as ferrites.

#### **2.2.1.6** *Superparamagnetism*

Ferromagnetic and ferrimagnetic materials can change its magnetic behavior if are produced in fine powder form in such a way that its grain size reaches certain critical value. When that value is achieved the thermal vibration energy of each particle has a magnitude comparable to the one of magnetic energy and thus even though magnetic moments are

prone to line up in the field direction the thermal vibration causes the magnetic moments to change its direction randomly; therefore there is no a net magnetic response and the material behaves as it is paramagnetic.

### **2.2.2 Magnetic Hysteresis**

Ferromagnetic and ferromagnetic materials exhibit regions inside the material where all magnetic moments are aligned in the same direction, this regions are called magnetic domains and are separated one of each other by a transition region called domain walls inside which the direction of magnetic moments gradually changes to match the direction of the neighboring domain. The presence of these domains leads to a nonlinear magnetization when an external field is applied because domain walls moves in such a way that the domains pointing in a direction close to field direction increases in size at expense of those domains having non favorable directions. This domain structure also causes a net magnetization in the material when the external field is removed since domain walls cannot be brought back to its original position; it is necessary to apply an external field opposite in sign to get the material into a demagnetized state. Figure 7 shows a typical hysteresis loop for ferromagnetic or ferromagnetic materials, the two loops corresponds to the same data; however the solid line represents magnetization ( $M$ ) while the dashed line represents magnetic induction ( $B$ ). If the material is placed in a continually alternating magnetic field, both magnetization and induction will cycle around a loop similar to the one depicted in figure 7 in the counter clock wise direction; the area under that trace will represent the energy absorbed by the material in one cycle of the alternating field.

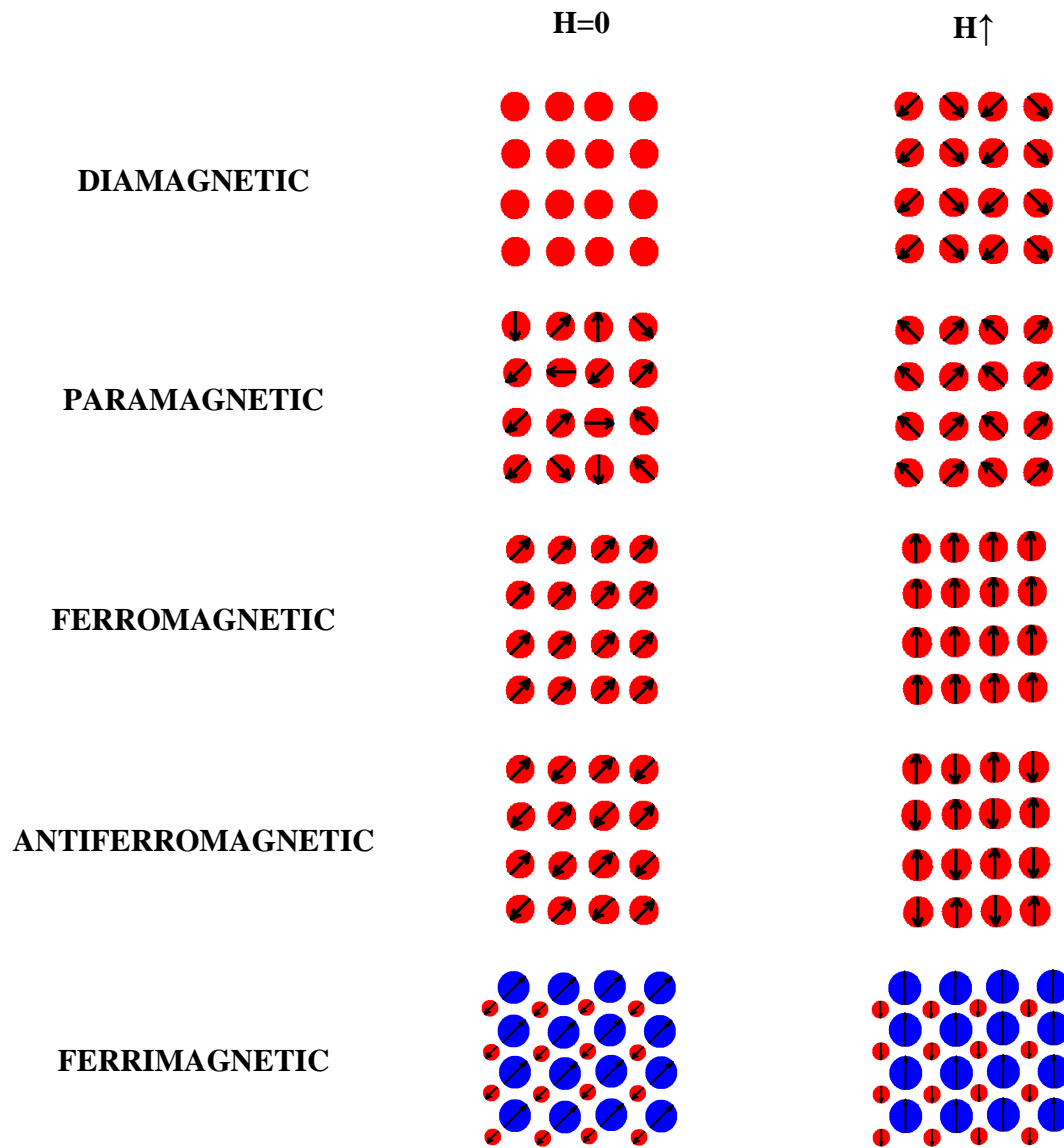


Figure 6. Schematic of magnetic behavior in materials.

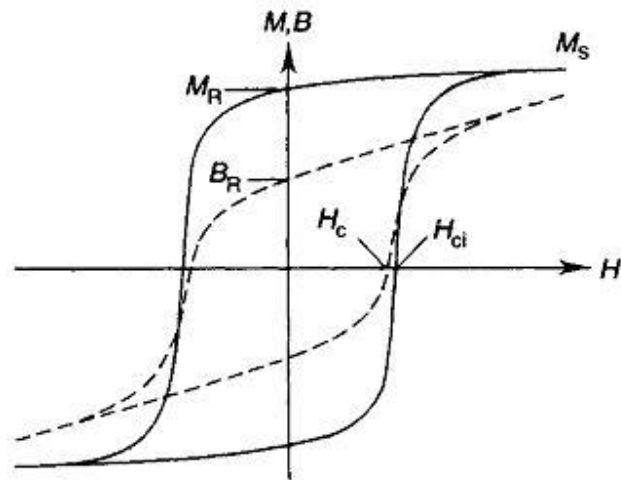


Figure 7. Typical hysteresis loop for ferro-ferri-magnetic materials [25]

### 2.2.2.1 Magnetic parameters

The hysteresis loop is a useful tool to characterize and classify ferromagnetic and ferro-magnetic materials. Various parameters can be picked up from this plot and are used to describe the magnetic behavior of these materials without the need of see the trace. The first parameter is called saturation magnetization and corresponds to the value of magnetization when all domains are oriented along with the applied magnetic field. The residual magnetization, commonly referred to as remanence ( $M_R$ ), corresponds to the value of magnetization exhibited by the material when the external magnetic field is removed. The third parameter known as coercivity ( $H_{ci}$ ) is the value of the magnitude of the reversed magnetic field needed to bring the magnetization to zero. In addition, for permanent magnets is also used the maximum energy product,  $(BH)_{MAX}$ , which refers to the maximum work that can be done by a magnet. Finally it must be noticed that there is no a thing such as saturation induction.

### 2.2.3 Permanent Magnets

As mentioned above if certain magnetic parameters of a ferromagnetic and ferromagnetic material are known then it is possible to determine the magnetic behavior of that material. Based on that information materials can be classified as soft magnetic materials and hard magnetic materials. The latter are also known as permanent magnets and are characterized by: high remanence, high coercivity, large hysteresis loop and high energy product.

### 2.2.4 Ferrites: Structural and Functional properties

Previously was introduced that magnetic behavior of materials relays on its atomic characteristics. Ceramic ferrimagnetic materials commonly referred to as ferrites exhibit magnetic behavior as a consequence of its crystalline structure. These materials have a complex FCC structure known as inverse spinel (figure 8) which can be thought as pile up of close packed oxygen planes and can be represented by the formula  $MFe_2O_4$ , where M represents any metallic ion or ions (ferrites containing more than one ion are known as mixed ferrites). One common material of this class is magnetite,  $Fe_3O_4$ , which possesses two types of iron ions: divalent iron  $Fe^{+2}$  and trivalent iron  $Fe^{+3}$  in a proportion 1:2, therefore its formula can be re written as  $FeO \cdot Fe_2O_3$ . In inverse spinel structures divalent ions are located in octahedral sites, half of trivalent ions occupy octahedral sites and the remaining trivalent ions occupy tetrahedral sites. When a magnetic field is applied, Fe ions in octahedral sites line up in the field direction while tetrahedral ions line up in the opposite direction, thus a net magnetic moment is exhibited by the material. With this in mind it could be notice that magnetic response o ferrites can be modified by substituting some Fe ions by other metallic ions exhibiting ferromagnetic behavior in elemental state.

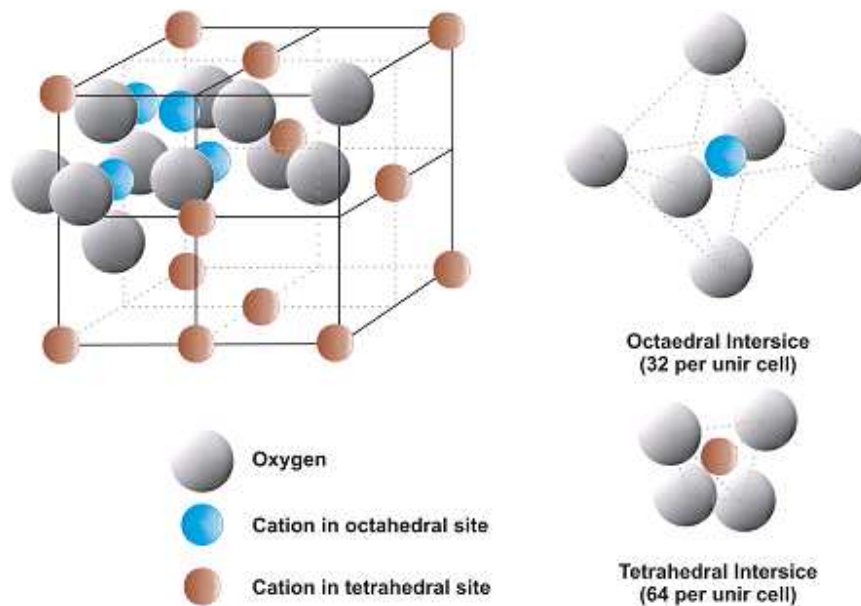


Figure 8. The spinel structure [26].

### 2.2.5 The Cobalt Ferrite Dispersoids

Within afore mentioned ferrimagnetic material, cobalt ferrite ( $\text{CoFe}_2\text{O}_4$ ) exhibits the same crystalline structure of magnetite (inverse spinel). The difference is that divalent iron ions have been substituted by cobalt ions which are also divalent. This change leads to an increase in coercivity when the material is produced in the single domain region [9, 27, 28]. The single domain diameter at room temperature (assuming room temperature at 300K) according to Kittel formula is 100nm and the superparamagnetic diameter at room temperature according to Néel is 10nm. Theoretical limits for saturation magnetization and coercivity at room temperature are 80.8emu/g and 5.3kOe respectively. This led to the conclusion that in the single domain region cobalt ferrite behaves as hard ferrite while the bulk material is considered a soft one; therefore, cobalt ferrite nanocrystals with diameter ranging from 10 to 100 nm became of interest for application such as high density data storage [9, 27, 28]. Cobalt ferrite in fine powder form can be produced by different

methods: chemical co-precipitation in aqueous media [9], chemical co-precipitation using oil in water microemulsions [27], mechanical alloying and glass crystallization [27]. Cubic magnetic materials exhibit anisotropy for magnetization being the easy axes along the cube edges  $\langle 100 \rangle$  or along cube diagonal  $\langle 111 \rangle$  [29]; in particular, cobalt ferrite single crystals have cubic magnetocrystalline anisotropy with three easy axes  $\langle 100 \rangle$  [28, 29].

### 2.3 POLYMER BASED NANOCOMPOSITES

Polymer based nanocomposites, also known as nanoscale filled polymer composites, had appeared as a new alternative to produce a new set of materials taking advantage of exceptional properties of materials at the nanoscale. Any filler possessing at least one dimension smaller than 100nm will be considered *nanofiller* or *nanodispersoids* in the forthcoming paragraphs [22]. For simplicity, nanofillers have been grouped into three categories according with its shape [22]: fiber or tube filler (radius  $< 100\text{nm}$  and aspect ratio greater than 100); plate like nanofillers which are commonly layer materials with thickness smaller than 100nm and aspect ratio greater than 25 in the other two dimensions; and approximately equi-axed fillers with a radius smaller than 100nm. Nanosize cobalt ferrite can be placed among the latter group and the importance of controlling the crystal size to obtain certain outstanding properties have been stated in previous sections.

In traditional polymer matrix composites one of the main concerns is the interface between polymer matrix and disperse phase [30] since this commonly this region determines the properties of the composite; one of the differences with nanocomposites is that the interfacial area of nano-filled polymer composites could be at least an order of magnitude greater than in conventional composites as can be seen in figure 9. In this figure, the strong

dependence of surface area per unit volume with particle diameter, assuming well dispersed spherical particles, is evidenced [22].

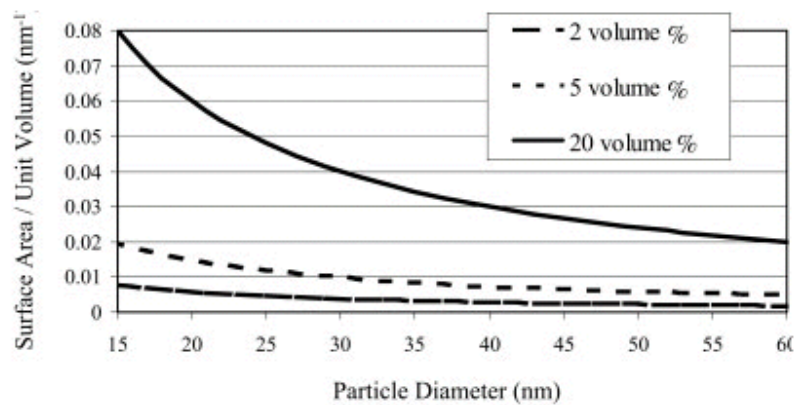


**Figure 9.** Variation of surface area per unit volume vs. particle size for various volumetric loads of homogeneously distributed dispersoids within a polymeric matrix[22]

The increase in interfacial area for nanocomposites carries out the formation of an interfacial region within the polymer matrix that could exhibit properties significantly different from those of the bulk polymer. In this regard, the degree of cure, chain mobility, chain conformation, and degree of chain ordering (short range crystallinity) could be considerably different in the interface region and thus can vary from this region to some point in the polymer matrix where the properties are again those of the bulk polymer [22]. Several researchers have been working on the study of this region and have found results that can sound contradictory and some others that have been already discussed; however certain general conclusion can be drawn: the properties of the composites are definitely influenced by the characteristics of interface region and thus the influence is related with the surface treatment imposed to nanofillers during fabrication process [22].

## 2.4 INTRODUCTION TO THERMAL ANALYSIS

From a wide viewpoint, thermal analysis (TA) is a group of measurements methods or techniques used to investigate the changes in physical properties (even the sample temperature) of a substance as a function of an imposed controlled temperature variation program [24, 31]. Even though different calorimetry techniques did not match the above definition [31] some authors frequently classify it as thermal analysis technique [24]. However, since this work does not deal with calorimetry techniques further discussion about this topic is not presented.

From a thermodynamic view point it is necessary to clarify that most of TA measurements are conducted out of thermal equilibrium since temperature is following a time dependent program and rarely enough time for the sample as whole to reach a given temperature and to achieve thermal equilibrium with its surroundings is allowed. With this in mind it is also important to note that results obtained by TA will depend on the conditions used to conduct the measurement (heating/cooling rates, load, atmosphere) as well as the sample properties (mass, dimension, geometry) [31]. It is usually recommended to use several TA methods and if possible to compare results with other techniques (spectroscopy, wet chemical mechanical, etc) to conduct interpretations.

The table 5 presents the different TA techniques and the properties that can be determined by each one according to the International Confederation of Thermal Analysis (ICTA) [24] and in the following sections a brief description of the TA techniques used to develop this work is addressed.

Property	Technique	Abbreviation
Mass	Thermogravimetry*	TG, TGA*
	Derivative thermogravimetry	DTG
Temperature	Differential thermal analysis	DTA
Dimensions	Thermodilatometry	TD
Mechanical properties	Thermomechanical analysis (Thermomechanometry)	TMA
	Dynamic mechanical analysis	DMA
Magnetic properties	Thermomagnetometry	TM
Optical properties	Thermoptometry or thermomicroscopy	---
Electrical properties	Thermoelectrometry	---
Acoustic properties	Thermosonimetry and thermoacoustimetry	TS
Evolution of radioactive gas	Emanation thermal analysis	ETA
Evolution of particles	Thermoparticulate analysis	TPA

\*The term 'thermogravimetric analysis' and the abbreviation 'TGA' are in common use but are not approved by the ICTA Nomenclature Committee.

**Table 5. Common thermal analysis techniques [24]**

### 2.4.1 Thermogravimetry (TG)

Thermogravimetry (TG) or thermogravimetric analysis (TGA) is a technique in which the changes in the mass of a given substance are measured against time or temperature. This measurements are carried out using a thermobalance which is an electronic microbalance placed inside a furnace with temperature controller all inside a closed chamber that allows atmosphere to be controlled, figure 10 shows an schematic view of a thermobalance. This thermal analysis technique is limited to assess thermal events and associated weight change, thus TG alone is useful to pick up information about desorption, decomposition, oxidation processes, accurate definition of conditions for drying or ignition of analytical precipitates, thermal stability of materials, shelf-life of drugs and polymers, etc. In addition, the

controlled atmosphere allows determining the behavior of materials when the temperature is varied in different environments and therefore information about optimal storage/usage conditions for certain materials can be obtained using TG.

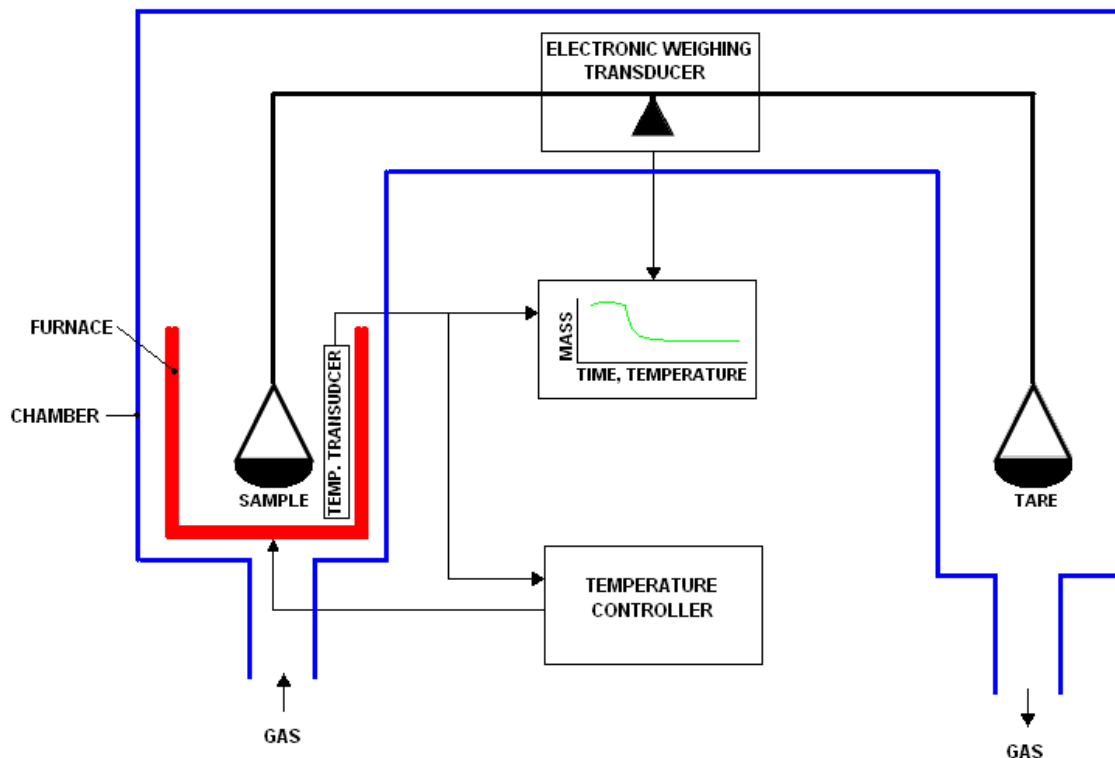


Figure 10. Schematic view of a thermobalance.

For the purpose of the present thesis, four types of curves could be expected on TG experiments which are shown in figure 11 and possible interpretations can be described as follows:

*Type (a) curves:* when the x axes is representing temperature this means that sample did not undergo decomposition or any reaction generating volatile products. In the case of x axes representing the time for an isothermal experiment this curves represents the thermal stability of the material and the result is interpreted as there were neither decomposition nor reactions producing volatiles in the time range studied for the given temperature. However,

in both cases if the sample underwent any solid state phase transformation along the selected time/temperature range, this information will not show evidence in the TG curve and thus another technique is to be used to discard this possibility.

*Type (b) curves:* the rapid loss weight at the beginning of the test could be characteristic of desorption of drying processes in both dynamic (i. e. with variation of temperature) and isothermal tests. However in the latter type of test this curve also can be interpreted as an isothermal measurement conducted at a temperature above the decomposition temperature for materials exhibiting stepped decomposition curves (figure 11 (d)).

*Type (c) curves:* this type of curve is typical for dynamic experiments; this is experiments in which the x axe represents temperature. These curves represent the decomposition of the material in a single step.

*Type (d) curves:* these curves are also common with temperature in the horizontal axis and represent a multi-stage decomposition process with intermediates of relative stability.

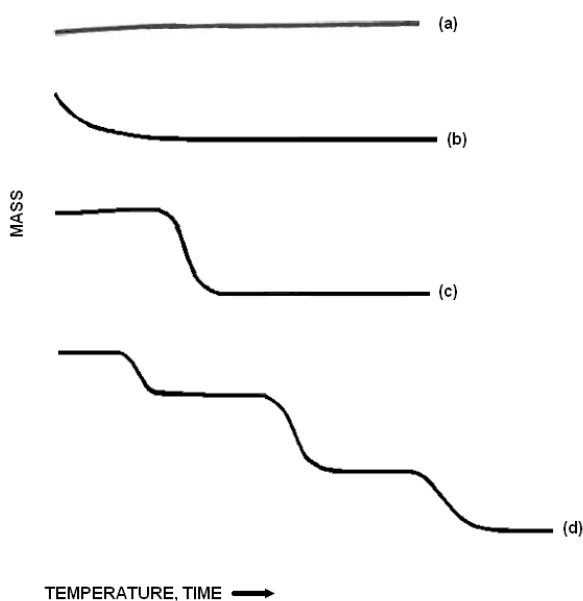


**Figure 11. Typical TG curves**

## 2.4.2 Dynamic Mechanical Analysis

This technique has received several names depending on who is talking about it. It is commonly called: dynamic mechanical analysis (DMA), forced oscillatory measurements, dynamic mechanical thermal analysis (DMTA), dynamic thermomechanical analysis (D-TMA), and even dynamic rheology. The name varies according to specialties or manufacturers. Disregarding the name, this technique can be described as applying an oscillating force to a sample and analyzing the material's response to that force [32].

### 2.4.2.1 Principles of the Technique

To understand the way this technique works and the information that can be obtained it is necessary to review some basic physical principles about the way applied forces and material's responses are related; the common practice is to relate them through a stress-strain curve in which the load is related to the applied stress (force/area) and the change in dimensions is related to the strain (elongation/original length) or rate of strain [24]. There are two extremes for stress/strain behavior which are elastic solids, which obey Hooke's law, i. e., that the applied stress is proportional to resultant strain (but is independent of the rate of strain), and liquids, which obey Newton's law, i.e., that the applied stress is proportional to rate of strain (not the strain itself). Both laws only hold for small values of strain or rate of strain and vary with the temperature at which the measurement is conducted [24], figure 12 show an example of stress-strain curves for the same material obtained at different temperatures. Actual materials however, exhibit a behavior that is placed between these two extremes and is referred to as viscoelastic behavior, i. e., the material responds partially as elastic solid and partially as viscous fluid. Even materials that

are though of as rigid, i. e. metals, will flow depending on the temperature at which the load is applied and/or the time allowed for the material to flow, certain author stated: “if you wait long enough everything flows” [32].

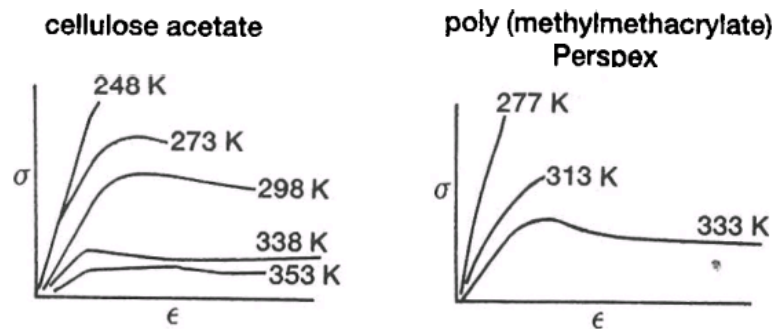


Figure 12. Variation of stress-strain curves with temperature [24]

So far the principles needed to understand the technique have been stated. Now it is possible to take a look on how the DMA works. Figure 13 shows a simple schematic of the instrument, as mentioned at beginning of this section in DMA an oscillatory force is applied to a material, mathematically this force can be expressed as:

$$F = F_0 \sin(\omega t) \quad (1)$$

Where  $F$  is the force at any time  $t$ ,  $F_0$  is the maximum force amplitude and  $\omega$  is the angular frequency of oscillation. This force causes a oscillatory stress in the sample which is described by the equation:

$$\sigma = \sigma_0 \sin(\omega t) \quad (2)$$

Looking at the two extremes of the materials behavior, elastic and viscous it can be found that the material at the spring-like or Hookean limit will respond elastically with the

oscillating stress and thus the strain at any time can be written as:

$$\varepsilon(t) = \frac{1}{E} \sigma_0 \sin(\omega t) \quad (3)$$

where  $\varepsilon(t)$  is the strain at a time  $t$ ,  $E$  is the Young's modulus and  $\sigma_0$  is the stress amplitude.

Since it was assumed an idealized elastic behavior stress and strain are linearly related and equation (3) can be rearranged as:

$$\varepsilon(t) = \varepsilon_{0e} \sin(\omega t) \quad (4)$$

where  $\varepsilon_{0e}$  is the strain corresponding to the maximum stress ( $\sigma_0$ ).

The other extreme is viscous behavior for which was stated before that stress is proportional to the strain rate, i. e., the first derivative of the strain, thus:

$$\varepsilon(t) = \eta \omega \sigma_0 \cos(\omega t) \quad (5)$$

where  $\eta$  is the viscosity. Equation (5) can be rearranged as:

$$\varepsilon(t) = \eta \omega \sigma_0 \sin\left(\omega t + \frac{\pi}{2}\right) = \omega \varepsilon_{0v} \sin\left(\omega t + \frac{\pi}{2}\right) \quad (6)$$

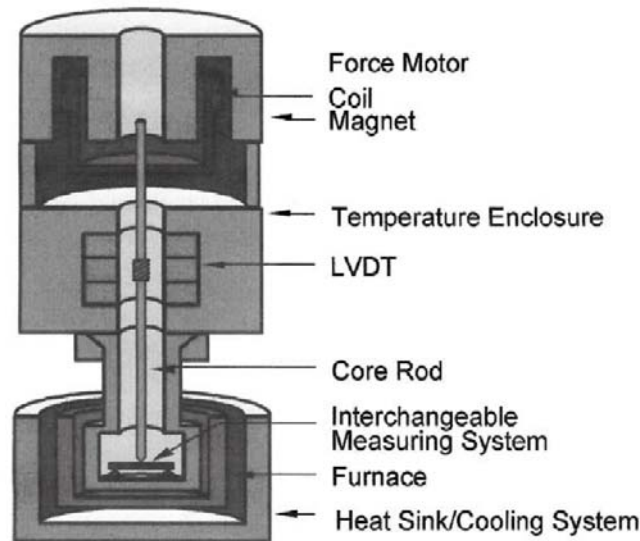


Figure 13. Schematic view of a DMA unit [32]

By comparing equations (4) and (6) it can be observed that elastic and viscous responses are shifted in frequency at an angle  $\pi/2$ . Previously, it was stated that actual materials possess a behavior lying between elastic and viscous extremes and therefore the response of these materials must be shifted in frequency at an angle  $\delta$  which value must be in the range  $0 < \delta < \pi/2$ . The response of an actual material is then given by:

$$\varepsilon(t) = \varepsilon_0 \sin(\omega t + \delta) = \varepsilon_0 [\sin(\omega t) \cos \delta + \cos(\omega t) \sin \delta] \quad (7)$$

Equation (7) can be separated into in-phase and out-of-phase strains that correspond to curves like those described by equations (4) and (6) respectively. The different curves corresponding to each type of response are summarized in figure 14.

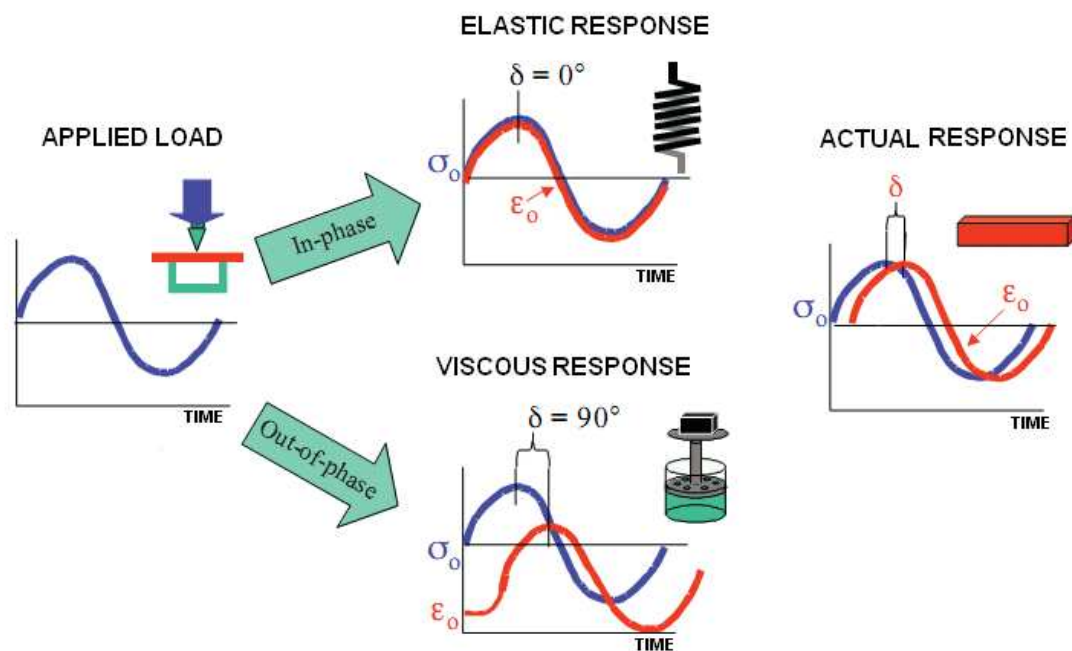


Figure 14. Response of materials for oscillatory loading [32]

From equation (7) it can be also defined an in-phase and out-phase module as:

$$\begin{aligned}\varepsilon' &= \varepsilon_0 \sin \delta \\ \varepsilon'' &= \varepsilon_0 \cos \delta\end{aligned}\quad (8)$$

The vector sum of these two components gives the overall or complex strain on the material:

$$\varepsilon^* = \varepsilon' + i\varepsilon'' \quad (9)$$

These terms are often written with  $M$  instead of the  $\varepsilon$  used so far and referred to as  $M'$  ( $M$  prime),  $M''$  ( $M$  double prime) and  $M^*$  ( $M$  complex) [32]. With this approach the term  $M'$  shows how elastic the material is (its spring-like nature), while  $M''$  shows its viscous behavior (liquid like nature). In terms of energy  $M'$  represents the amount of energy that is stored by the material and thus is also referred to as storage modulus while  $M''$  represents the fraction of energy that is dissipated as heat which is also referred to as loss modulus. The ratio of loss modulus to elastic modulus is also known as  $\tan \delta$ , tangent of the phase lag or damping and is a dimensionless property that indicates how well the material can disperse energy or in other words how well a material will absorb or loose energy. It is very important to note that even when  $M'$  is an analogous of Young's modulus the two parameters are no exactly the same property because Young's modulus is normally calculated over a range of stresses and strains, as it is the slope of a line, while the  $M'$  comes from what can be considered a point on the line; and the tests are very different, as in the stress–strain test, one material is constantly stretched, whereas it is oscillated in the dynamic test [32].

DMA tests can be done at a fixed temperature, a fixed frequency, varying the temperature, varying the temperature, varying the frequency and using combinations of these modes.

### 2.4.2.2 Application of DMA to polymers characterization

For the purpose of this work temperature scans on polymers, i. e., tests in which a polymeric material is oscillated at a fixed frequency while the temperature is increased, are going to be briefly addressed and discussed. This method is often used to determine thermal transitions in polymers. Typical curves for a temperature scans are depicted in figure 15.

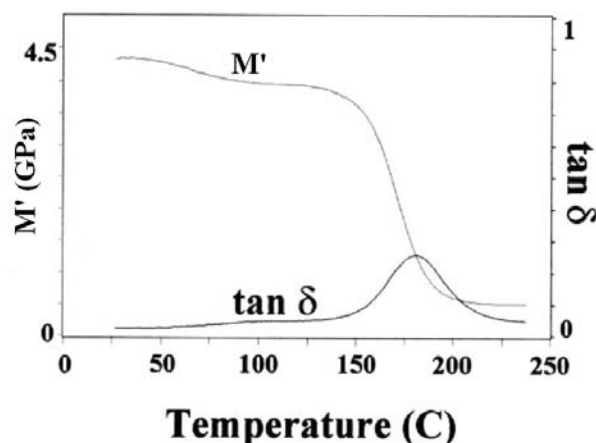


Figure 15. Typical output profiles from a DMA-temperature scan [32]

To explain the transitions that take place in the polymer molecules as the temperature is raised a simple approach is that using what is referred to as crankshaft model which assumes the molecule as a collection of mobile segments that have some degree of free movement [32], one example molecule with its possible free movements is shown in figure 16. In a thermoplastic polymer, once the temperature begins to increase from very low temperature the molecules start to acquire energy and therefore mobility which is related to changes in its viscoelastic behavior, i. e.,  $M'$ ,  $M''$ ,  $M^*$  and  $\tan \delta$ . The figure 17 shows an idealized  $M'$  vs. temperature plot for a thermoplastic and the transitions corresponding to each type of motion in the crankshaft model molecule of figure 16. The transitions that occur at temperatures lower than  $T_g$  are known as sub  $T_g$  transitions, high order transitions or second order transitions and are not always as sharp step as those depicted in figure 17,

sometimes they appear as changes in slope of  $M'$  modulus accompanied of a small dome like shape in the  $\tan \delta$  trace; an example of this situation is shown in figure 18.

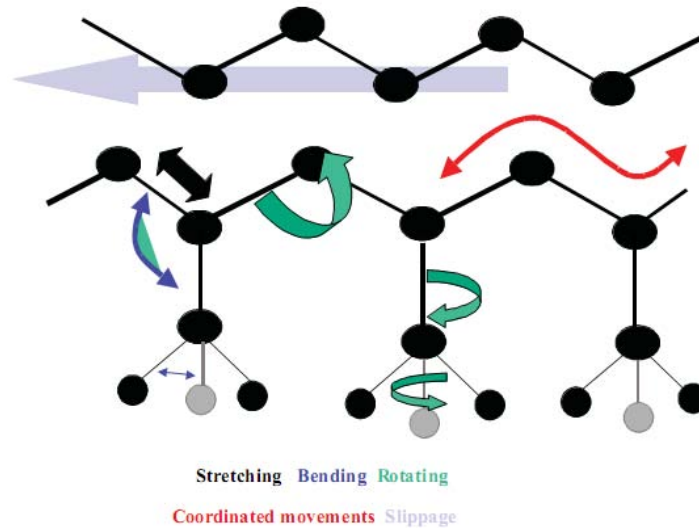


Figure 16. Crankshaft model of a polymer molecule [32]

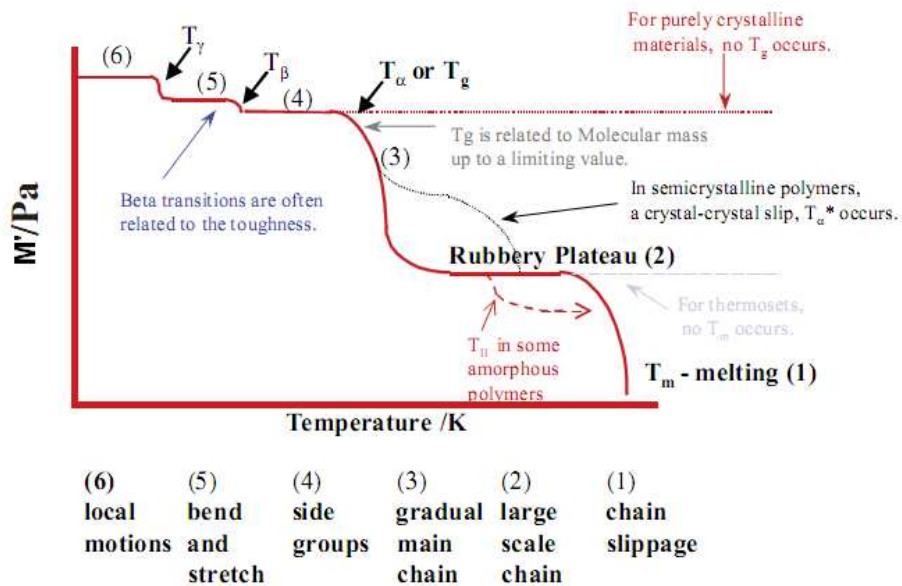


Figure 17. Idealized DMA curve for a thermoplastic polymer [32]

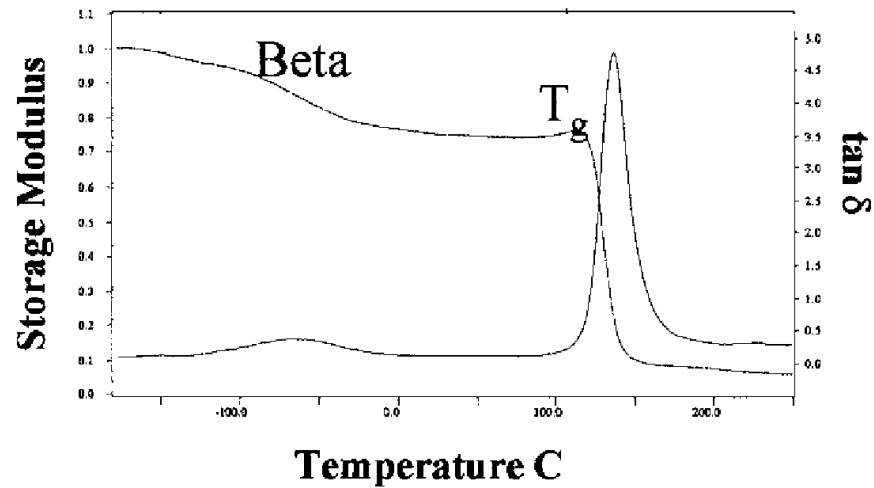


Figure 18. Actual DMA curve showing structural transitions in polymers [32]

Commonly glass transition temperature is determine as the onset of peak in the Tan  $\delta$ -T curve or the onset of the  $M'$  drop in the  $M'$ -T plot as shown in Figure 18. The way selected could depend on the application or an specific standard. This transition ( $T_g$ ) is related to large chain segments beginning to move as consequence of supplied energy represented by raise in temperature [32]. It is also important to note that pure crystalline polymers will not exhibit glass transition temperature, this kind o transition is characteristic of semicrystalline or amorphous polymers.

### 3. METHODOLOGY

#### 3.1 MATERIAL SELECTION

##### 3.1.1 Polymer Matrix: Polyimide (PI)

Typical polymers used as matrices in composites include polycarbonate (PC), epoxy resins and polyimide [24, 30]; however as mentioned in the introduction a matrix for a composite intended to be used in MEMS must be compatible with MEMS fabrication techniques. From this viewpoint the range of possible materials is narrowed. Regarding epoxy resins, only the SU-8 resin [17] met this requirement, however the need of a specific wave length UV light for its curing became a constraint for this research due to the lack in this kind of equipment. The other possibility, and final selection, is polyimide (PI) which has been widely used as dielectric and microelectronics. In addition this material has been studied in researches regarding fabrication of nanocomposites [7, 10, 12, 24, 33].

##### 3.1.2 The Magnetic Disperse Phase: Cobalt Ferrite Nanoparticles

The magnetic disperse phase for a nanocomposite for possible application in MEMS must exhibit high coercivity and high magnetic remanance. This cobalt ferrite ( $\text{CoFe}_2\text{O}_4$ ) was selected based on their outstanding magnetic properties, which were optimized by a novel method developed at our NANOMaterials processing laboratory in the Department of Engineering Science and Materials-University of Puerto Rico Mayaguez. The selection was therefore done to take advantage of the unusual high coercivity achieved in this particular nanosize ferrite particles.

## 3.2 MATERIALS SYNTHESSES AND PROCESSING

### 3.2.1 Synthesis of Cobalt Ferrite Nanocrystals

Cobalt ferrite nanocrystals were synthesized by a modified coprecipitation method. An aqueous solution of 0.11M Fe(III) and 0.55M Co(II) was continuously added by a peristaltic pump at 1ml/min into the reaction vessel (a stainless steel beaker) containing an aqueous solution of 0.48M NaOH under boiling conditions and mechanically stirred at 500 RPM. The vessel was kept under heating conditions using a propane gas burner for one hour to allow dehydration and atomic rearrangement involved with the conversion of the precursor hydroxide into the ferrite structure while stirring also remains; the chemical reaction is presented in figure 19 with the experimental setup in figure 20 and an schematic of the synthesis process in figure 22. Ferrite nanocrystals were magnetically recovered, washed out three times with distilled water and dried for 24 hours at 80°C [9]. Figure 21 shows the high resolution transmission electron microscope image of the ferrite nanocrystals used in this study.



Figure 19. Chemical reactions involved with the formation of cobalt ferrite

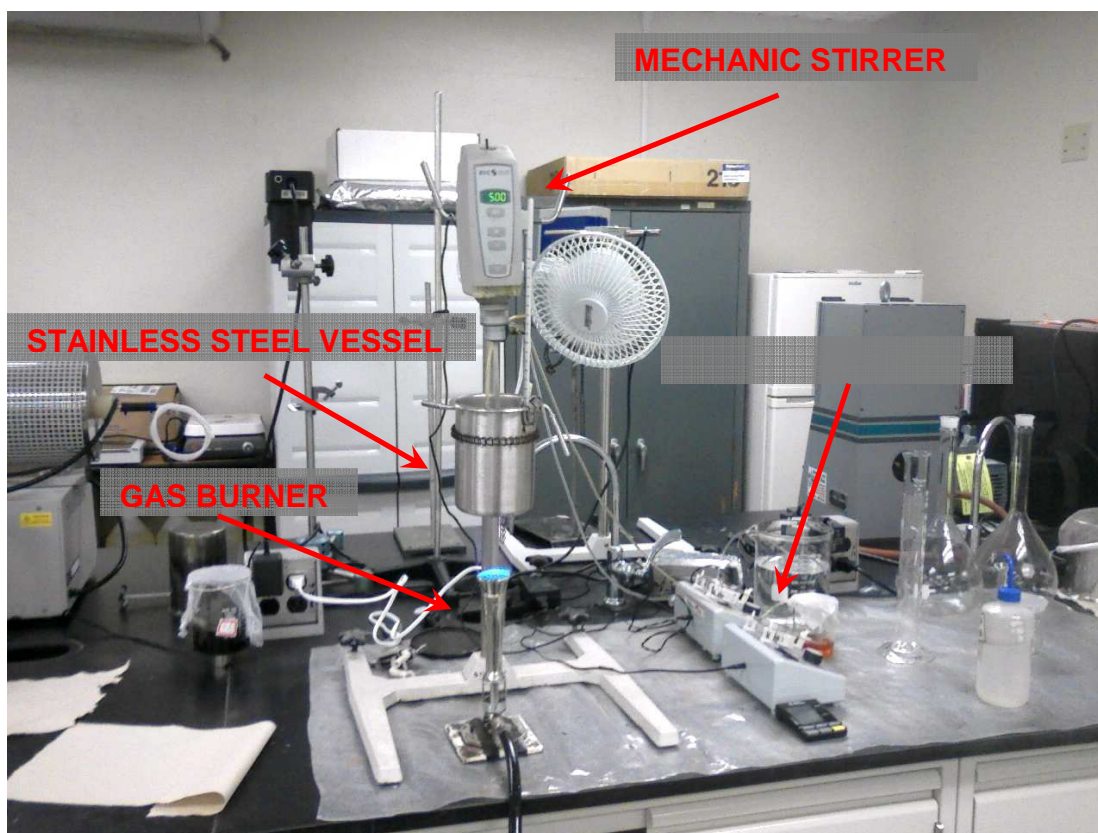


Figure 20. Experimental setup used to synthesize cobalt ferrite

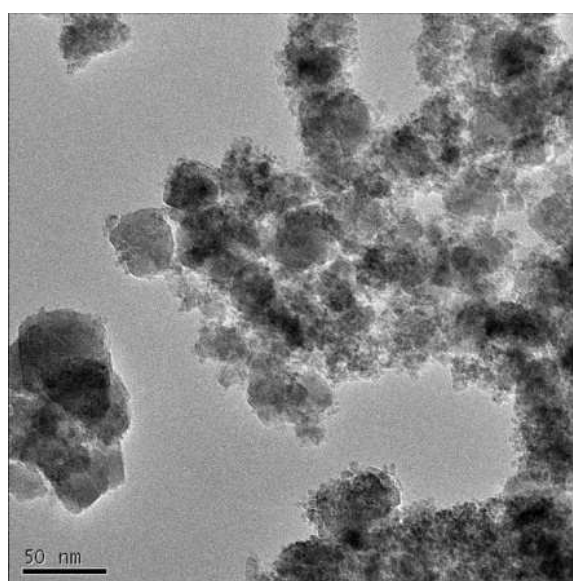


Figure 21. HRTEM micrograph of cobalt ferrite nanocrystals used in this thesis.

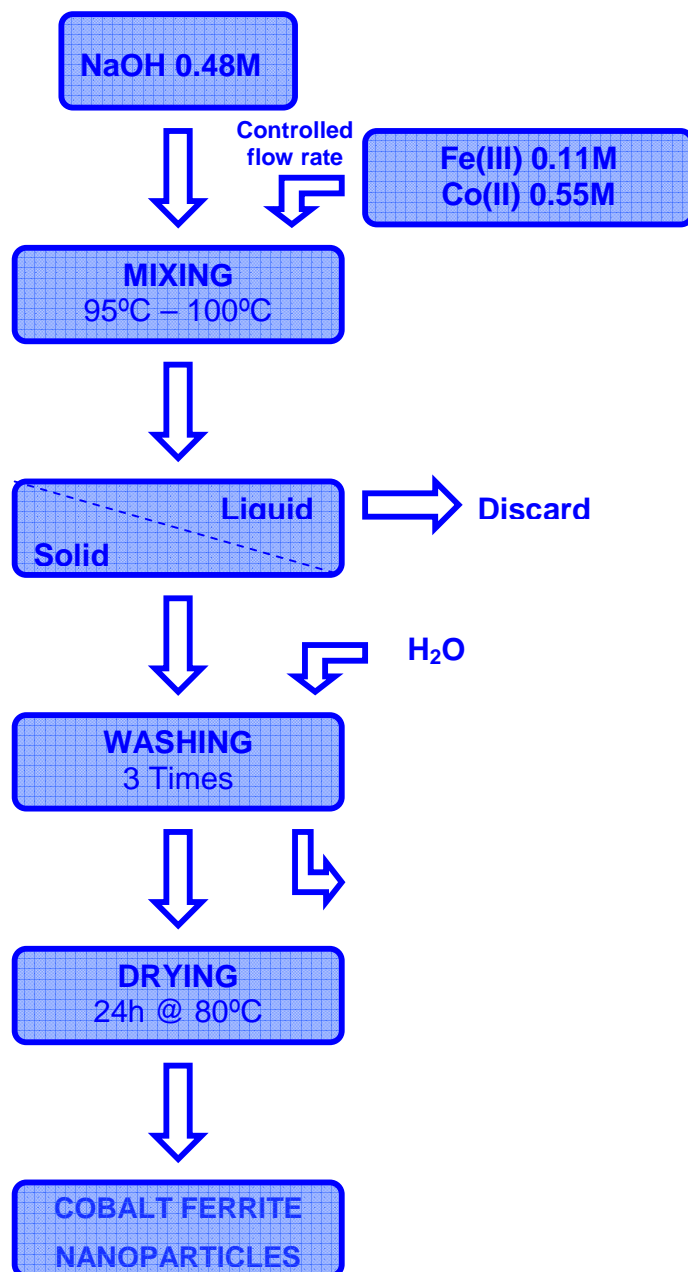


Figure 22. Experimental procedure for cobalt ferrite synthesis

### 3.2.2 Synthesis of Polyimide

There are commercially available polyimide precursors in which the first step of synthesis, the one leading to the formation of precursor polyamic acid, was carried out by the manufacturer. These precursors are generally supplied as a solution where polyamic acid is dissolved in a suitable solvent. Therefore, in order to obtain the desired polyimide structure the mentioned precursor solution has to be poured in a mold or dispensed onto a substrate to get the final shape followed by thermal processing at different temperatures in the *softbaking* and *curing* stages. The former is carried out at temperatures ranging from 85°C to 140°C depending of the intended piece thickness [21]; the main objective of this stage is to evaporate the solvent obtaining solid material. The second thermal process, also known as thermal imidization or hardbake, is typically carried out by selecting a suitable heating rate (say, 3-6 °C/min) from room temperature to 400°C followed by dwelling for 30 minutes. The curing conditions depend on the polyimide formulation and, therefore, are commonly suggested by the precursor manufacturer based on trial-and-error approaches to avoid compositional and structural defects. It is also important to note that the curing process must be conducted inside a nitrogen atmosphere to avoid surface oxidation of the polymeric constituents that tends to occur above 200 °C; that is the reason why the curing furnace must be cooled under 200 °C prior to material removal. The objective of this curing treatment is to achieve what is called cyclodehydration of the polyamic acid which consists of elimination of OH and H groups from the acid molecule and the formation of the carboxylic group – nitrogen bonding, as depicted in figure 3. The specific curing cycle considered in the present work is addressed and described in a later section. In the present thesis, benzophenone tetra-carboxylic dianhydride-oxydianiline-metaphenylene diamine

formulation precursor from DuPont was selected [7]. This precursor has trademarked name PI2555 and it is presented in a NMP solution form. The corresponding repeat unit is presented in figure 23 whereas the general properties for this precursor are summarized in table 6.

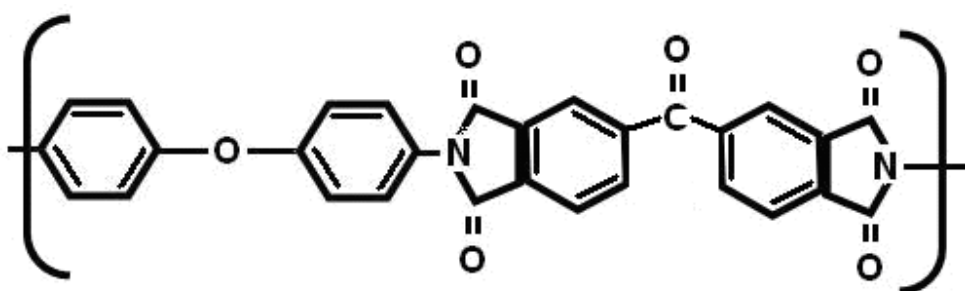


Figure 23. PI2555 polyimide repeat unit

PROPERTY/UNIT	RANGE
Solids %	18.0 to 20.0
Viscosity, poise	12.0 to 16.0
n-Methyl-2-Pyrrolidone %	75.0 to 85.0
Aromatic Hydrocarbons	15.0 to 25.0
Chloride ppm	0.00 to 2.00
Density, g/ml	0.960 to 1.160
Sodium ppm	0.000 to 1.000
Potassium, ppm	0.00 to 0.50
Iron ppm	0.00 to 1.00
Copper ppm	0.00 to 0.50
Total Metals ppm	0 to 10
Ash %	0.000 to 0.100

Table 6. Specification for PI2555 (as supplied by DuPont Company)

### 3.2.3 Preparation of Polyimide-CoFe<sub>2</sub>O<sub>4</sub> Nanocomposites

In order to prepare the composites it is necessary to disperse the cobalt ferrite nanocrystals in a PI precursor solution (PI2555). Two methods were used to achieve that objective. First

a high energy approach that makes use of an IKA T-8 basic homogenizer (figure 23) with a S18N-19G dispersing tool (figure 24). The second option consisted in the use of a low-energy approach using a Cole Parmer labmill 8000 one-tier mill (figure 25). Nanocomposites of 0.1, 1, 10 and 20 % volume fractions were prepared. For the sake of comparison bare polyimide films were also produced using the same processing technique and thus assess the influence of each of these methods on the films properties.



**Figure 24. IKA T-8 basic homogenizer (right) and the corresponding dispersing accessory (left).**

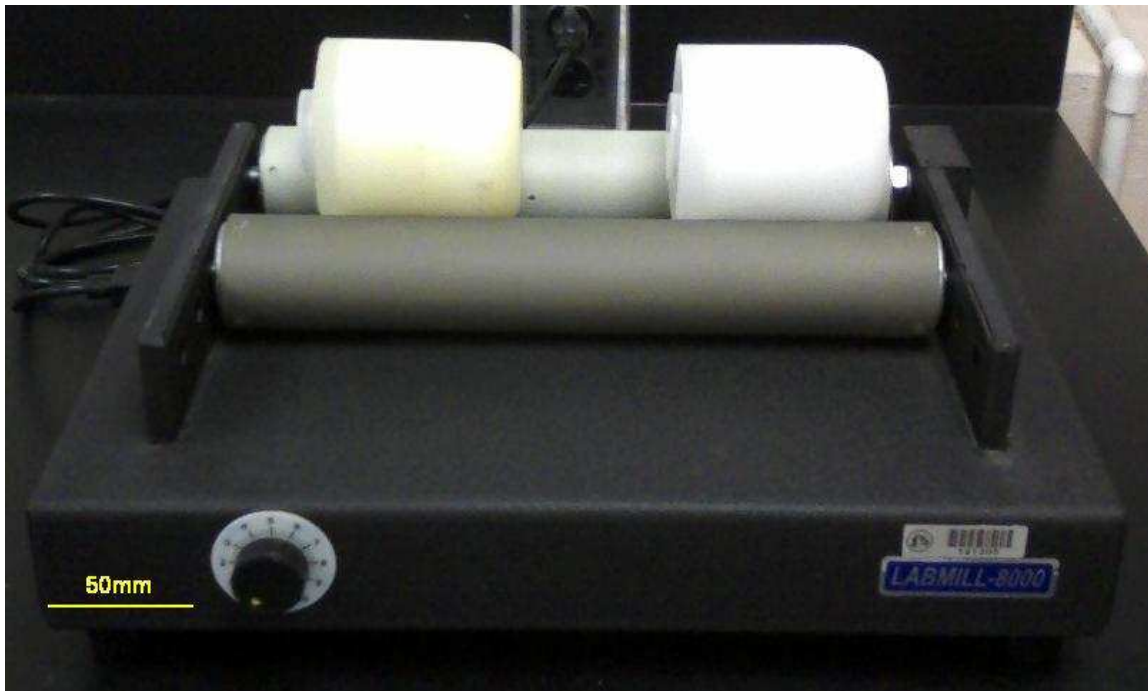


**Figure 25.** Cole Parmer labmill 8000 one-tier mill.

### 3.2.3.1 *Composite Preparation by High Energy Dispersion*

Thirty milliliters of the polyimide precursor (Dupont PI2555) was mixed with isopropyl trisostearyl titanate ( Kenrich Petrochemicals KR-TTR) which is a reagent commonly used in the industry to improve the dispersion of inorganic materials in polymer matrices [7] through reaction with free protons at the inorganic interface that in turn will form a organic-titanium monomolecular layers on the inorganic surface which also actuates as coupling agent between organic/inorganic materials. Figure 26 shows the structural representation of the KR-TTR molecule and table 7 summarizes its properties. The amount of KR-TTR to be added was selected based on manufacturer's rule of thumb, which establishes 0.2wt. % of polymer or 0.2 to 0.5 wt. % of filler, whichever is the greater; in this work both cases has occurred because of the selected ferrite volume fractions. Suitable amounts of ferrite powder were added to the previous solution to achieve the desired volumetric loads (0.1%,

1%, 10% and 20%). These volumetric loads were calculated based on the average solids content of PI2555 precursor and the theoretical densities of pure PI and cobalt ferrite [7, 9]. The ferrite-polymer precursor solution was mixed using afore mentioned homogenizing devices for 1 hour of contact rotating at 10,000 RPM. The latter contact time was selected based on the time at which a solution containing 20% volumetric ferrite load became homogeneous in color.

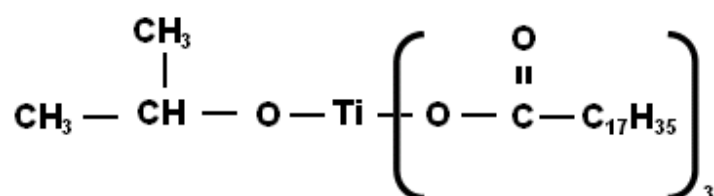


Figure 26. Chemical structure of KR-TTS

PROPERTY/UNIT	VALUE
Physical Form	Liquid
Solids (in IPA solvent), %	95
Color , Gardner	Approx. 18
Viscosity, cps @ 25°C	50-200
Specific Gravity @ 16°C	0.95±0.02
Flash Point, °F (TCC)	200
Initial Boling Point, °F (ASTM)	300
pH (Saturated Solution)	5-6

Table 7. Typical properties of KR-TTS (supplied by Kenrich Petrochemicals)



**Figure 27. Burundum grinding media used in the present research.**

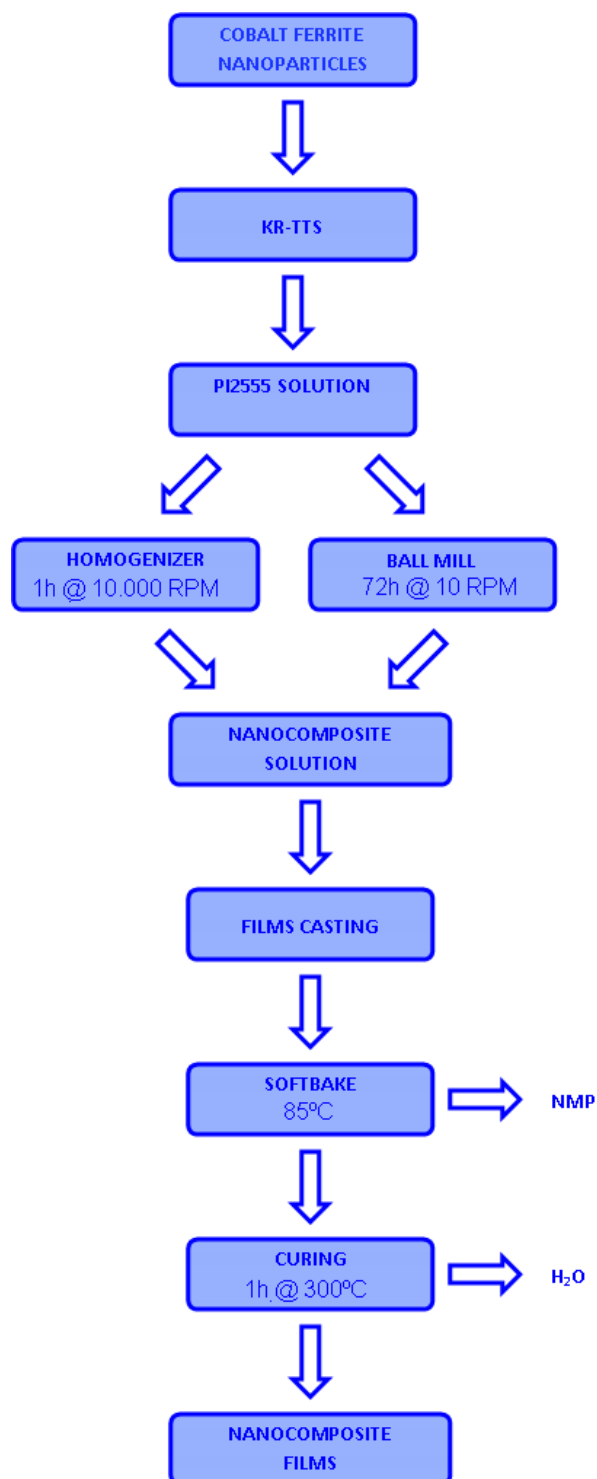


Figure 28. Experimental procedure for nanocomposite film synthesis and processing

### **3.2.3.2** *Composite preparation by Low Energy Dispersion*

To prepare the composites by this method, 40 milliliters of PI precursor were mixed with KR-TTS following the same directions of the preceding section with suitable amounts of ferrite for the selected volume fractions (the same mentioned in the preceding section). This solution was put into a glass flask containing 24 burundum (which is 90 to 99%  $Al_2O_3$ ) grinding media (Cole-Parmer) of cylindrical shape with 0.5 inch in diameter and 0.5 inch height (figure 27) in such a way that 40% of flask volume were occupied by this media, 40% by polyimide/ferrite and the remaining volume was free space. The flask was placed onto the one-tier mill (figure 25) for 72 hours at 10 RPM which the minimum spindle speed of the used ball mill and in order to achieve settings similar to those reported by Lagorce (72 hours @ 6RPM) [7].

### **3.2.4 Pure Polyimide and Composite Films Processing**

Solvent-cast free-standing films of polyimide and the corresponding composites were fabricated by pouring 0.6 to 1 ml of the precursor solution into a mold consisting of a glass substrate and a 316L stainless steel ring with 29.4 mm in diameter (figure 29) that confined the solution into a circular shape. The mold containing the precursor solution was heated on a hotplate at 85°C until almost all solvent was removed (qualitatively established as the moment when films are solid to the touch); the former processing stages were carried out under controlled atmosphere with 99.998% gas nitrogen to keep relative humidity as low as possible and always under 50% to avoid chain scion which is caused by water molecules when get in contact with poly(amic) acid molecules of PI precursor. Produced films were peeled out from the substrate and thermally cured inside a tube furnace (carbolite MTF

2/38/400 with eurotherm 3508 controller) under controlled conditions. Curing was carried out by following this sequence: (i) heating of the films from room temperature to 200°C at a 4°C/min rate; (ii) 30 minutes of heating at 200°C; (iii) heating up to 300°C at 2.5°C/min; (iv) dwelling during 60 minutes; and (v) cooling down inside the furnace (furnace is turned off until room temperature is reached). The whole curing cycle took place in a 99.998% nitrogen atmosphere to avoid oxidation of produced films that would occur if PI gets in contact with oxygen above 200°C. The preparation and processing of composite films is shown schematically in figure 28 while the curing cycle is described graphically by figure 30.

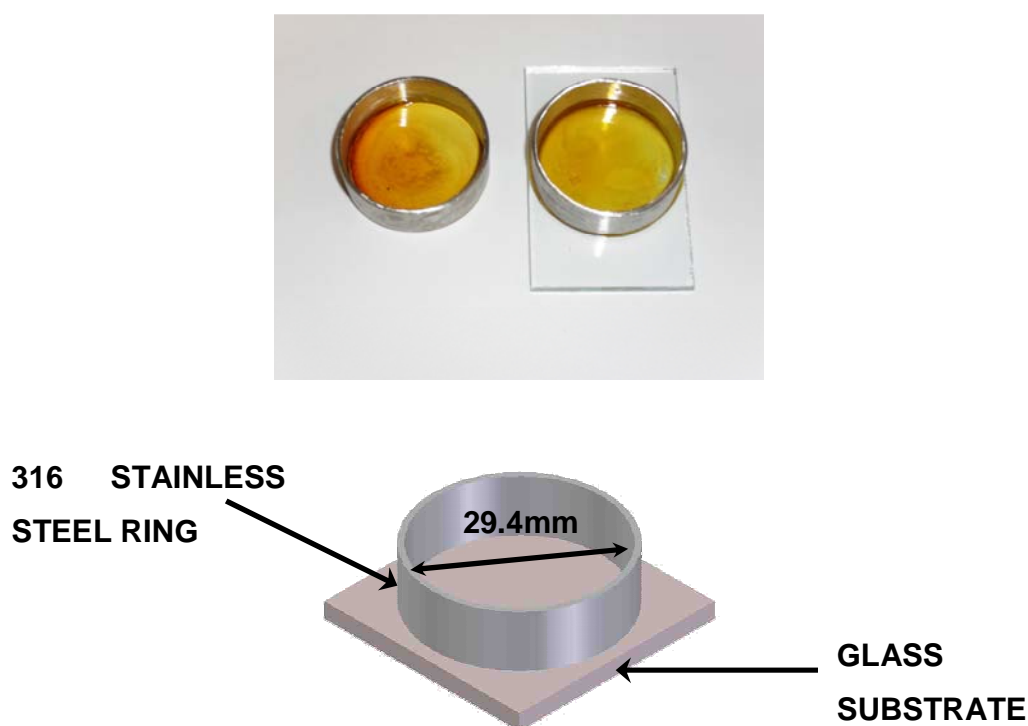


**Figure 29.** Stereo images of produced films and scheme of the used molds.

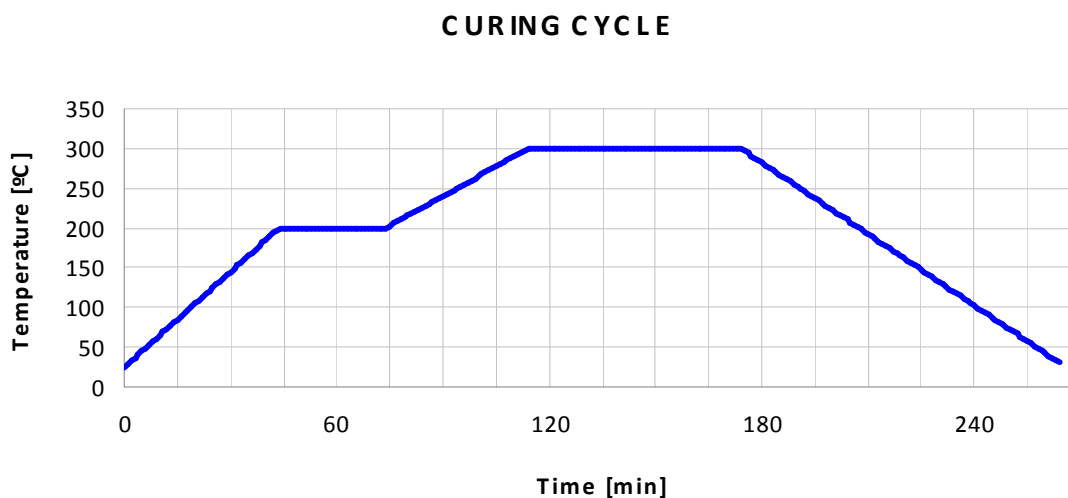


**Figure 30.** Details of the curing cycle used to produce pure PI and PI-based nanocomposite films.

### 3.3 MATERIALS CHARACTERIZATION

The techniques used to characterize the bare polymer matrix, disperse phase and composites are addressed below:

#### 3.3.1 X-Ray Diffraction (XRD)

Structural analysis of bare PI films, composites films and cobalt ferrite powders were carried out using the Cu-K $\alpha$  radiation and  $\beta$ Ni filter in a Siemens D500 powder x-ray diffractometer (Figure 31). All patterns were recorded in the  $2\theta$  range of 5 - 75° with a 0.02° step and one sample per second rate.

X-ray Diffraction (XRD) is one of mostly used techniques to identify the crystalline phases present in materials and to measure the structural properties (grain size, phase composition, preferred orientation, and defect structure) of these phases. XRD is also used to find

atomic arrangements in amorphous materials such as polymers; however since the used equipment is a powder diffractometer for the polymer phase only a qualitative analysis could be done since parameters such as interplanar distance “d” of partially crystalline solids is calculated from the transmission spectra which can not be recorded in this type of equipment. The basic features of a powder diffractometer are shown in Figure 32.

Diffraction phenomenon is the consequence of x-ray radiation being scattered by atoms regularly arranged in a lattice possessing interatomic distances of a magnitude comparable to the wave length of the incident radiation. The simplest case for a crystalline material diffracting x-ray radiation is show schematically in Figure 33. X-ray beams scattered by adjacent atomic planes must be in phase for diffraction to occur, other wise destructive interference of the waves occur and no signal is detected. Thus, from Figure 33, the condition for constructive interference is that optical path difference between the incident and scattered beam (segment ABC) must be an integer number (n) of X-ray wavelength. Mathematically, this condition is described by Bragg’s law:

$$n\lambda = 2d \sin \theta \quad (10)$$

where n is the number of integer wave length of difference in optical path,  $\lambda$  is the wavelength of the used radiation and  $\theta$  is the diffraction angle. This equation was used to determine “d” values for ferrite nanoparticles, while the average crystallite size was calculated by Debye-Scherrer’s equation:

$$t = \frac{0.9\lambda}{B \cos \theta} \quad (11)$$

where  $\lambda$  is the wavelength of the used radiation,  $\theta$  is the diffraction angle and B is the broad of the peak at the half of its height.



Figure 31. Siemens D500 XRD – Engineering Science and Materials Department at UPRM.

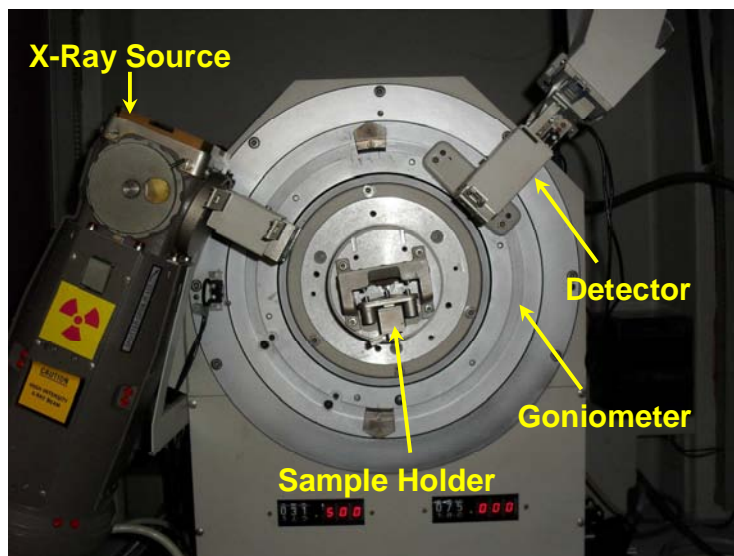


Figure 32. Basic features of the Siemens D500 powder diffractometer

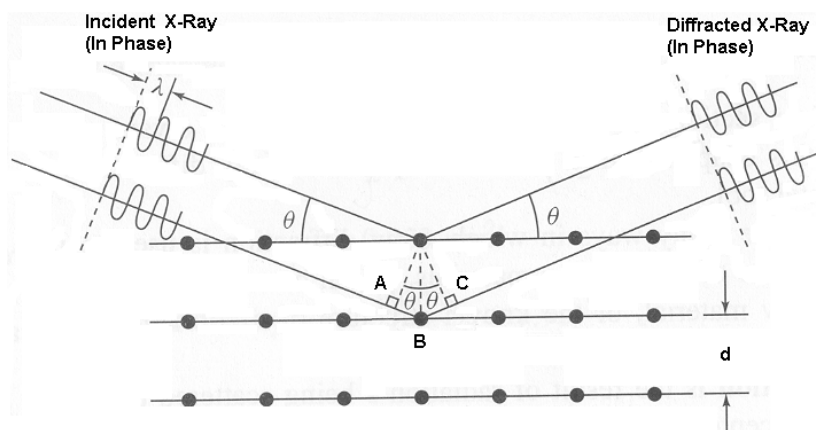


Figure 33. Schematic of the diffraction phenomenon.

### 3.3.2 Fourier Transform Infrared Spectroscopy (FT-IR)

Fourier-transform infrared (FTIR) spectroscopy was used to confirm the completion of the thermal imidization process and thus the development of PI structure in both bare matrix films and fabricated composites films. FTIR spectra were obtained in a Scimitar FTS 2000 Digilab spectrometer (Figure 34)

FTIR provides information about functional groups present in solid or liquid samples based on the presence of atomic bonding that can interact with an infrared radiation beam. It must be noted that this technique is particularly useful for organic compounds and therefore polymers which lies within that classification. However, chemical bonds vary widely in their sensitivity to probing by infrared techniques; for example, carbon-sulfur bonds often give no infrared signal while silicon-oxygen bonds can produce signals intense enough to be detected when probing very small quantities (in the order of  $10^{13}$  bond/cc). Thus, the potential utility of infrared spectrophotometry (IR) is a function of the chemical bond that needs to be detected. Fortunately the organic materials used for this work (PI) produce

infrared signals that allow determining the chemical bonding and thus the functional groups that form its molecules.



**Figure 34. Scimitar FTS 2000 Digilab Spectrometer – Physics Department UPRM.**

### **3.3.3 The Vibrating Sample Magnetometer (VSM)**

Magnetic behavior of bare PI and cobalt ferrite powders as well as the variation in magnetization and coercivity of the nanocomposites with the volumetric load of the disperse phase was determined by room-temperature magnetization measurements in a Lake Shore-7400 vibrating sample magnetometer, VSM (figure 35).

Currently VSM is the most widely used equipment used to conduct room temperature and high temperature magnetization measurements of liquids, solids, powders and films. In this technique the sample is placed inside a uniform magnetic field to magnetize it and is physically vibrated which causes an induced voltage in a pick pickup coil that is proportional to the sample's magnetic moment. In a typical setup (Figure 36), the induced

voltage is measured through the use of a lock-in amplifier using the vibrating device signal as its reference.



**Figure 35. Lake Shore 7400 Series VSM – Engineering Science and Materials Department UPRM.**

One drawback of this technique is that the sample, in general, has to be rather short to fit between poles of the electromagnet that imposes the magnetic field and therefore the method is, in certain cases, not well suited to the determination of the magnetization curve or hysteresis loop because of the demagnetizing effects associated with the short specimen. Magnetic moments as small as  $5 \times 10^{-4} \text{ A m}^2$  ( $5 \times 10^{-5} \text{ emu}$ ) are measurable with a VSM. Its accuracy is better than 2% [34].

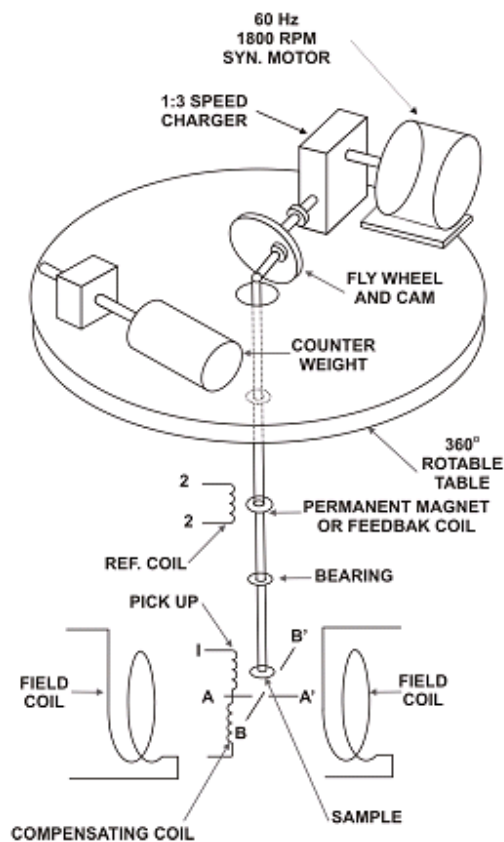


Figure 36. Schematic of a Vibrating Sample Magnetometer [26]

## 3.4 THERMAL ANALYSIS

### 3.4.1 Thermogravimetry (TG)

Thermogravimetry (TG) was used to determine the temperature of degradation and the thermal stability as a function of time of both, bare PI and nanocomposite films. Five percent of weight loss was set as the critical value, i.e. the maximum allowance in weight variation based on previous work done by Dunson [21]. For the particular case of thermal stability test the parameter were selected taking into account that a microchip that is soldered onto a printed circuit board can reach a temperature of 350°C for two hours

therefore thermal stability tests for polymers to be used in microelectronics are conducted for two hours at 400°C [21]; however, to find out if there is a critical time for thermal stability overnight (8 hours) experiments were arbitrarily selected. Thus, thermal stability tests were carried out by keeping the films at 400°C for 8h in a Mettler Toledo TGA/SDTA 851e thermogravimetric analyzer (figure 37) under a 99.9% extra dry gas nitrogen atmosphere. The same set-up was used to determine the degradation temperature of the films by heating them from room temperature to 600°C at 5°C/min. For all tests sample size was between 3 to 5 mg.

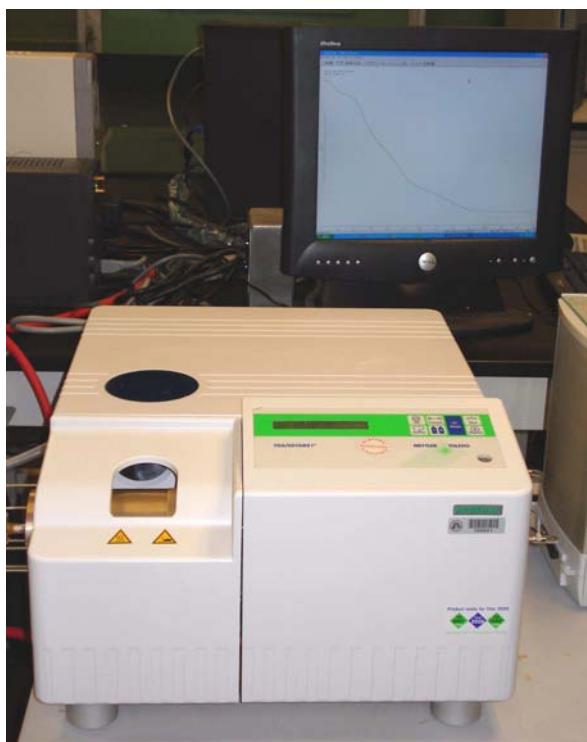


**Figure 37. Mettler Toledo Thermogravimetric Analyzer – Engineering Science and Materials Department UPRM.**

### 3.4.2 Dynamic Mechanical Analysis (DMA)

The viscoelastic behavior of bare polyimide and composites films was evaluated in a Mettler Toledo DMA/SDTA 861e dynamical mechanical analyzer (figure 38) for an applied 1Hz sine wave tensile load while the temperature was increased at a 5°C/min from room temperature to 400°C for these measurements in air atmosphere. Samples were of rectangular shape 10.5mm long and 5 to 6 mm wide.

These measurements give information about afore explained  $M'$ ,  $M''$ ,  $M^*$  and  $\tan \delta$ , however for the purpose of this work only measurements of  $\tan \delta$  (also known as tangent of the phase lag) and the storage (elastic) modulus  $M'$  as a function of temperature were analyzed since they provide the major amount of information about material's behavior as explained in previous section.

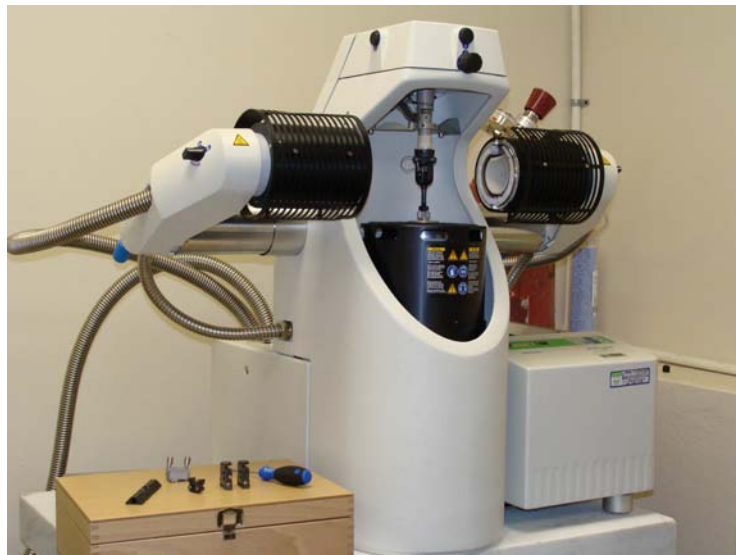


Figure 38. Mettler Toledo Dynamic Mechanical Analyzer – Engineering Science and Materials Department UPRM.

## 4. RESULTS AND DISCUSSION

### 4.1 STRUCTURAL ANALYSIS

Structural analysis of produced composite materials was carried out to verify the development of polymer matrix and crystalline dispersoids. In this regard X-ray diffraction (XRD) and Fourier transform infrared spectroscopy (FTIR) were used to identify the crystalline phases and the functional groups of the polymeric matrix, respectively.

#### 4.1.1 FTIR Analyses

FTIR spectrum for the polyamic precursor is shown in figure 39 and Figure 40 shows the FTIR spectra for bare polyimide and nanocomposite films containing 0.1%, 1% 10% and 20% volume fractions of cobalt ferrite nanoparticles produced after curing the ferrite-PI precursor mixture treated by the high-energy IKA T-8 homogenizer as dispersing tool. Films with the same volume fractions were also produced using the ball mill to disperse ferrite particles. The obtained FTIR spectra are presented in Figure 41. Disregarding the dispersion technique, main bands at  $1780\text{ cm}^{-1}$  (C=O asymmetrical stretching),  $1710\text{ cm}^{-1}$  (C=O symmetrical stretching),  $1370\text{ cm}^{-1}$  (C-N stretching) and  $710\text{ cm}^{-1}$  (C=O bending) were identified and assigned to imide groups in the polyimide structure. The absence of bands in the  $3200\text{ cm}^{-1}$  - $2900\text{ cm}^{-1}$  range corresponding to OH and NH stretching as well as the vanishing of the band at  $1660\text{ cm}^{-1}$  (NH bending) suggests the completion of the imidization process by removal of H and OH species from the structure of the polyamic acid precursor.

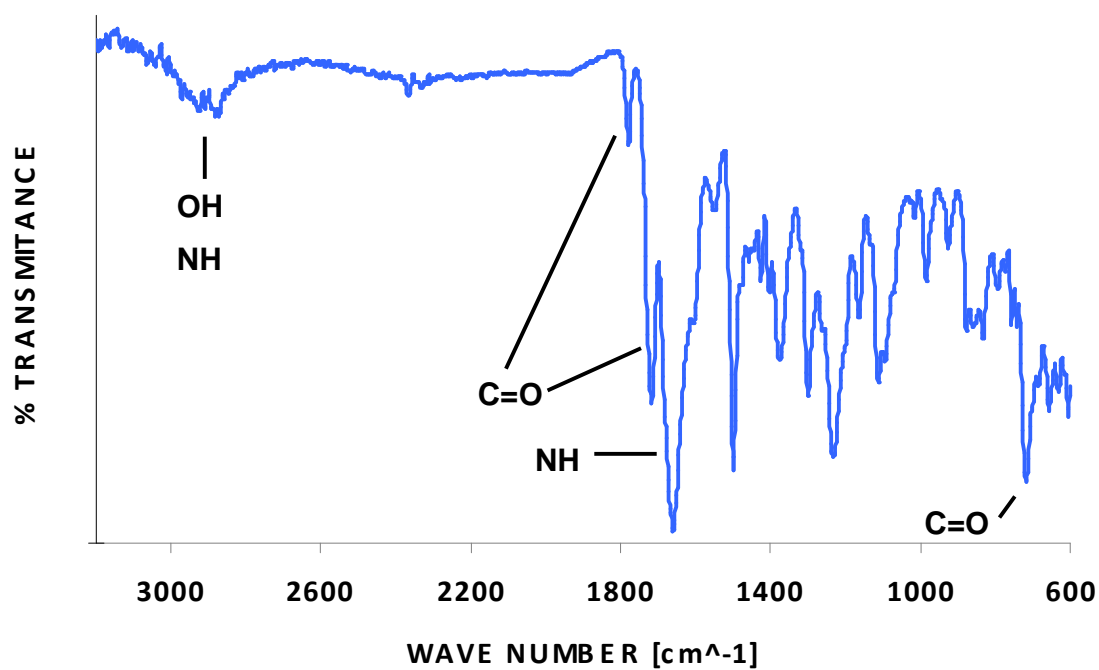


Figure 39. FTIR Spectra for the polyamic precursor

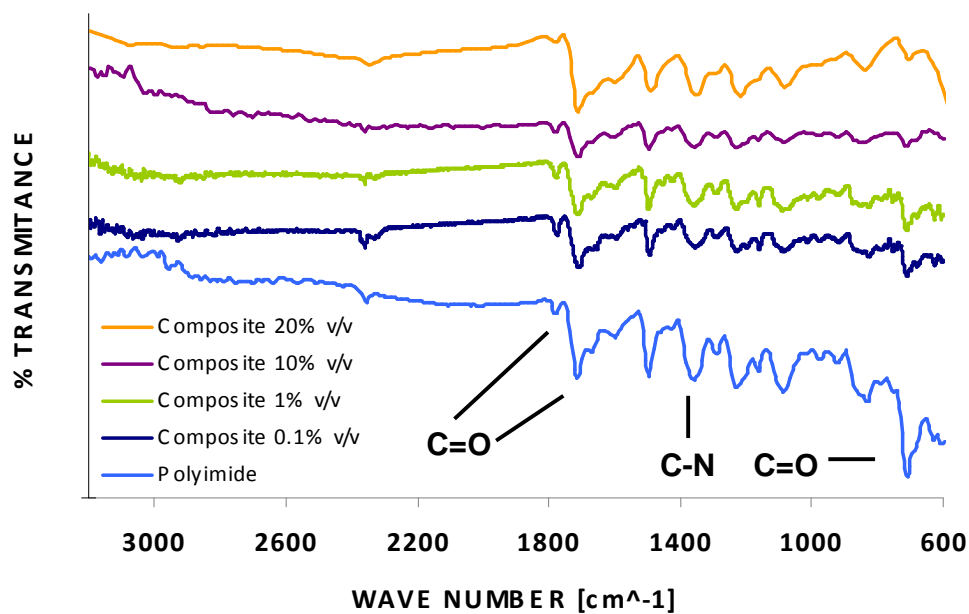
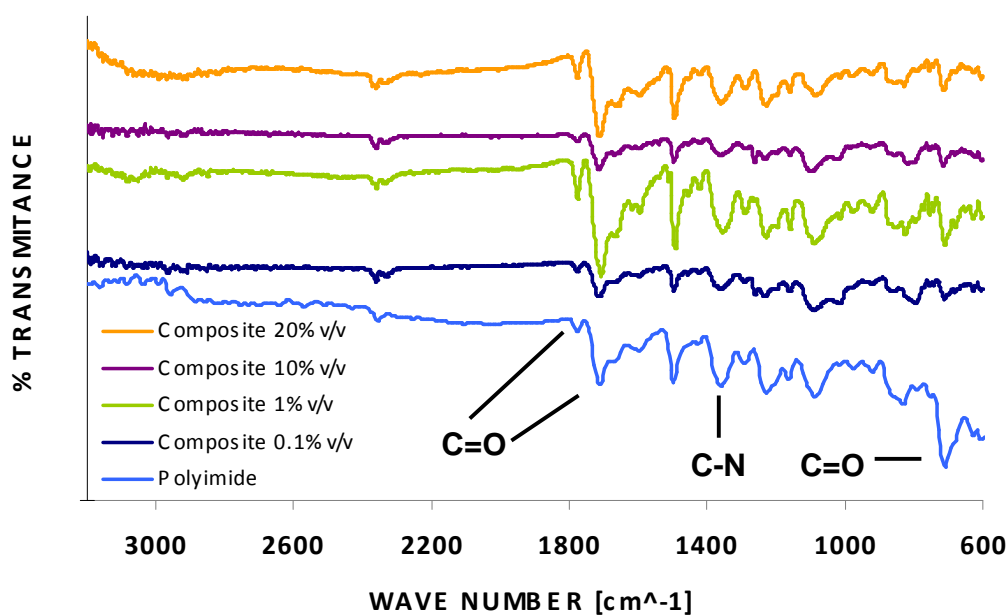


Figure 40. FTIR Spectra of bare polyimide and different volume fraction composite films produced after curing the dispersion treated by the IKA T-18 high-energy homogenizer



**Figure 41.** FTIR Spectra of bare polyimide and different volume fraction composite films produced after curing the dispersion treated by the Labmill 8000 ball mill.

Obtained information was in agreement with previous works by Dunson [21] and Zhan [12] who identified similar bands in processed polyimide and maghemite-polyimide composites. Accordingly, it was clear that dispersion techniques being assessed do not have remarkable influence in the molecular structure of the polymeric matrix in produced composites as well as in bare polyimide films.

#### 4.1.2 XRD Analyses

XRD analyses of the polyimide matrix, isolated disperse cobalt ferrite nanoparticles and the corresponding nanocomposites confirmed the formation of the expected structures using both the homogenizer (Figure 42) and the ball mill (Figure 43) as dispersing approaches. Only well-defined peaks corresponding to the spinel cubic structure of cobalt ferrite

dispersoids were detected. The corresponding average crystallite size and lattice parameter were estimated at 20 nm and 8.34Å, respectively. These values are in good agreement with those reported by Y. Cedeño et al. [9]. The broad XRD peak centered on 18° in bare polyimide films indicates a short-range molecular order, which is also encountered in the 0.1%, 1% and 10% volume fraction nanocomposites produced using both dispersion techniques. However, for the composites containing 10% ferrite volume fraction the peak is located at a lower diffraction angle; this shift in  $2\theta$  value would suggest an increase of the interplanar distance in the polymer that is attributed to the close interaction between polymer chains and incorporated ferrite nanocrystals. Furthermore, the molecular ordering in the polymeric matrix was no longer evident when the volume fraction of ferrite in the nanocomposites was increased to 20%; the incorporation of ferrite nanoparticles in the composite would have inhibited the development and/or ordering of the polymeric chains disregarding the dispersion used dispersion technique. As mentioned in the theoretical background section since a powder diffractometer was used only qualitative information about polyimide crystalline structure can be gather, i. e. to determine whether the polyimide exhibits a regular atomic array or not. Furthermore, reviewed works did not provide information about polyimide crystalline structure beyond the interplanar distance in such array. Finally, based on these results there was found no effect of dispersion technique on the structural features of produced nanocomposites.

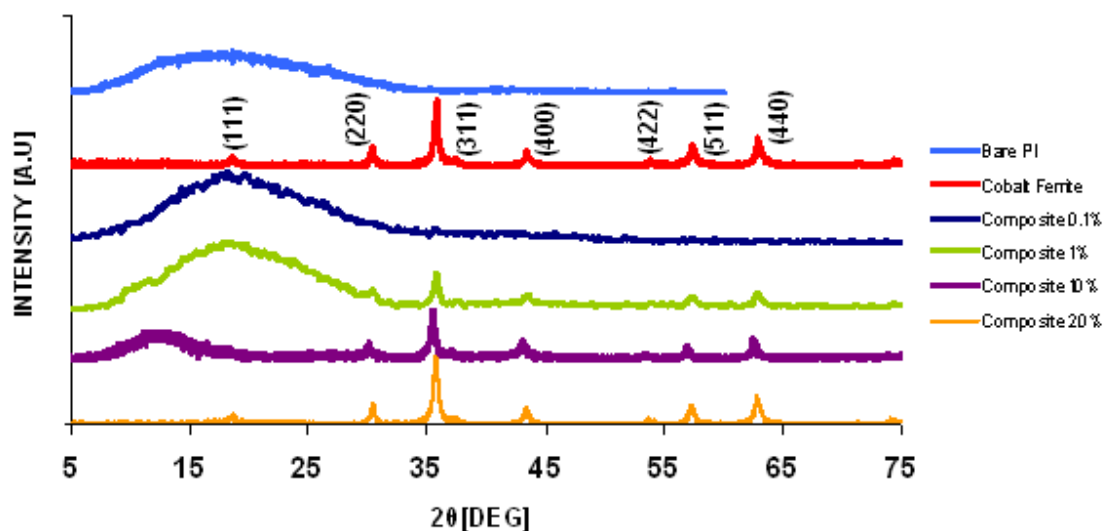


Figure 42. XRD patterns for cobalt ferrite powder, bare polyimide and different volume fraction composite films produced after dispersing the ferrite nanoparticles in PI precursor using the IKA T-8 homogenizer

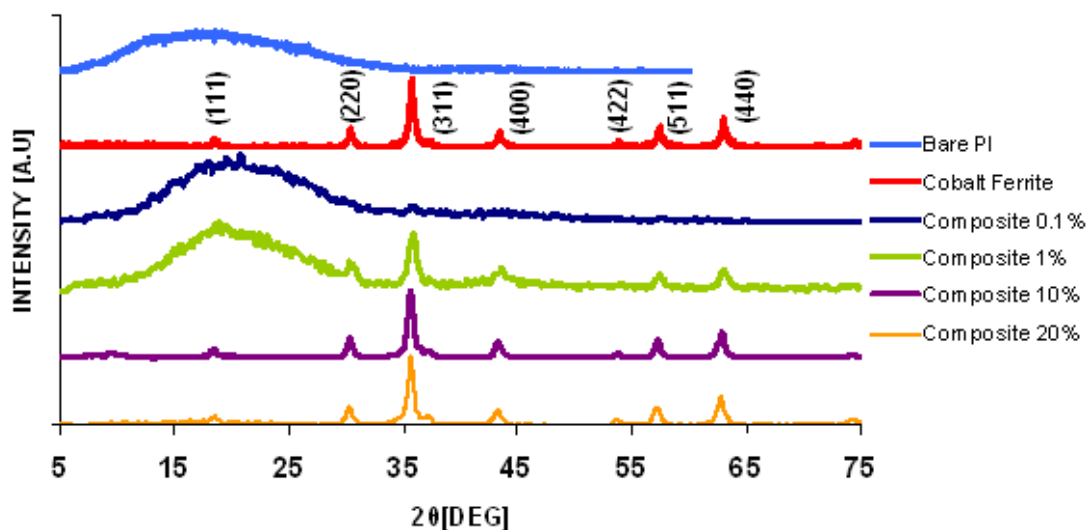
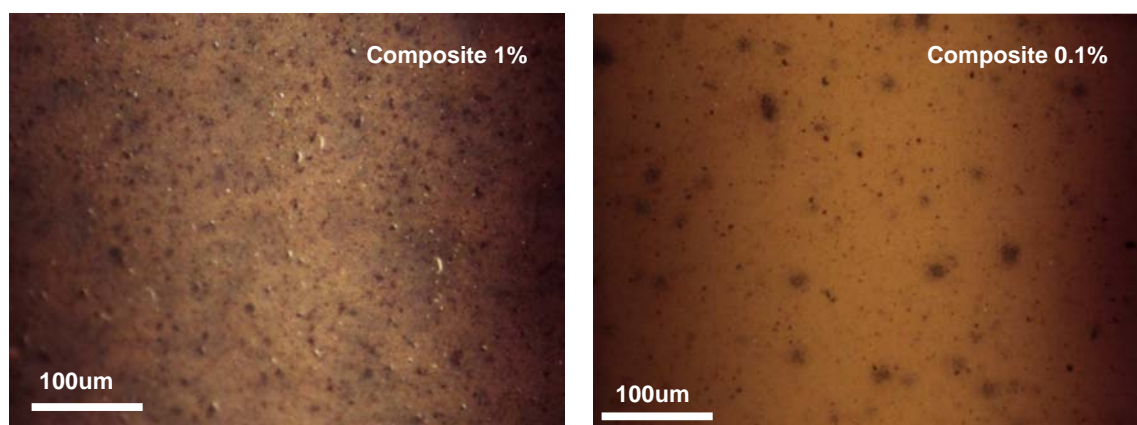


Figure 43. XRD for cobalt ferrite powders, bare polyimide and different volume fraction composite films produced after dispersing the ferrite nanoparticles in PI precursor using the Labmill 8000 ball mill.

## 4.2 DISPERSION ASSESSMENT

Composite films of 0.1% and 1% ferrite volume fractions were prepared in order to qualitatively assess the dispersion achieved with both dispersing techniques (high-energy homogenizer and ball mill). For this purpose stereographic images at 100X magnification were taken of films produced at various volumetric loads of the disperse phase. Figure 44 shows the stereographic images corresponding to the composites prepared using the IKA T-8 homogenizer; a good distribution of the particles can be observed for both volume fractions; even when there are ferrite clusters, they were homogeneously distributed. However, It is important to note that those clusters were formed during the drying step after the ferrite synthesis. Despite of this unavoidable aggregation, these particles were reasonably well dispersed within the polymeric matrix by the selected dispersion technique. Similar results were found for the composite films produced after dispersing the ferrite particles in the matrix by using the ball mill set-up (Figure 45).



**Figure 44.** 100X Stereographs of composites produced after curing the ferrite-precursor solution using the IKA T-18 high energy homogenizer

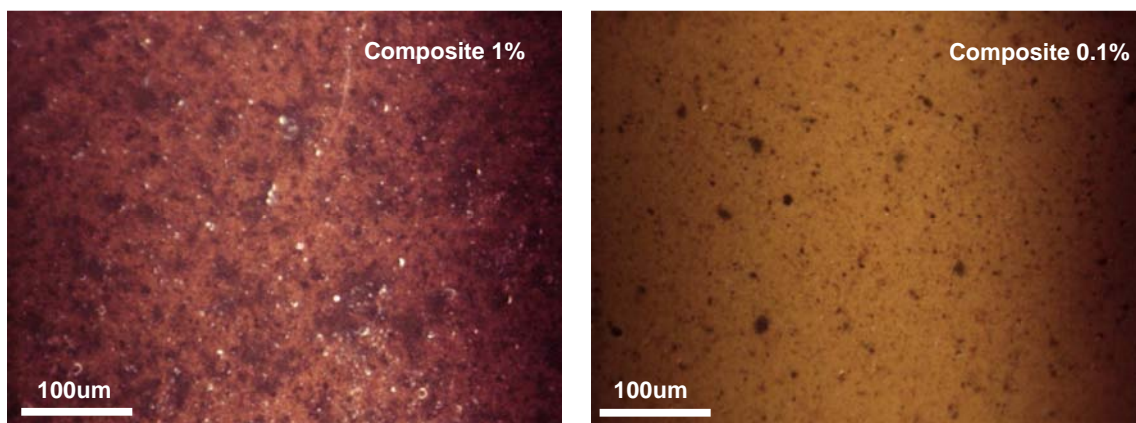


**Figure 45.** 100X Stereographs of composites produced after curing the ferrite-precursor solution using the Labmill 800 ball mill.

### 4.3 MAGNETIC CHARACTERIZATION

Room-temperature M-H loops for isolated ferrite nanoparticles and nanocomposite films synthesized at 0,1%, 1%, 10% and 20% ferrite volume fractions produced using the two dispersion methods under evaluation were measured applying the magnetic field along parallel and perpendicular directions with respect to the film surface in order to verify the isotropic magnetic behavior of the composite films. Figures 46 to 49 shows the MH loops for the pure ferrite and the corresponding nanocomposites produced after curing the ferrite-PI precursor suspension by the IKA T-8 high-energy homogenizer. Regarding the magnetic properties of the pure cobalt ferrite nanoparticles, the maximum magnetization was 42.5emu/g; the lack of saturation in the corresponding M-H loop can be attributed to the significant presence of superparamagnetic particles in the polydisperse powders. In turn, the saturation observed in the M-H loops for the nanocomposites films can be a

consequence of the immobilization of the ferrite nanocrystals in the polymeric matrix. As observed in the corresponding M-H loops, the saturation magnetization of the nanocomposites varied from as a function of the ferrite weight load. As expected, the coercivity remained constant (2.9kOe) in any case. This behavior was also evidenced for volumetric fractions as low as 0.1% (Figures 48 and 49).

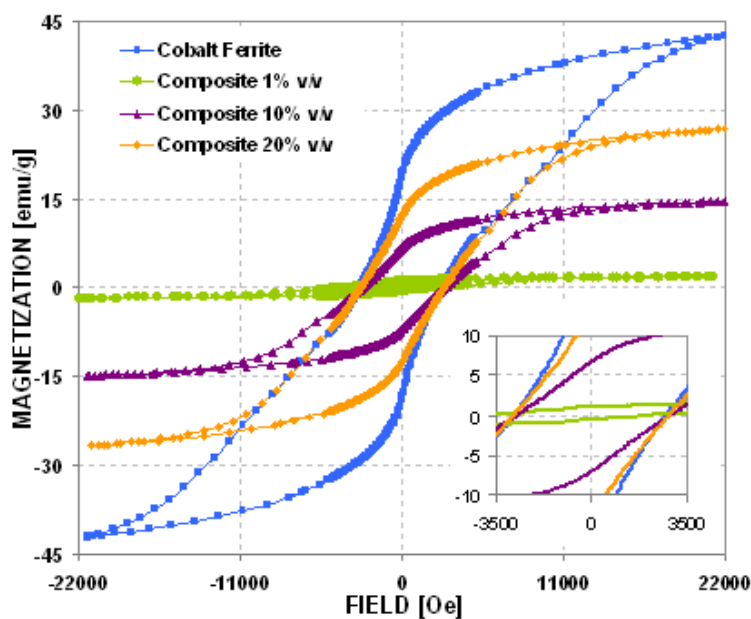


**Figure 46.** Room temperature M-H loops for cobalt ferrite powders and composite films produced at different volume fractions. High-energy homogenizer was used as a dispersing tool. The external field was applied along the parallel direction

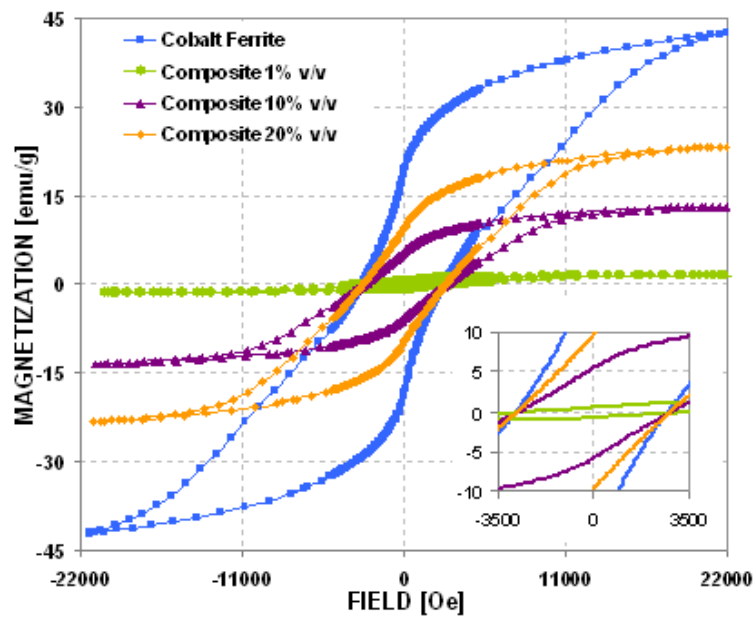


Figure 47. Room temperature M-H loops for cobalt ferrite powders and composite films produced at different volume fractions. High-energy homogenizer was used as a dispersing tool. The external field was applied along the transverse direction

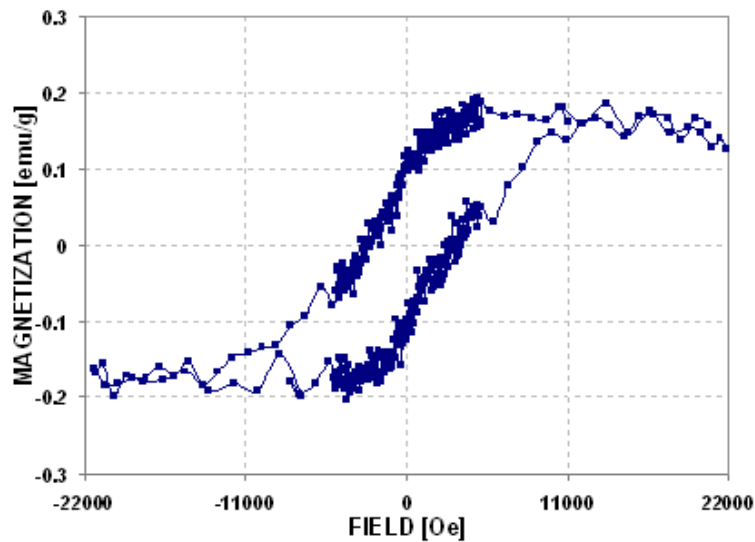
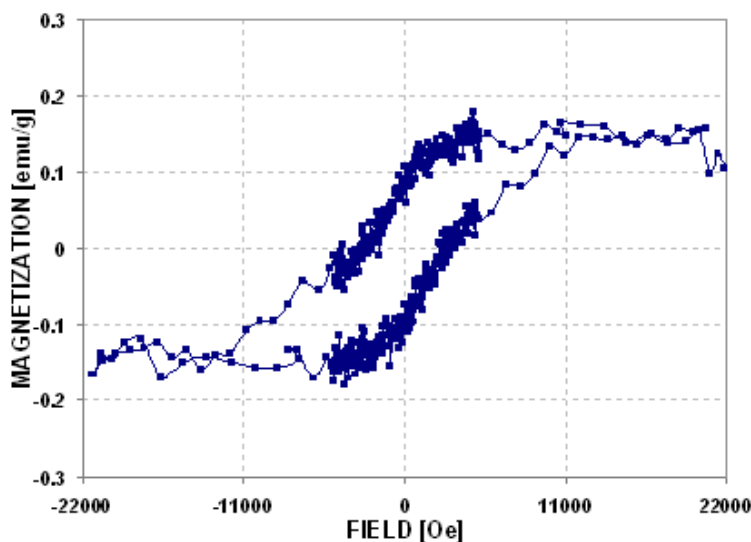


Figure 48. Room temperature M-H loop for composite film containing 0.1% v/v cobalt ferrite. High-energy homogenizer was used as a dispersing tool. The external field was applied along the parallel direction



**Figure 49.** Room temperature M-H loop for composite film containing 0.1% v/v cobalt ferrite. High-energy homogenizer was used as a dispersing tool. The external field was applied along the transverse direction

Pure cobalt ferrite powders used to produce composite films by using ball milling as dispersing tool exhibited maximum magnetization of was 45.8emu/g (Figures 50 and 51); these powders also lacked of saturation in the corresponding M-H loop as a consequence of the presence of polydisperse crystals. Nanocomposite films produced this way also presented well saturated MH loops. As previously said, saturation was due to immobilization of the ferrite nanocrystals in the polymeric matrix. The saturation magnetization of the nanocomposites also varied as a function of the ferrite weight percentage. The coercivity remained constant (2.6 kOe) in any case, even for low volume fraction values (0.1%) as shown in Figures 52 and 53.

Based on the above considerations, a negligible variation with the direction of the external magnetic field in both, the saturation magnetization and coercivity, was observed (Figures

46 to 53). This fact suggests the formation of isotropic magnetic nanocomposite films. The isotropic behavior is attributed to the effective dispersing techniques as was also in agreement with our previous observation on this respect.

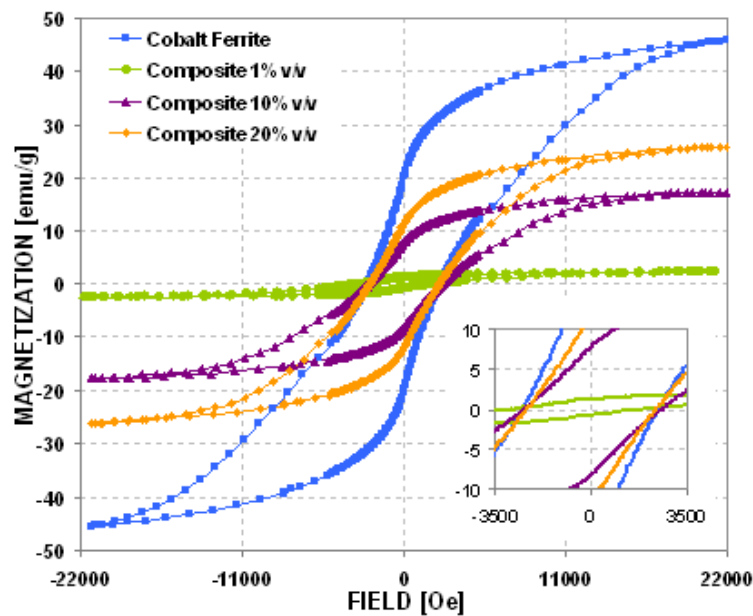


**Figure 50.** Room temperature M-H loops for cobalt ferrite powders and composite films produced at different volume fractions. Low-energy ball mill was used as a dispersing tool. The external field was applied along the parallel direction

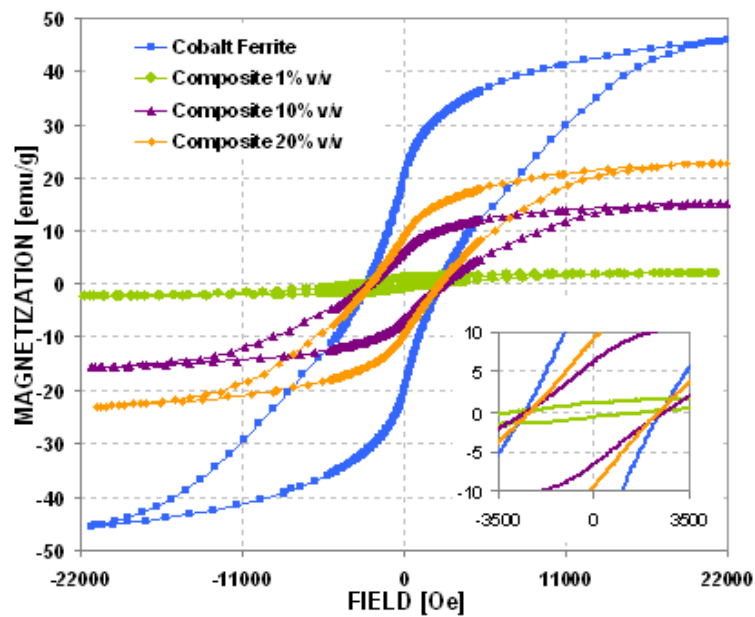


Figure 51. Room temperature M-H loops for cobalt ferrite powders and composite films produced at different volume fractions. Low-energy ball mill was used as a dispersing tool. The external field was applied along the transverse direction

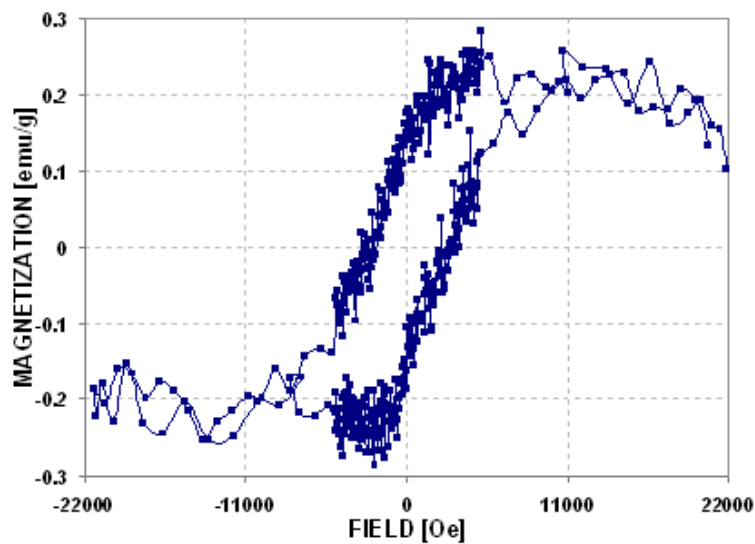
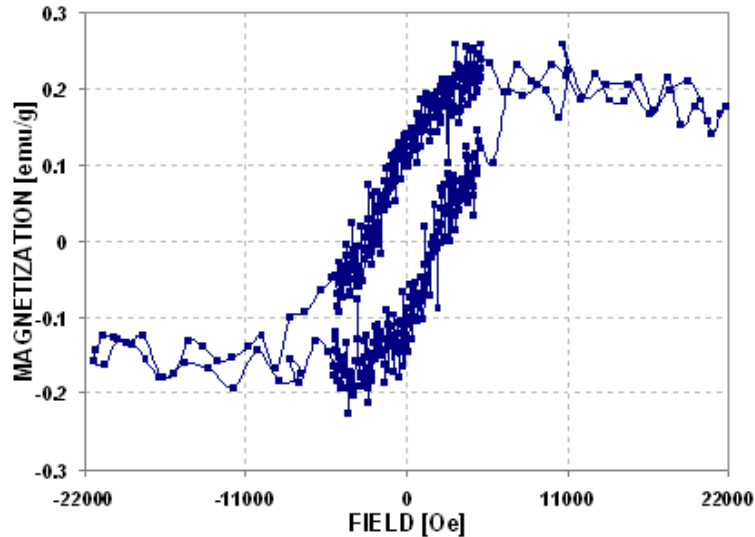


Figure 52. Room temperature M-H loop for composite film containing 0.1% v/v cobalt ferrite. Low-energy ball mill was used as a dispersing tool. The external field was applied along the parallel direction



**Figure 53.** Room temperature M-H loop for composite film containing 0.1% v/v cobalt ferrite. Low-energy ball mill was used as a dispersing tool. The external field was applied along the transverse direction

Since polyimide has no magnetic response, the saturation magnetization ( $M_s$ ) in produced composites should be attributed to the mass of magnetic dispersoids. If so, this magnetization should follow the rule of mixtures based on mass fraction. To verify this hypothesis, cobalt ferrite weight percentages (wt%) corresponding to 1, 10 and 20% volume fraction were calculated and used with the saturation magnetization of ferrite powders to estimate the theoretical saturation magnetization using the aforementioned rule of mixtures. The calculated values are compared with the experimental ones. The corresponding data is presented in Tables 8 and 9, and Figures 54 and 55.

Volume Fraction [%]	Weight Percentage [%]	Theoretical Ms [emu/g]	Experimental Ms [emu/g]
1	4.76	2.181	2.360
10	37.47	17.169	17.678
20	55.30	25.339	26.053

**Table 8.** Theoretical and experimental values of saturation magnetization for films produced at different volume fractions. Low-energy ball mill was used as a dispersing tool.

Volume Fraction [%]	Weight Percentage [%]	Theoretical Ms [emu/g]	Experimental Ms [emu/g]
1	4.76	2.024	1.758
10	37.47	15.935	14.802
20	55.30	23.518	26.760

**Table 9.** Theoretical and experimental values of saturation magnetization for films produced at different volume fractions. High-energy homogenizer was used as a dispersing tool.

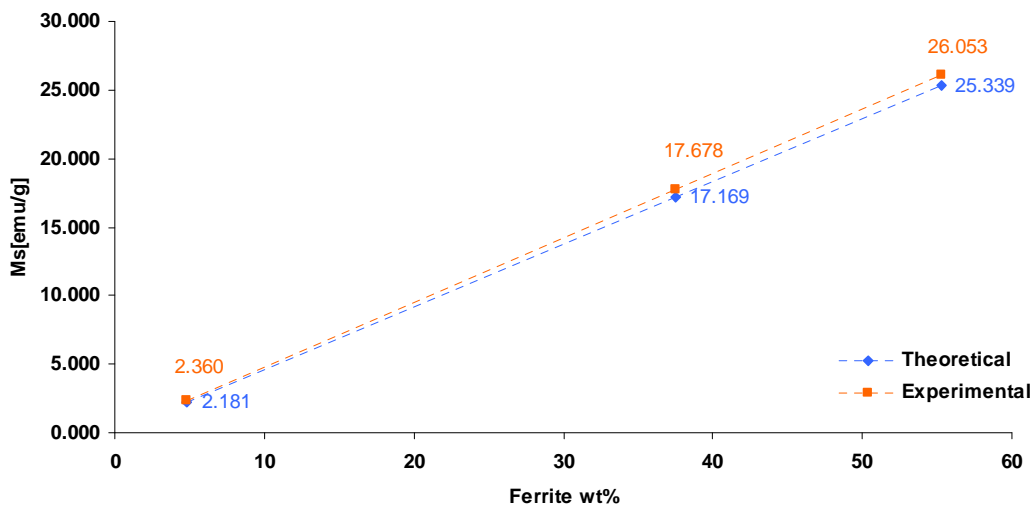


**Figure 54.** Theoretical and experimental values of saturation magnetization for films produced at different volume fractions. Low-energy ball mill was used as a dispersing tool.. The dotted lines are presented as eye guides only.

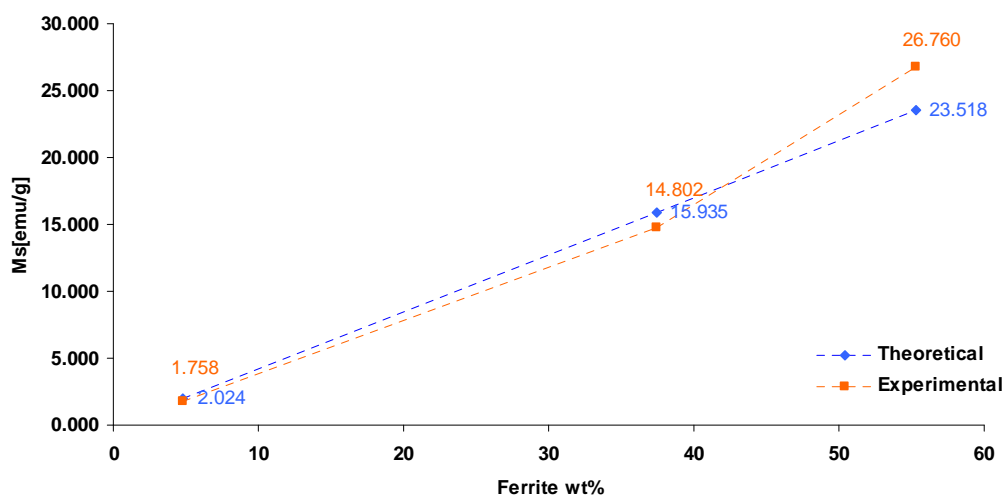


**Figure 55.** Theoretical and experimental values of saturation magnetization for films produced at different volume fractions. High-energy homogenizer was used as a dispersing tool. The dotted lines are presented as eye guides only.

Based on the above results and taking into account that both weight percentage and volume fractions were calculated from the components used in the composites fabrication, it was proved that saturation magnetization of composites follows a rule of mixtures based on mass fraction. On this basis, saturation magnetization measurements can be used as a method to accurately determine the volume or mass fraction of produced composites.

Based on the above results and considerations, produced composites can be used as permanent magnets for application in MEMS according to the discussion of section 1.3.2.

#### 4.4 THERMAL ANALYSES

So far, selected nanocomposites fabrication procedures have shown satisfactory results from a functional viewpoint. Therefore, two additional characterization techniques were

used to assess the viability of those fabrication routes from a thermal behavior viewpoint. Thermogravimetry, (TG), was used to assess the thermal degradation behavior and thermal stability of produced films. Any TG characterization test should be complemented by an additional test to evaluate the mechanical behavior of the material as a function of the temperature. For this purpose, dynamic mechanical analysis (DMA) was also used to qualitatively evaluate changes in the mechanical behavior of produced nanocomposite films.

#### **4.4.1 Thermal Degradation Tests**

In the design of conventional composite materials it is desirable to keep certain properties of the matrix unchanged as much as possible. On this basis, thermal degradation tests (TG) were run to determine the temperature at which bare polyimide and the corresponding composites were degraded. For this purpose, and based on practical considerations provided by Dunson [21], five percent of weight loss was set as the critical value, i.e. the maximum allowance in weight variation due to thermal decomposition of the material. Figure 56 shows the thermal degradation curve corresponding to bare polyimide films in which a degradation temperature of 537°C was established. This temperature value is in good agreement with the 550°C temperature established in the polyimide datasheet. For the sake of comparison, a polyimide film produced after treatment of the precursor solution by the high-energy IKA T-8 homogenizer was also produced and its thermal degradation behavior determined. The corresponding % weight loss-temperature profile (Figure 57) exhibited a stepped curve with the onset of the thermal degradation process located around 330 °C and a corresponding thermal degradation temperature of 515°C. This behavior

suggest that the high spindle speed of the high-energy homogenizer aside from dispersing the inorganic particles is also promoting the chains scission in the polymer matrix at earlier temperatures. Undoubtedly, the intensive dispersion conditions will affect the thermal stability of this type of polymeric matrixes.

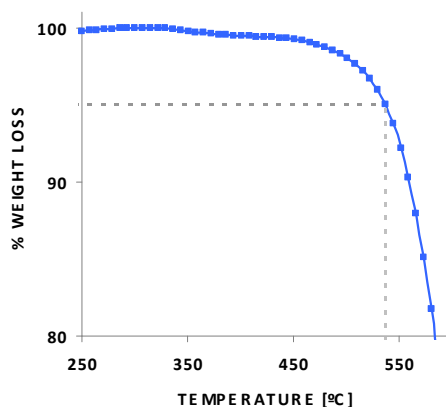


**Figure 56.** Thermal degradation curve for bare PI produced without using the high-energy homogenizer.

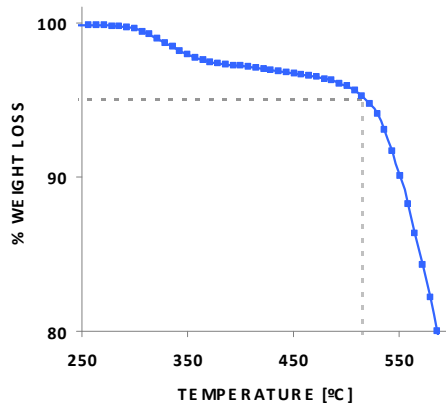


**Figure 57.** Thermal degradation curve for PI synthesized after using high-energy IKA T-18 homogenizer.

Figure 58 shows the thermal degradation curves for composites with 0.1% and 1% volume fractions produced using the ball mill (A and C) and the IKA T-8 homogenizer, (B and D).

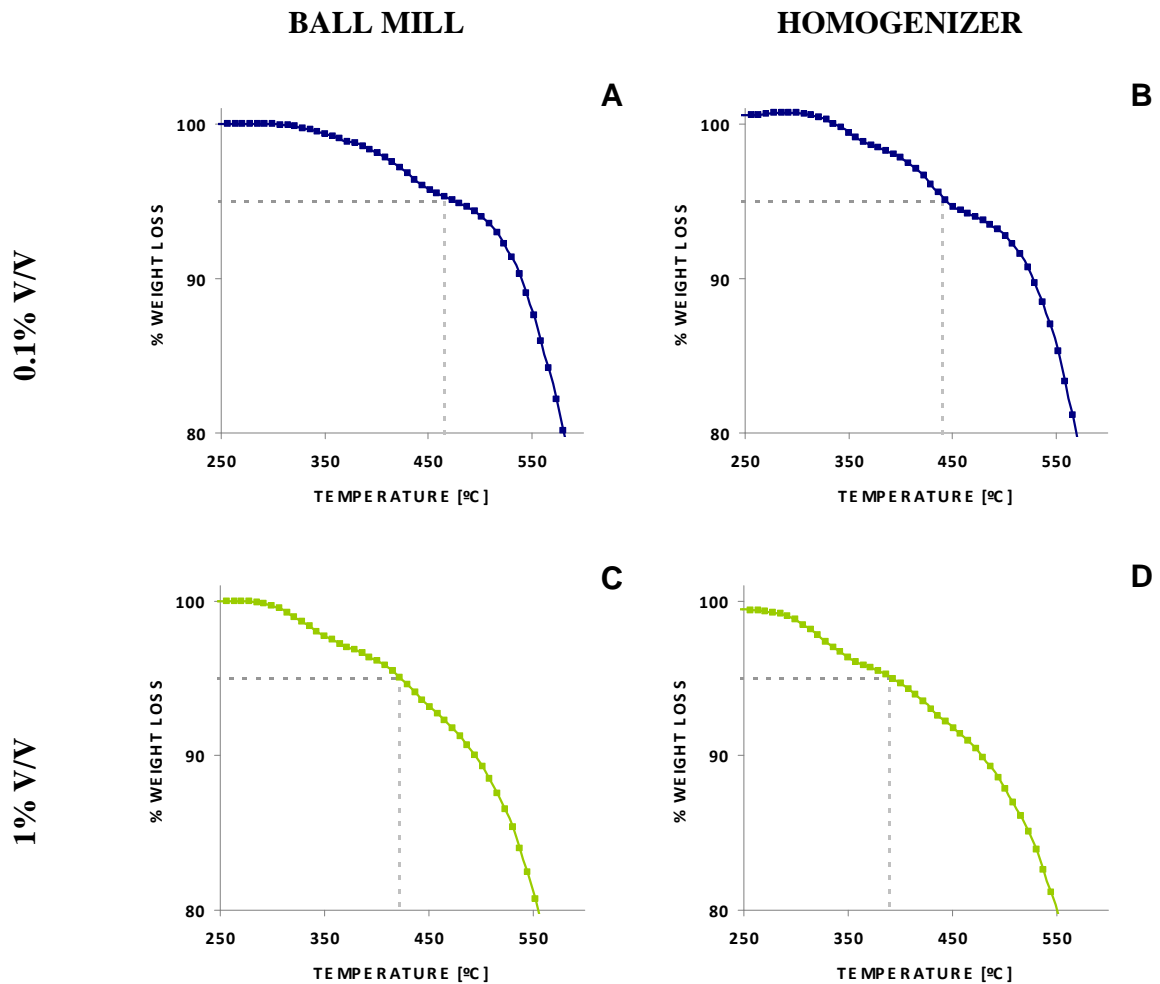


**Figure 58. Thermal degradation curves for composites containing 0.1% and 1% ferrite volume fractions**

Figure 59 shows the thermal degradation curves for composites with 10% and 20% volume fractions produced after using ball milling (A and C) and IKA T-8 homogenizer (B and D) as dispersing tools. Both, Figure 58 and Figure 59, show that produced composite films experienced a pronounced weight loss starting between 300°C and 350 °C which became larger as the volume fraction was increased. The weight loss in the nanocomposites could

have been attributed to an incomplete imidization process; however, FTIR and NIR results did not show the presence of OH<sup>-</sup> groups and N-H bonds that would have reinforced this interpretation. In the case of the films produced using the high-energy homogenizer, an even more pronounced weight loss with the increase in temperature was found. This fact would suggest a synergistic effect of the increase in volume ferrite volume fraction, also observed for the films produced in the ball mill, and the chain scission as suggested by Figure 57; the presence of cobalt ferrite particles should have hindered inter-chain bonding in the polyimide. A graphical interpretation of this mechanism is shown in Figure 60. This nanoparticle-chain interaction is also reinforced by the XRD analyses which shown a decrease in the degree of crystalline character of polymer matrix as ferrite volume fraction was increased. Consequently, thermal degradation temperatures of films produced after dispersion of the nanoparticles in the precursor solution by ball milling were higher than that of films containing the same ferrite volume fraction but dispersed by the high-energy homogenizer.

Relevant results of thermal degradation tests are summarized in Table 8. It is important to note that reviewed papers dealing with polyimide based composites did not carry out thermal stability test and thus the only possible comparison to be done in this work is the one presented with respect to the thermal response exhibited by bare polymeric matrix.

<b>Ferrite Volume Fraction [%]</b>	<b>Dispersion Technique</b>	<b>Onset of Degradation [°C]</b>	<b>Degradation Temperature[°C]</b>
0.1	Homogenizer	328	440
1		299	390
10		335	407
20		336	379
0.1		336	466
1	Ball Mill	314	422
10		335	430
20		350	422

**Table 10. Summary of Thermal Degradation Results**

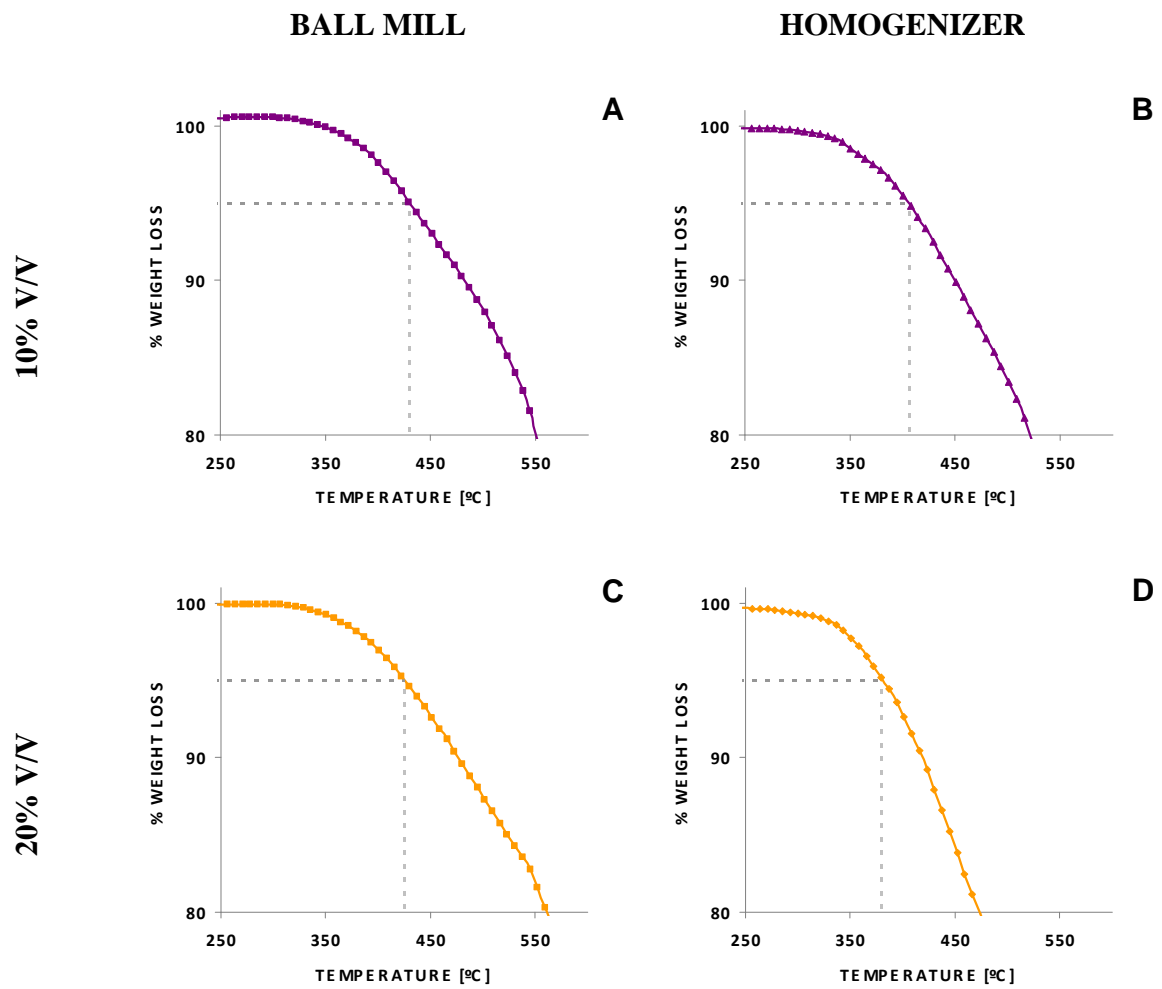
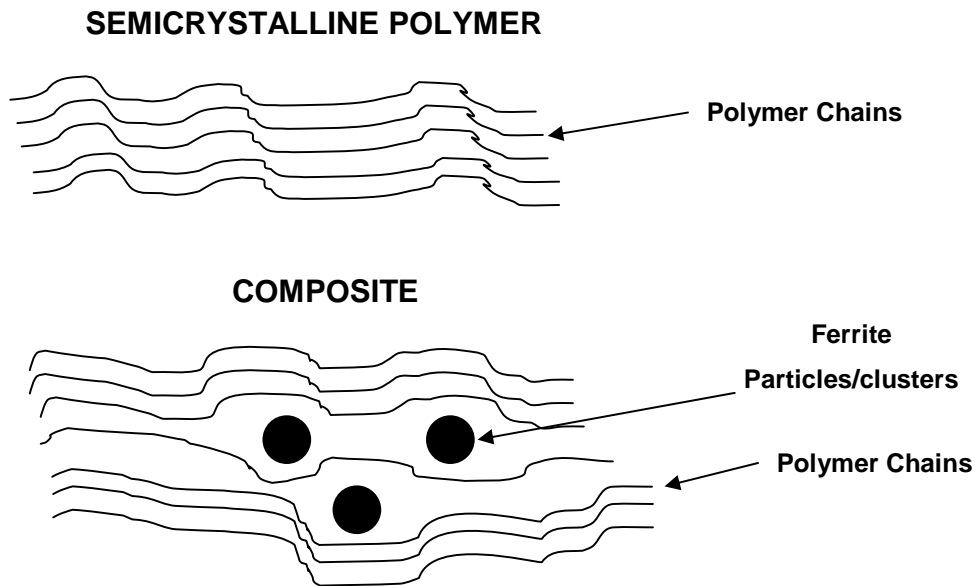


Figure 59. Thermal degradation curves for composites containing 10% and 20% ferrite volume fractions.



**Figure 60.** Schematic interpretation of the ferrite particles-polymeric matrix interaction.

#### 4.4.2 Thermal Stability

As mentioned before (section 3.4.1) polyimide coatings to be used in microelectronics have to withstand temperatures of 350°C during the soldering process of integrated circuits. Furthermore, it is also possible to attain similar but localized temperatures in MEMS devices. Therefore, the assessment on how the material behaves when subjected to fixed temperature along a determined time becomes indispensable. Accordingly, thermal stability of produced films was evaluated by following a protocol common suggested by Dunson [21] that is based on the sample weight loss as a function of time at 400°C. The corresponding data are shown in Figures 61 to 64 and revealed an almost constant weight loss rate of the produced composites with heating time. This rate of weight loss was more pronounced for a larger volumetric load of the ferrite phase (Table 11) and varied from 0.48%/h to 1.87%/h (when volume fraction increased from 0.1 to 20%) for films produced

using the low-energy ball mill and varied from 0.42%/h to 3.03%/h (when volume fraction increased from 0.1 to 20%) for films produced using the high-energy homogenizer.

Bare PI film (Figure 61) exhibited a negligible weight loss rate, evidencing its high thermal stability. Similar behavior was observed for the PI film that was pre-treated by the high-energy homogenizer (Figure 62). In general, the weight loss rates were higher for nanocomposite films produced using the homogenizer as dispersion method and increased for higher volume fractions as mentioned previously. The maximum rate of weight loss was 3.03%/h in the composite produced using ball milling as dispersing method versus 1.87%/h for the composite produced after dispersing the nanoparticles by using the high-energy homogenizer. The ferrite volume fraction was 20% in both cases. These results are in good agreement with the tendency observed in the thermal degradation data previously discussed where the higher weight loss was observed in those composite films produced after using the homogenizer as dispersing tool. These results are also in agreement with the hypothesis of ferrite particles acting as obstacles for interchain bonding as well as with the hypothesis stating that the high energy imposed by the homogenizer to the precursor solution is causing chain scission. Thus, for films produced with the homogenizer a synergistic effect of polymer chain and particle volume fraction would explain the higher weight loss rate is since shorter polymer chains would require even less energy (compared with films produced using the ball mill as dispersing tool) to separate one of each other and/or to degrade.

Based on the results obtained so far, only composite films produced by using ball milling as dispersing tool and containing 0.1% and 1% v/v of cobalt ferrite would meet the requirements described in section 3.4.1. As well as in the case of thermal degradation previously discussed, there is no published information regarding thermal stability of

polyimide matrix composites and thus the only comparison criteria is the thermal behavior of bare polyimide which, ideally, would be expected to remain at least the same in composites

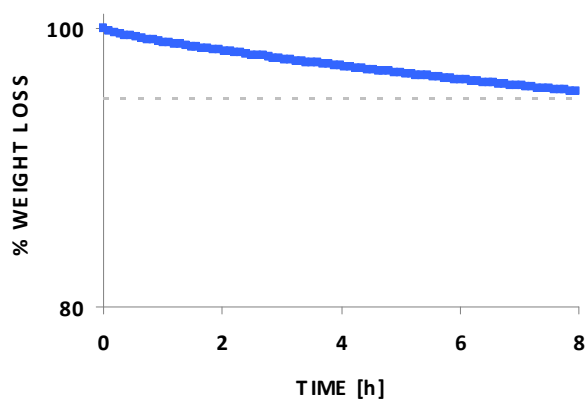


Figure 61. Thermal stability curve for bare PI

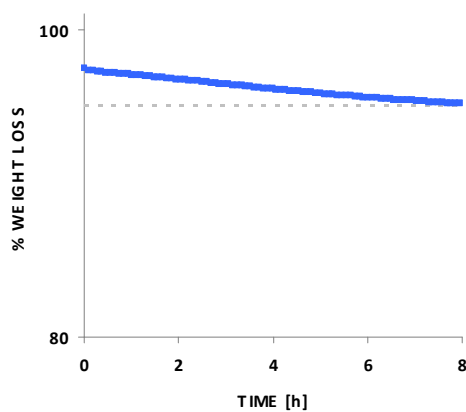


Figure 62. Thermal stability curve for bare PI pre-treated with the high-energy IKA T-8 homogenizer

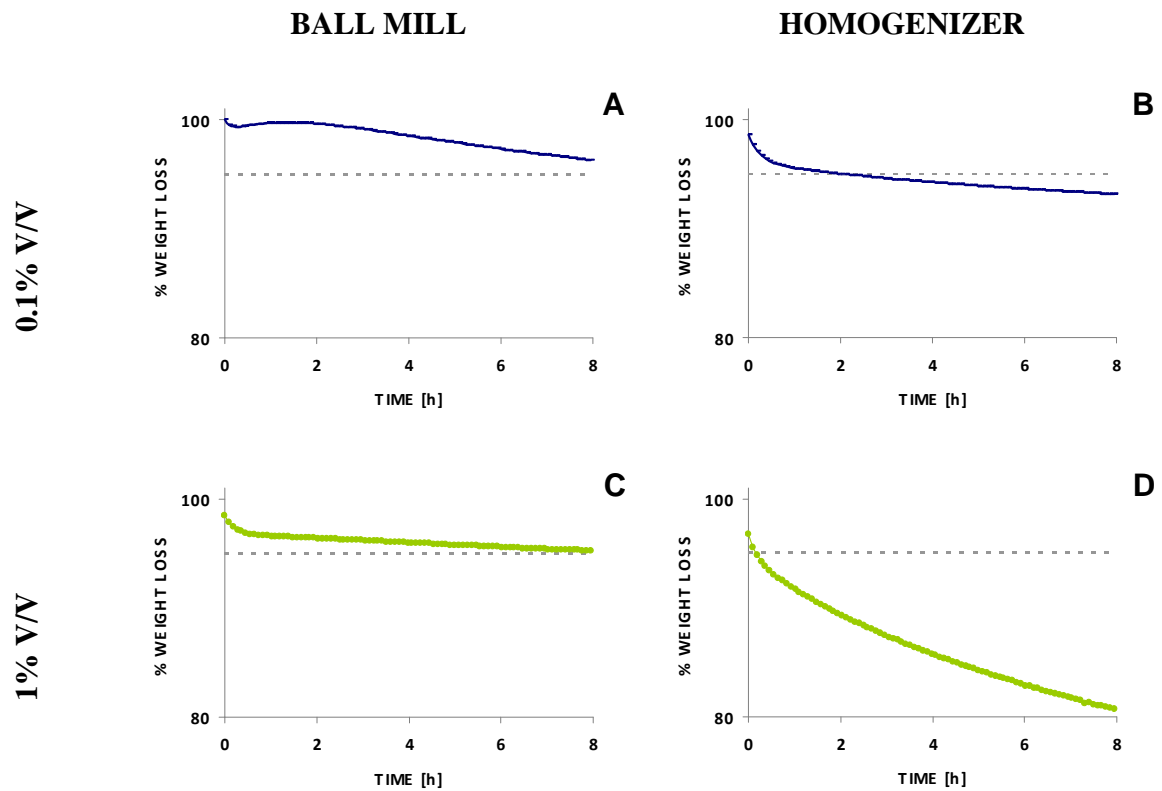


Figure 63. Thermal stability curves for composites containing 0.1% and 1% ferrite volume fractions

Composite Volume Fraction [%]	Weight Loss Rate [%/h]	
	Ball Mill	Homogenizer
0.1	0.48	0.42
1	0.23	1.73
10	1.75	2.06
20	1.87	3.03

Table 11. Weight loss rates for composite films produced at different volume fractions

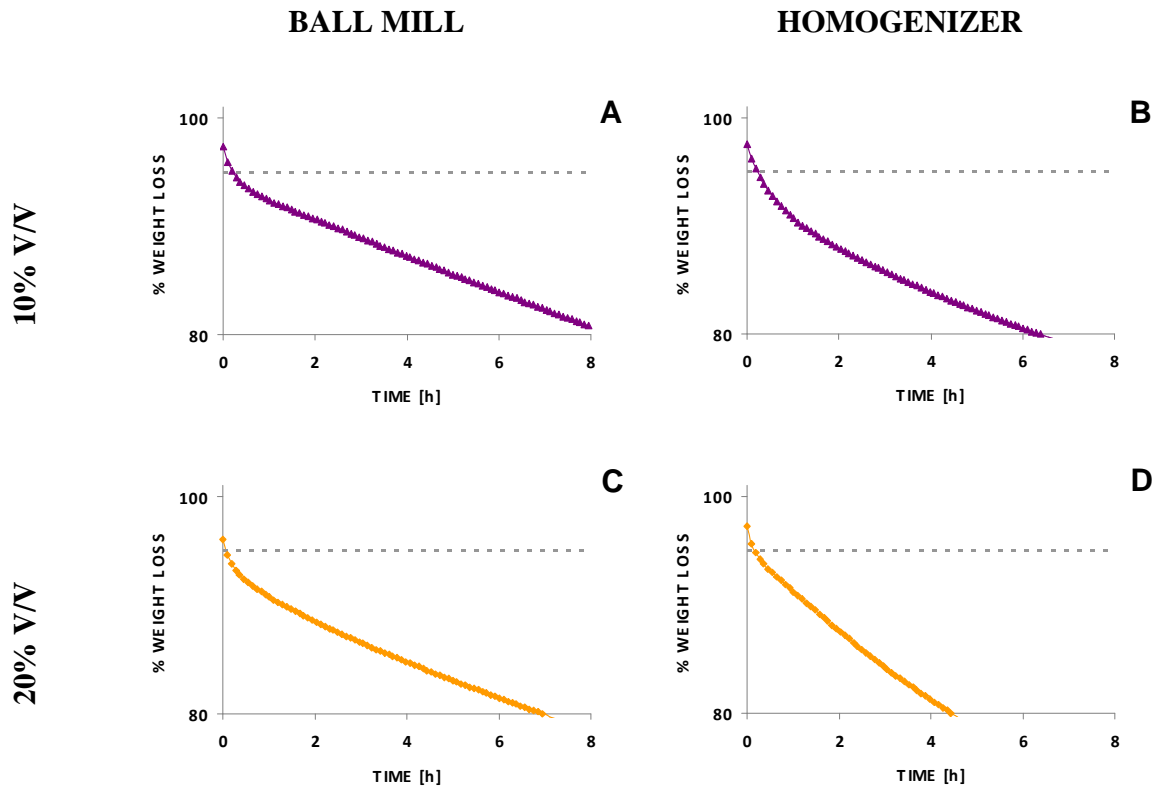


Figure 64. Thermal stability curves for composites containing 10% and 20% ferrite volume fractions

#### 4.4.3 Dynamical Mechanical Analysis

As Figure 65 evidences, composite films produced with the high energy IKA T-8 homogenizer exhibited a reduction in storage (elastic) modulus,  $M'$ , compared to the plot for bare polyimide. This reduction in  $M'$  was larger as ferrite volume fraction in the film increased from 0.1% to 20%. This decrease in  $M'$  will produce a less stiff material or, in terms of energy, a material that can store less energy in the form of elastic strains. Evidently, an increase in the v/v ratio of the disperse ferrite phase caused a significant drop in the corresponding  $M'$ . Since polyimide is a linear chain polymer with complex monomers, it begins to degrade even before proper melting. This particular behavior of

polyimides explains the sloped  $M'$ - $T$  profile that can be considered as an indicative of the development of different molecular relaxations. Furthermore, the stepped profile of the  $M'$ - $T$  plots corresponding to the composite films would suggest a molecular relaxation of the polymer matrix. This molecular relaxation could have been promoted by the intercalation of the ferrite nanoparticles between the polymeric chains in the nanocomposites.

On the other hand, the variation of  $\text{Tan } \delta$  as a function of temperature is shown in Figure 66. As explained in earlier sections,  $\text{Tan } \delta$  is a relationship of the loss modulus  $M''$  to the storage modulus and thus is a relationship of the viscous-like to the elastic behavior of the material being evaluated. Under this basis, the information provided by this figure suggested an increase in the viscous-like behavior for the composite films; an explanation also supported by the drop in  $M'$  plots above discussed. Moreover, the trends observed in Figures 65 and 66 indicate that an increment in the volumetric load of the disperse phase will lead to the rise in the  $\text{Tan } \delta$  values because, as mentioned before, the increase in nanoparticles volume fraction should have hindered the interchain binding. Furthermore, the observed dependence of  $M'$  and  $\text{Tan } \delta$  on the volumetric load of ferrite nanoparticles in the films are in good agreement with their thermogravimetric behavior, discussed previously.

The glass transition temperature,  $T_g$ , of the homogenized films was determined from the data shown in Figures 65 and 66. In Figure 66,  $T_g$  corresponds to the temperature at which a maximum value of  $\text{Tan } \delta$  was achieved. Accordingly,  $T_g$  values varied from 228°C in pure PI to 267°C in the composite films.  $T_g$  was also estimated as the onset of  $M'$  drop (Figure 65). In this later case,  $T_g$  varied from 205°C, in pure PI, to approximately 230°C for nanocomposites disregarding the volume fraction. Unfortunately, as mentioned several times before this is a pioneering work in its class and therefore there are no available

references to compare with.

Figure 67 shows  $M'$ - $T$  plots corresponding to nanocomposite films produced in the ball mill. As in the case of those films produced with the homogenizer a reduction of the  $M'$  module is evidenced compared with bare polyimide. However films obtained using this dispersion technique do not show a stepped curve which suggests a more compact polyimide microstructure. These results reinforce the observations in thermal stability and thermal degradation tests where films produced in the ball mill showed a less pronounced weight loss.

The glass transition temperature,  $T_g$ , for films produced in the ball mill was determined in the same way discussed above for homogenized films. From the  $M'$ - $T$  graph (Figure 67) it was found that  $T_g$  increased from 230°C, in bare PI, to around 250°C for the produced nanocomposites (0.1%-20% v/v of ferrite phase). In turn,  $T_g$  estimated from the  $\tan \delta$  plots (Figure 68) was around 280 °C in the case of composites and near 270°C for bare polyimide. Detailed values for glass transition temperatures obtained from  $M'$ - $T$  plots are summarized in Table 11 whereas Table 13 summarizes the results from the  $\tan \delta$ -Temperature measurements. The films produced by using the ball milling dispersing approach exhibited glass transition temperature values higher than the ones obtained for the homogenizer-dispersed films. This fact suggests the development of longer chains in the former composites, which also reinforces the hypotheses formulated from the thermogravimetry tests. DMA measurements did not suggest a systematic variation of measured properties as function of the ferrite volume fractions; thus, it can only be suggested that increase in the  $T_g$  values observed for all composite films was attributed to the presence of solid particles (ferrite nanocrystals), which should have delayed the polymer yielding process. The latter would also suggest an apparent matrix/dispersoids

interaction when a stress is applied to the composite films that could be associated with the schematic shown in Figure 60. This load transfer mechanism, however, requires a more dedicated study that is beyond the scope of the present work.

Composite Volume Fraction [%]	Glass Transition Temperature [°C]	
	Ball Mill	Homogenizer
0.1	255	234
1	263	215
10	242	241
20	258	232

Table 12. Glass transition temperature determined from  $M'$ -T plots for composite films produced at different ferrite volume fractions

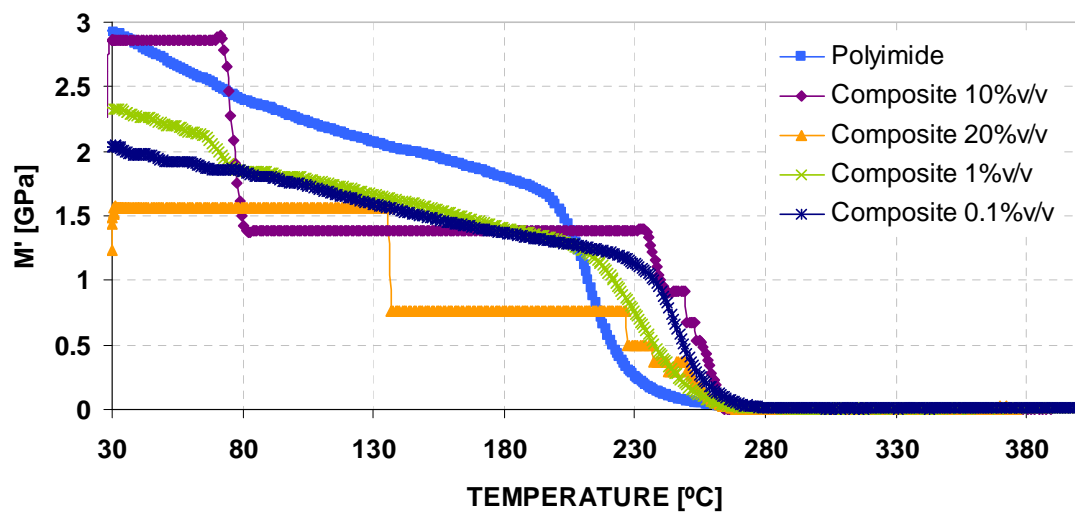


Figure 65. Storage Modulus ( $M'$ ) against Temperature for bare PI and different volume fraction films previously dispersed by using the high-energy IKA T-8 homogenizer

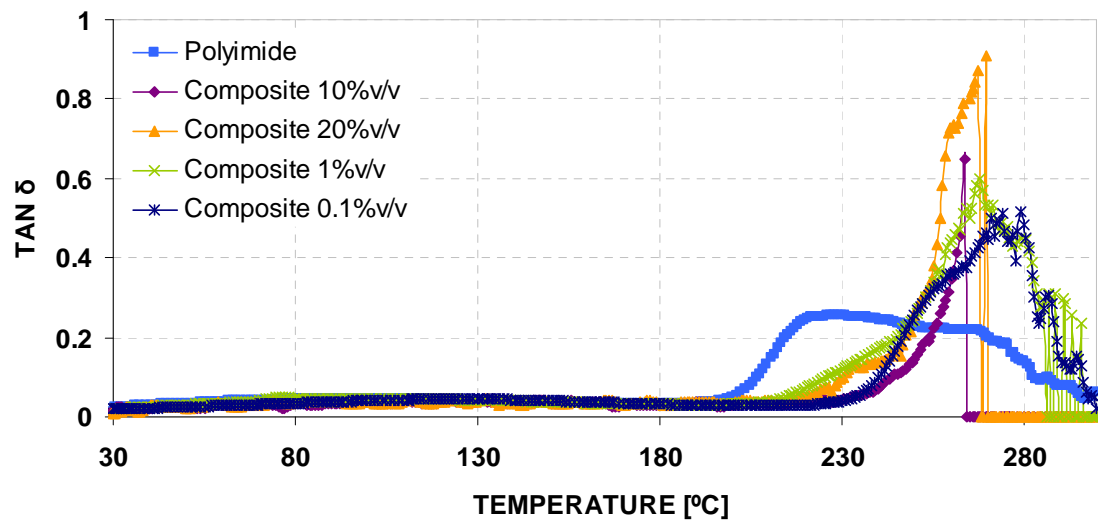


Figure 66. Variation of Tan  $\delta$  with temperature for bare PI and different volume fraction films previously dispersed by using the high-energy IKA T-8 homogenizer

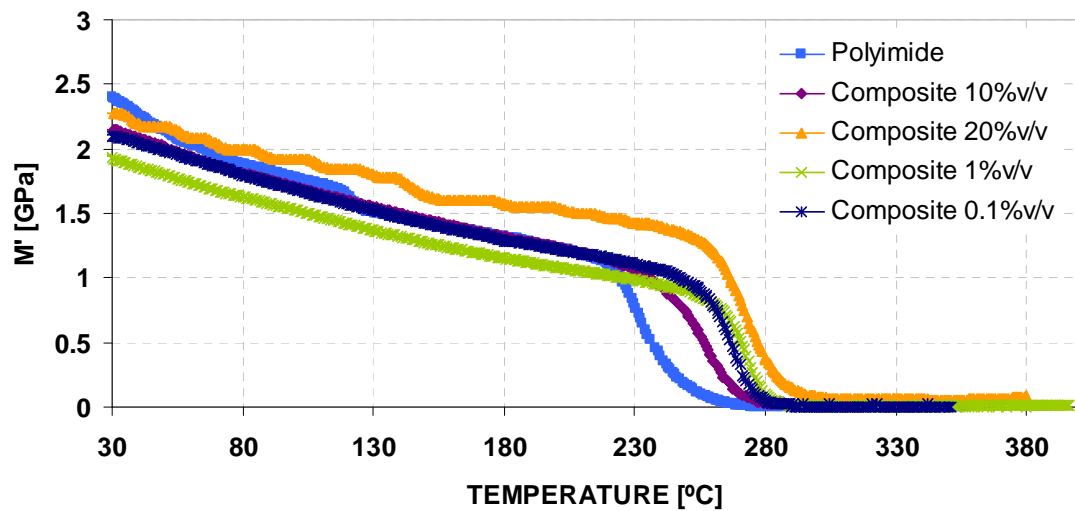


Figure 67. Storage Modulus ( $M'$ ) against Temperature for bare PI and different volume fraction films previously dispersed by using ball milling.

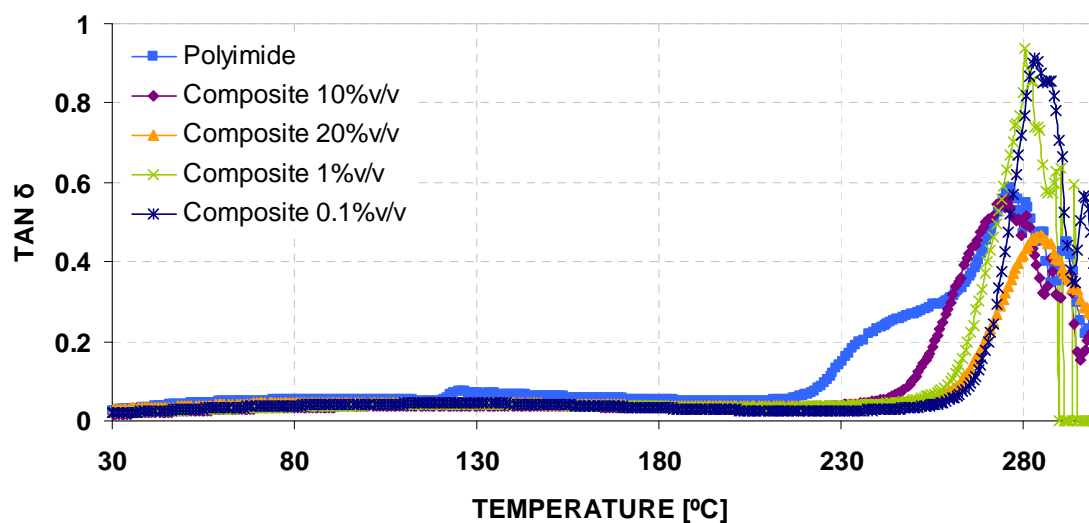
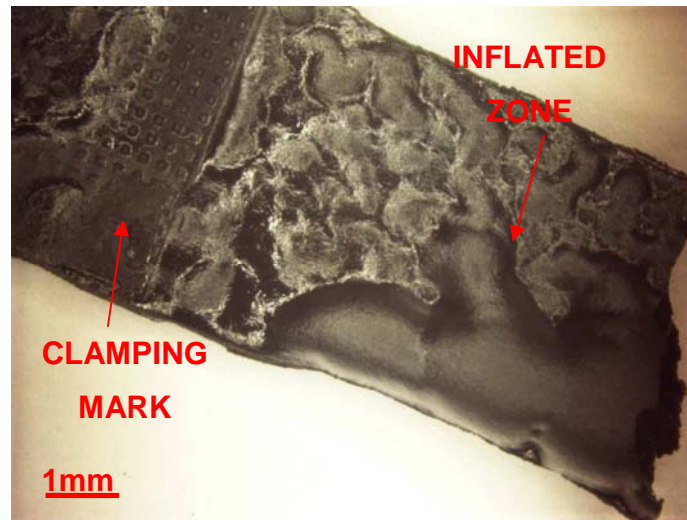


Figure 68. Variation of Tan  $\delta$  with temperature for bare PI and different volume fraction films previously dispersed by using ball milling

All results obtained from the DMA characterization of our films were in nice agreement with the considerations deduced from the degradation and thermal stability tests performed on the same films which suggested a lack in the development of polyimide microstructure due to the presence of ferrite nanocrystals in the composite. This phenomenon was more evident for composite films containing 10% and 20% ferrite volume fractions. However, this effect was only evidenced macroscopically by the inflation exhibited by the films containing 20% ferrite volume fraction shown in Figure 69.

Compostie Volume Fraction [%]	Glass Transition Temperature [°C]	
	Ball Mill	Homogenizer
0.1	281	280
1	283	268
10	276	264
20	285	270

Table 13. Glass transition temperature determined from Tan $\delta$ -T plots for composite films produced at different ferrite volume fractions



**Figure 69. Inflated composite film. 20% ferrite volume fraction film produced using the Labmill 800 ball mill. DMA tested from room temperature to 400°C.**

Optical observations inside the inflated zone revealed that highest volume fraction composites (20%) undergo solidification problems that could be caused either by ferrite particles acting as obstacles for the polyamic acid solids to coalesce and form a solid structure or trapped thermal imidization byproducts which produced the fibrous-like microstructure shown in Figure 70. Further work must be conducted towards determining the cause of this phenomenon and therefore to propose a solution. If the trapped byproducts were the actual cause, modifications of the curing cycle could be carried out to slow down the rate of reaction allowing byproducts to diffuse out of the films. However, if the hypothesis of ferrite acting as obstacles were the actual one, a more detailed study must be conducted towards establishing the volume fraction limit to obtain composite films exhibiting satisfactory dynamical mechanical behavior. Finally if it can be assured that the composites analyzed here are not to withstand temperatures above 100°C they can be used without concerns regarding its thermo-mechanical behavior. Based on the above

considerations all composites evaluated in this work can be considered to be use in the fabrication of MEMS devices such as the microactuators reported by Lagorce [7] with the only restriction relating on its operation temperature as mentioned before. Other devices like micromotors or micropumps could also be fabricated using these composites if a detailed analysis assured the operation temperature remaining below 100°C.

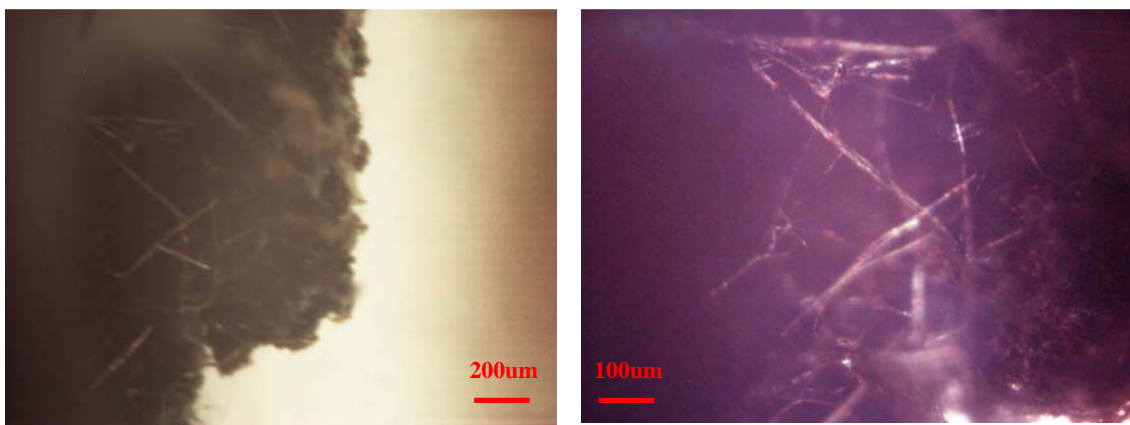


**Figure 70.** Fibrous-like microstructure of inflated film. 20% ferrite volume fraction film produced using the Labmill 800 ball mill. DMA tested from room temperature to 400°C.

## 5. CONCLUDING REMARKS

Polyimide-cobalt ferrite nanocomposite films having well-tuned magnetic properties were synthesized. As suggested by the structural characterization of produced films, the inclusion of ferrite nanoparticles in the polyimide matrix would inhibit the development and/or ordering of the polymeric chains. Although the magnetization of the nanocomposites was found to be strongly dependent on the volumetric load of the ferrite nanoparticles, the corresponding coercivity remained constant. M-H measurements also suggested the magnetic isotropic behavior in the nanocomposite films. Isotropy was also evidenced by dispersion assessment carried out using near infrared spectroscopy and stereographic imaging which showed a good distribution with poor dispersion of the disperse phase evidenced by the presence of ferrite cluster that formed during the drying of ferrite powders and could not be separated by the used dispersing devices.

Regardless of the later challenges, in this work has been demonstrated that molecular structure of polymer matrix could be developed even though inorganic nanoparticles were present and producing nanocomposites exhibiting satisfactory dispersion as suggested by functional and structural analysis. The later statement can be considered a positive outcome taking into account that selected disperse phase were particles with high coercivity which led to a 'natural' trend to aggregate.

Thermal analysis results suggest that these clusters hinders the inter chain binding process and cause a detrimental in the thermo mechanical behavior of the composite compared with bare polyimide. This effect is of critical importance for temperatures above 100°C in any

case. Therefore, produced polyimide-ferrite nanocomposites can be used without any concern about their physical and structural stability for applications involving temperatures up to 80°C.

This work was a pioneering effort towards the characterization of polymer matrix nanocomposites from a wide viewpoint which included structural, functional, thermal and mechanical behavior assessments for the developed materials.

Further work must be focused on the use of either another drying technique or another synthesis route for cobalt ferrite nanoparticles such as the use of cobalt and iron acetates in organic solvents in such a way that the drying step is avoided and polyimide precursor can be mixed directly with the synthesis solvent in order to avoid the formation of the aforementioned clusters which acted as obstacles for inter-chain binding. Another alternative to overcome this difficulty is the surface treatment of inorganic particles with another coupling agent different from the one used in this work (KR-TTS), however the work by Zhan [12] has demonstrated to achieve good distribution but poor dispersion of the inorganic fillers as well as the results shown in this work.

## REFERENCES

- [1] Bhushan, B. *Nanotribology and nanomechanics of MEMS/NEMS and BioMEMS/BioNEMS materials and devices*. *Microelectronic Engineering* 84, 387–412, 2007.
- [2] S. Spearing, *Materials issues in microelectromechanical Systems (mems)*, *Acta mater*, 48, 179-196, 2000.
- [3] Jin Qian, Ya-Pu Zhao. *Materials selection in mechanical design for microsensors and Microactuators*. *Materials and Design* 23, 619–625, 2000.
- [4] Gad-el-Hak, M. *The MEMS handbook*. CRC Press. 2006.
- [5] Tsung-Shune Chin, *Permanent magnet films for applications in microelectromechanical systems*, *Journal of Magnetism and Magnetic Materials*, 209, 75-79, 2000.
- [6] L. García-Cerda, M. Escareño-Castro, M. Salazar-Zertuche, *Preparation and characterization of polyvinyl alcohol–cobalt ferrite nanocomposites*, *Journal of Non-Crystalline Solids*, 353, 808–810, 2007.
- [7] L. Lagorce, M. Allen, *Magnetic and Mechanical Properties of Micromachined Strontium Ferrite/Polyimide Composites*, *Journal of microelectromechanical systems*, vol. 6, no. 4, 307-312, 1997.
- [8] D. Askeland, P. Phule, *The science and engineering of material*, Fifth edition, Thomson, 2005.
- [9] Y. Cedeño-Mattei, O. Perales-Pérez, M. Tomar, F. Román, *Tuning of Magnetic Properties in Cobalt Ferrite Nanocrystals*, *Journal of applied physics*, 103, 07e512, 2008.
- [10] S. K. Lim, K. J. Chung, Y. Kim, C. K. Kim, C.S. Yoon, *Synthesis of iron oxide nanoparticles in a polyimide matrix*, *Journal of Colloid and Interface Science*, 273, 517–522, 2004.
- [11] J. H. Kim, J. Kim, K. H. Baek, D. H. Im, C. K. Kim, C. S. Yoon, *Fabrication of CoPt nanoparticles with high coercivity on a polymer film*, *Colloids and Surfaces A: Physicochem. Eng. Aspects*, 301, 419–424, 2007.

- [12] J. Zhan, G. Tian, L. Jiang, Z. Wu, D. Wu, X. Yang, R. Jin, *Superparamagnetic polyimide/ $\gamma$ -Fe<sub>2</sub>O<sub>3</sub> nanocomposite films: Preparation and characterization*, *Thin Solid Films*, 916, 6315-6320, 2008.
- [13] I. G. Yanez-Flores, R. Betancourt-Galindo, J. A. Matutes Aquino, O. Rodríguez-Fernandez, *Preparation and characterization of magnetic PVC nanocomposites*, *Journal of Non-Crystalline Solids*, 353, 799–801, 2007.
- [14] J. Slama, A. Gruskova, R. Vıcen, S. Vıcenova, R. Dosoudil, J. Franek, *Composite material with substituted Li ferrite for high-frequency applications*, *Journal of Magnetism and Magnetic Materials*, 254–255, 642–645, 2003.
- [15] M. Pasquale, C. P. Sasso, M. Velluto, S. H. Lim, S.H, *Stress sensing with Co based ferrite composites*, *Journal of Magnetism and Magnetic Materials*, 242–245, 1460–1463, 2002.
- [16] C. P. Sasso, M. Pasquale, L. Giudici, S. H. Lim, S.M. Na, *Piezomagnetic coefficients of polymer bonded Co-ferrites*, *Sensors and Actuators*, 129, 159–162, 2006.
- [17] A. Voigt, M. Heinrich, C. Martin, A. Llobera, G. Gruetzner, F. Pérez-Murano, *Microelectronic Engineering*, 84, 1075–1079, 2007.
- [18] K. Baba, F. Takase, M. Miyagi, *Ferromagnetic particle composite polymer films for glass and semiconductor substrates*, *Optics Communications*, 139, 35-38, 1997.
- [19] M. Makleda, T. Matsuib, H. Tsudab, H. Mabuchib, M. El-Mansya, K. Morii, *Magnetic and dynamic mechanical properties of barium ferrite–natural rubber composites*, *Journal of Materials Processing Technology*, 160, 229–233, 2005.
- [20] S. Sindhua, S. Jegadesanb, A. Parthibanb, S. Valiyaveettil, *Synthesis and characterization of ferrite nanocomposite spheres from hydroxylated polymers* *Synthesis and characterization of ferrite nanocomposite spheres from hydroxylated polymers*, *Journal of Magnetism and Magnetic Materials*, 296, 104–113, 2006.
- [21] Dunson, D. *Synthesis And Characterization Of Thermosetting Polyimide Oligomers For Microelectronics Packaging*. Virginia Polytechnic Institute 2000.
- [22] P. M. Ajayan, L. S. Schadler, P. V. Braun, *Nanocomposite Science and Technology* Wiley-Vch, 2003.
- [23] F. Hasanain, Z. Y. Wang, *New one-step synthesis of polyimides in salicylic acid*, *Polymer*, 49, 831-835, 2008.
- [24] M. Brown, *Introduction to thermal analysis: techniques and applications*, Chapman and Hell, 1995.

- [25] J. H. Westbrook, R. L. Fleischer, *Magnetic, electrical and optical properties and applications of intermetallic compounds*, Wiley, 2000.
- [26] B. Renteria. *Preparation and characterization of polyaniline-based magnetic nanocomposites for emi shielding applications*, University of Puerto Rico Myaguez, 2007.
- [27] Pillai, V. Shah, D. *Synthesis of high-coercivity cobalt ferrite particles using water-in-oil microemulsions*. Journal of Magnetism and Magnetic Materials, 163, 243-248, 1996.
- [28] Grigorova, M. Blythe, H. Blaskov, V. Rusanov, V. Petkov, V. Masheva, V. Nihtianova, D. Martinez, Ll. Muñoz, J. Mikhov, M. *Magnetic properties and Mossbauer spectra of nanosized CoFe<sub>2</sub>O<sub>4</sub> powders*. Journal of Magnetism and Magnetic Materials, 183, 163-172, 1998.
- [29] R. Newnham, *Properties of Materials: anisotropy, symmetry, structure*, Oxford University Press, 2005.
- [30] M. Piggot, *Load bearing fibre composites*, second edition, Kluwer academic editors, 2002.
- [31] P. Gallagher, *Handbook of thermal analysis and calorimetry*, Volume 1: principles and practice, Elsevier, 1998.
- [32] K. Menard, *Dynamic mechanical analysis: a practical introduction*, CRC, 1999.
- [33] Pan, C. T *Perpendicular magnetic anisotropic field for polyimide-based microactuator with excimer laser ablation*. Sensors and Actuators A, 113, 240–247, 2004.
- [34] D. Jiles. *Introduction to magnetism and magnetic materials*. Chapman and Hall, 1<sup>st</sup> edition, 1991.
- [35] P. Gallagher, *Handbook of thermal analysis and calorimetry*, Volume 2: Applications to polymers and plastics, Elsevier, 1998.
- [36] B. Stuart. *Infrared spectroscopy: fundamentals and applications*. Wiley.
- [37] D. A. Burns, E. W. Ciurczak. *Handbook of near infrared analysis*. Third Edition, CRC Press, 2008.
- [38] A. C. Comer, D. S. Kalika, B. W. Rowe, B. D. Freeman, D. R. Paul. *Dynamic relaxation characteristics of Matrimid polyimide*. Polymer, 50, 891-897, 2009.
- [39] ASTM. *Standard practice for plastics: Dynamic mechanical properties: determination and report procedures*. ASTM D4065-01, 2001.